Studies on Effect of Excitation Frequency on Neutral Radicals in Very High Frequency Capacitively Coupled Plasma

Takayuki Ohta

2004

Nagoya University

名古屋大学図書

41370405

報告番号 甲第 6268 号

Contents

1. Introduction

1.1 Various applications of plasma processing 1
1.2 Smart plasma process 3
1.3 Very high frequency capacitively coupled plasma 5
1.4 Radical temperature 8
1.4.1 Importance on the radical temperature 8
1.4.2 Previous studies on the radical temperature 11
1.5 Previous studies on the plasma chemistry using SiH_4 and SiF_4 gases 13
1.6 Purpose and composition of this thesis 16
Reference for Chapter 1

2. Experimental apparatus and plasma diagnostic techniques

2.1 Experimental apparatus 23
2.2 Plasma diagnostic techniques 33
2.2.1 Ultraviolet Absorption Spectroscopy (UVAS) 33
• Ring dye laser
• Hollow cathode lamp
2.2.2 Infrared Diode Laser Absorption Spectroscopy (IRLAS) 38
2.2.3 Laser Induced Fluorescence (LIF) 42
2.2.4 Actinometric Optical Emission Spectroscopy (AOES) 47
2.2.5 Microwave interferometer 49
2.2.6 Double probe 50
2.2.7 Pyrometer 53
Reference for Chapter 2

3. Measurement of Si, SiF, SiF_2 radicals and SiF_4 molecule in SiF_4 plasma

3.1 Introduction 55
3.2 Measurement of Si, SiF, SiF_2 radicals and SiF_4 molecule 56
3.3 Spatial distribution 71
3.4 Summary 78
Reference for Chapter 3

4. Effect of excitation frequency on the translational temperature and absolute density of Si atoms in SiF_4 plasma

4.1 Introduction 82
4.2 Estimation of translational temperature of Si atom 83
4.3 Effect of excitation frequency on the translational temperature and absolute density of Si atoms 86
4.4 Mechanism for translational temperature of Si atom 89
4.5 Summary 97
Reference for Chapter 4

5. Effect of excitation frequency on absolute density and translational temperature of Si atom in SiH_4 plasma with Ar, H_2, and N_2 dilution gases

5.1 Introduction 99
5.2 Behavior of Si density 101
5.3 Behavior of Si translational temperature 109
5.4 Summary 117
Reference for Chapter 5

6. Effect of excitation frequency on thin film formation in SiH_4 plasma

6.1 Introduction 120
6.2 Estimation for contribution of radicals to film deposition 120
6.3 Summary 126
Reference for Chapter 6

7. Conclusions

7.1 Summary of this thesis 128
7.2 Scopes for future works 130

Acknowledgments
List of Papers

Chapter 1
Introduction

1.1 Various applications of plasma processing

The non-equilibrium plasma processes are indispensable for manufacturing ultra-large-scale integration circuits (ULSIs), thin film transistors (TFTs) of liquid crystal displays (LCDs), solar cells, and so on. Plasma processing is now the most important key-technology, because the low temperature process and so on are all to be realized in the large area process.

In the fabrication of ULSIs, the dielectric layers for insulation and passivation of metal layers for interconnection are deposited and the unmasked area of the semiconductor, the dielectric, or metal layer are etched by plasma processing. The number of device components on a chip for dynamic random access memory (DRAM) and microprocessor (MPU) follows an exponential growth as Moore predicted, permitting over millions and soon billions of transistors to be integrated on a chip. In 2014, the 1 Terabit DRAM or MPU with 3.6 billion transistors will be expected. Therefore, the interconnecting technology is getting more complicated. The number of interlayer dielectrics has increased in advanced logic devices with quarter micron design rules. ULSIs is mostly occupied with interconnect wiring delay which has come to play a dominant role in determining the total signal delay in ULSIs rather than basic gate delay.[1]-[3] It is important to reduce the wiring resistance and parasitic capacitance in order to improve the signal transmission rate.[4] One of the effective methods to reduce the parasitic capacitance is to use interlayer materials with low dielectric constant (low-k) instead of SiO_2.[4]-[6] Interlayer insulating films using low-k materials such as SiOF, SiOCH, and a-C:F are synthesized by plasma enhanced chemical vapor deposition (PECVD). For the fabrication of complementally metal-oxide-semiconductor (CMOS), gate insulated layer such as SiN, SiON thin films are synthesized by

PECVD.[7],[8] Moreover, plasma processes also etch these layers such as SiO_2, the dielectric films, or metal films, since plasma processes have some advantages such as anisotropic etching characteristic and dry process. Therefore, all ULSI processing steps over sixty percent are performed through the use of plasmas. The reduction of production cost of ULSIs has been achieved by increasing the number of component per chip in a large wafer and by performing a process at a high rate. Moreover, a demand for the low cost is also being achieved, through the use of larger silicon wafers. The wafer size used in production today is 8 inch in diameter and 12 inch are in operation. Therefore, the problem that exists for the equipment manufacturers is how to scale up the equipment and provide the same process yield.

Hydrogenated amorphous silicon (a-Si:H) and microcrystalline silicon (μc-Si) thin films were used for the solar cell and TFTs for LCDs, because Spear *et al.* reported the electrical conductivity of these films can be controlled over many orders of magnitude by doping with impurities.[9] The solar cell is the clean energy source without consuming fuels such as oil, coal, and uranium, and emitting CO_x, NO_x, SO_x, and radioactive wastes which affect the environment. The a-Si:H films are generally synthesized by PECVD. The formation of a-Si:H films has some advantages, such as ability to deposit films on various materials, in a large area and at a low process pressure. In order that the solar cell can be widely used as an electric energy source, it is important to improve its convection efficiency, which is now lower than a crystal silicon solar cell, to reduce the production cost much above.[10] a-Si:H and μc-Si films have also been applied to TFTs for LCDs, because the films be formed uniformity on the area of almost 1 square meter at low temperatures by using PECVD. Recently, μc-Si films are attractive, because they have high carrier mobility compared with a-Si:H films. PECVD is a useful method for the direct formation of μc-Si films at a low temperature over a large area compared with other methods such as the thermal chemical CVD,[11],[12] the solid phase crystallization of a-Si:H,[13],[14] and the eximer laser annealing of a-Si:H.[15]-[18]

Accordingly, the plasma processing has been widely used for many manufacturing. For the development of the plasma processing, improvement of the device production

equipment and optimization of the process conditions has ever been performed. However, in order to produce the films and etch with optimized characteristics, realize the fine processing, and stabilize the processing, it is important to understand the gas-phase kinetics and the plasma-induced sub-surface reactions in the plasma processing.

1.2 Smart plasma process

Figure 1-1 shows the schematic diagram of the macroscopic phenomena for the plasma processing. The internal processes in the plasma are classified as follows;

(1) The primary reactions are generation of active species by the electron impact dissociation of the injection gas. Primary decomposition products consist of positive and negative ionic species, excited species, and neutral radicals.

(2) The neutral radicals can react with parent molecules, and the steady-state of the plasma formed through the secondary and higher-order reaction processes among various species.

(3) The neutral radicals and reaction products generated in the plasma transport onto the surface of the substrate through diffusion. The positive ions are also transported towards the substrate with a high energy by the sheath electric field formed in front of the substrate.

(4) The formation of thin film through the surface-reaction processes between the active species incident onto the surface and the solid material deposited on the surface, such as the adsorption, desorption, and surface-migration processes.

Therefore, plasma processing, which has gas-phase reaction and surface reaction, is very complicated. The plasma processing is much affected by the behavior of the species such as molecules and radicals in the gas-phase and it is necessary to investigate the kinetics of species.

Up to now, plasma processing has been investigated by the external parameters such as input power, gas pressure, substrate temperature, and so on, and process conditions have been optimized by comparing with the process performance. However,

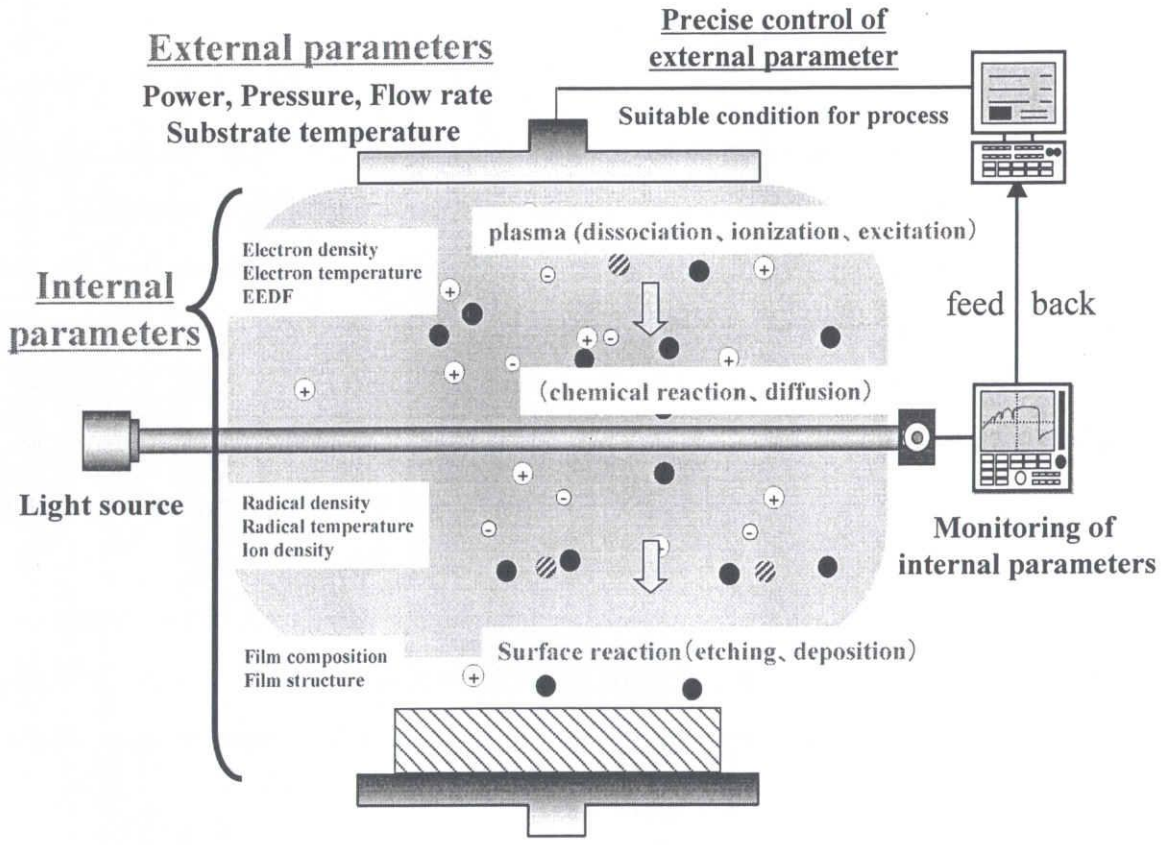

Figure 1-1 Smart plasma process.

the performance control by this way has a limit and the results obtained using the conventional parameter, that is, external parameter will not give us the common fundamental information. In order to perform of plasma process with highly precise control, it is necessary to carry out the monitoring of the internal parameters such as electron density, electron temperature, gas density and so on, and plasma processing should be performed with using the internal plasma parameters. During the plasma processing, the internal parameters are monitored and fed back to the control system, and the process will be controlled precisely to make conditions suitable for deposition and etching; which is called "smart plasma process". It will be the new plasma processing system in the next generation, which is proposed as a new concept by Hori and Goto.[19]

1.3 Very high frequency capacitively coupled plasma

Up to now, radio frequency (RF) 13.56 MHz and microwave 2.45 GHz have mainly employed in plasma processing such as PECVD, reactive ion etching (RIE), and surface treatment. Recently, the process development is demanded for higher deposition and etching rates, and improvement of film quality and anisotropy. With increasing in the size of silicon wafers, the plasma uniformity is also become a critical parameter for the reduction of costs. This is a major driving force for optimizing a process window in terms of pressure, input power, coupling techniques and frequency range for plasma excitation. So far, several high-density plasma (HDP) sources have developed for large area process and high plasma density at low pressure. HDP such as electron cyclotron resonance plasma (ECRP), inductively coupled plasma (ICP), surface wave plasma (SWP), ultrahigh frequency plasma (UHFP), neutral loop discharge plasma (NLDP), helicon wave plasma (HWP) and so on are shown in **Table 1-1**. HDP can open the new reaction pathways allowing better performance comparing with conventional RF 13.56 MHz capacitively coupled plasma (CCP). HDP usually shows the high electron temperature and density and hereby provides a high deposition rate. In HDP, the dissociation rate of feed gases amounts to over 90 % and various kinds of radicals with

Table 1-1 High density plasma sources.

	Non-Magnet			Magnet		
	ICP	UHFP	SWP	NLDP	ECRP	HWP
Gas Pressure (Pa)	0.1 - 10	0.01 - 5	1 - 100	0.1 - 1	0.01 - 10	0.1 - 10
Frequency (MHz)	13.56	500	2450	13.56	2450	13.56
Electron Density (cm^{-3})	10^{11}-10^{12}	10^{11}-10^{12}	10^{10}-10^{12}	10^{11}-10^{12}	10^{11}-10^{13}	10^{11}-10^{13}
Electron Temperature(eV)	4 - 5	1 - 2	1 - 3	1 - 2	2 - 10	4 - 5

high densities are produced.

Recently, it is expected to change of the electron energy distribution function (EEDF) for controlling radical composition in the plasma suitable for each individual process. However, it is difficult to control a plasma and especially EEDF, which is affected by many parameters in the plasma process. The effect of excitation frequency attracts much attention to change EEDF. **Table 1-2** shows the various excitation frequencies used by each plasma sources.[20],[21] The frequencies of CCP and ICP expand the frequency region from 13.56 to 100 MHz. SWP and ECRP which usually used 2.45 GHz are generated at lower frequency region below 500 MHz.

The very high frequency capacitively coupled plasma (VHF-CCP) has some advantages for plasma processing compared with the conventional RF 13.56 MHz CCP. The interest of VHF-CCP is demonstrated by modelings[22]-[26] and experiments.[27]-[39] The effect of excitation frequency has been investigated in a particle in cell Monte Carlo simulation model and in a fluid model. [22]-[24] Raising the excitation frequency of the discharge at a constant amplitude of the applied voltage increases the plasma density approximately in proportion to the square of the excitation frequency.[22],[23],[26] The sheath thickness and ion energy decrease with increasing the excitation frequency. Therefore, a higher frequency operation enables to increase ion directionality due to fewer collisions in the sheath and a reduction of ion bombardment on the substrate.[22]-[25] VHF-CCP also expands the effective area of plasma by trapping the electron drift motion with the time-varying field because the loss of electrons in the discharge volume is mainly controlled by diffusion.[26] The EEDF changes with increasing the excitation frequency at the RF voltage of constant because the electron

Table 1-2 Various excitation frequencies on plasma sources.

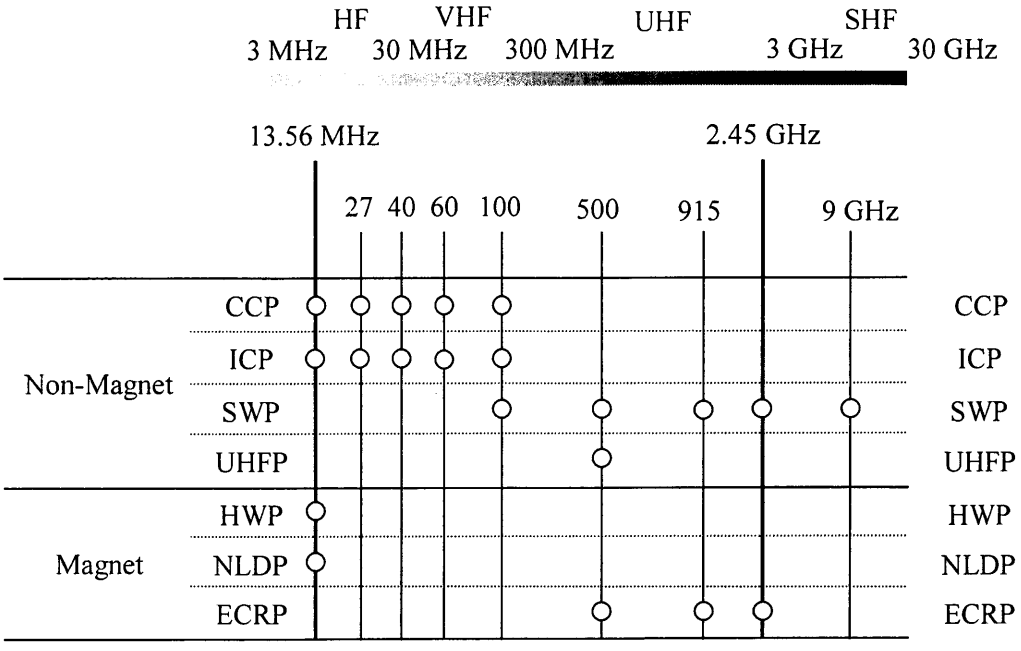

heating mode changes from the bulk heating (Druyvesteyn EEDF) to the surface heating (bi-Maxwellian EEDF) with increasing the excitation frequency. Accordingly, the electron temperature decrease with increasing the excitation frequency.[39] Therefore, the VHF-CCP has several important advantages compared with RF 13.56 MHz CCP. Moreover, thin-film formation and etching can be performed all over the area larger than 30 cm in diameter with high uniformity, using simple parallel plate electrode geometry with large plasma volume without magnetic fields.

Various merit of VHF-CCP in materials processing have been reported from the experience in the reactive ion etching[27]-[29] and microcrystalline silicon deposition.[30]-[38] In the etching, it is reported that VHF-CCP attained a high etch rate, improvement of the selectivity due to effective decomposition of injection gases, reduction of the self-bias voltage, and so on. Koshiishi *et al.* reported that the reduction of micro-loading effect without sacrificing selectivity has been realized.[29] In the microcrystalline silicon deposition, many experiences were accumulated in obtaining the higher growth rate, better uniformity, and reduced intrinsic stress of a-Si:H film deposition. Howling *et al.* reported that high frequency operation enables a large

reduction of powder formation.[30] Takai *et al.* reported that increasing excitation frequency led to the reduction of the electron temperature, resulting in reduction of the high order silane-related radicals in the plasma. Accordingly, a-Si:H films were formed with considerably less the photo-induced degradation.[31] Moreover, Finger *et al.* reported that the decrease of the deposition temperature was demonstrated without the loss of the material quality.[32] These experiences have been reported with the good performance of VHF-CCP processes such as synthesizing thin films. However, it has not been reported enough on the plasma chemistry such as radical density, radical temperature, and so on in VHF-CCP. The plasma chemistry of the VHF-CCP and the effect of the excitation frequency on radical species still has never been clarified in detail. Therefore, it is important to clarify the neutral radical chemistry in VHF-CCP and the diagnostics of radicals in VHF-CCP is indispensable.

1.4 Radical temperature

1.4.1 Importance on the radical temperature

The neutral gas temperature is one of the most important internal plasma parameters for understanding and controlling the plasma process, because the gas temperature has a considerable effect on the density profiles, the transport of reactive radicals, the reaction of radicals, and so on. The effects of the radical temperature are shown in **Figure 1-2**.

The diffusion constant of radicals is described in the following equation based on the Chapman-Enskog theory with the Lennard-Jones intermolecular potential,[40]

$$D = \frac{3}{16} \frac{\sqrt{\frac{4\pi k_B T}{M_{AB}}}}{n\pi\sigma_{AB}^2 \Omega_D} f_D , \tag{1-1}$$

where k_B is the Boltzmann constant, T is the temperature of the radical, M_{AB} is $2[(1/M_A)+(1/M_B)]^{-1}$ which M_A and M_B are the molecular weights, n is the number density of molecules in the mixture, σ is the intermolecular distance where the potential value is zero, Ω_D the collision integral for diffusion, and f_D is a correction term which is

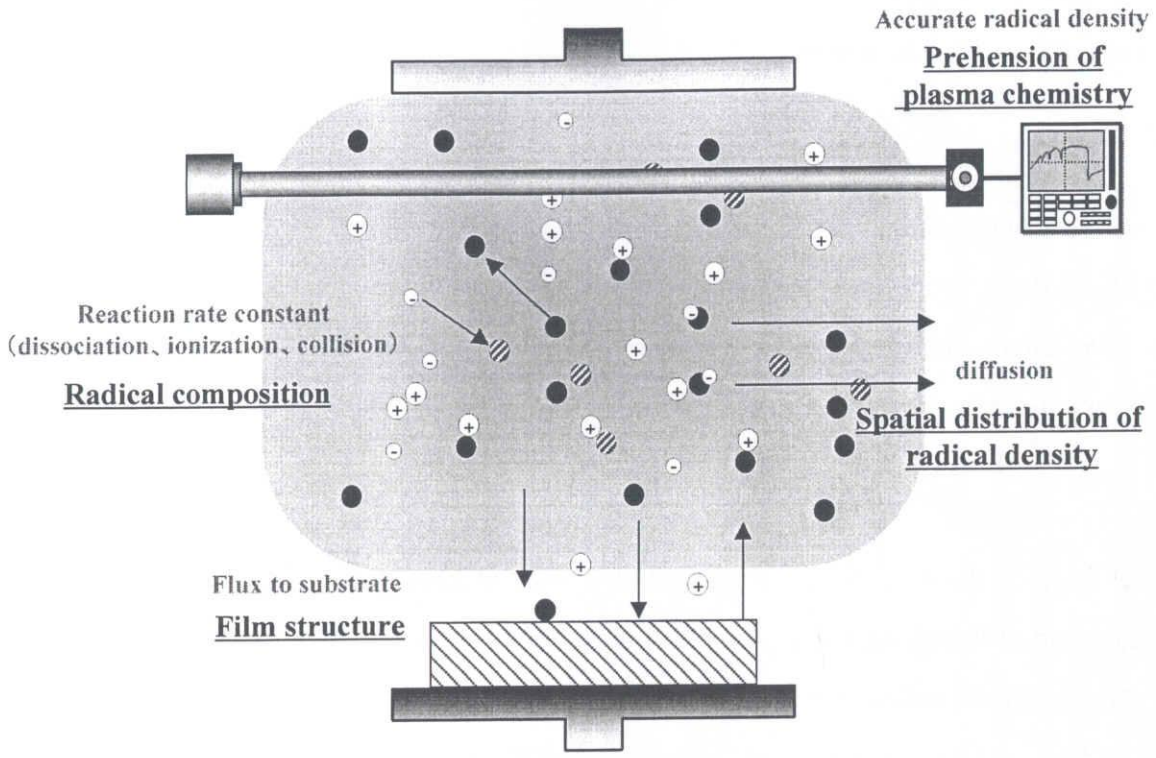

Figure 1-2 the effect of radical temperature.

on the order of unity. Therefore, the transport of radicals, that is, the spatial distribution of the radical density in the plasma is much affected by the temperature. Recently, the uniformity of the process is hardly demanded in ULSIs manufacturing processes for reducing the cost, so the control of the radical temperature is important.

Incident flux of radicals on the substrate is also affected by the temperature. Assuming that radicals come toward the substrate at the thermal velocity, the flux of radical Γ to the substrate is given by[41]

$$\Gamma = \frac{n}{4}\sqrt{\frac{8k_B T}{\pi m}}, \tag{1-2}$$

where n is the radical density and m is the mass of the radical. The radical temperature affects the structure and composition of thin films.

Moreover, many chemical reaction rates are strongly related to functions of the temperature of the species, and are described by Arrhenius equation,

$$k \propto \exp\left(-\frac{E}{RT}\right), \tag{1-3}$$

where E is the activation energy and R is the gas constant. Reaction rates are also a function of the temperature. The plasma chemistry such as radical composition is much affected by the radical temperature.

The measurement of radical densities is important to understand the plasma processes and to control them. The diagnostics of radicals have been performed using laser induced fluorescence and absorption spectroscopy, and the measured values have to be corrected for the partition function that is a function of the gas temperature to obtain the absolute densities. For example in absorption spectroscopy technique, the absolute density of radical is estimated by the following equation assuming the Doppler broadening for the absorption line in the low pressure condition,

$$N = \frac{1}{A}\frac{\Delta\nu_D}{2}\sqrt{\frac{\pi}{\ln 2}}\frac{8\pi\nu_0^2}{c^2}\frac{g_1}{g_2}k_0, \tag{1-4}$$

$$\Delta\nu_D = \frac{2}{c}\sqrt{2R\ln 2}\nu_0\sqrt{\frac{T}{M}}, \tag{1-5}$$

where A is the Einstein constant, $\Delta\nu_D$ is the Doppler width, R is the gas constant, g_1 and

g_2 are the statistical weights of the lower and upper levels, respectively, v_0 is the wave number of the line center, k_0 is the maximum absorption coefficient at the line center, and c is the velocity of the light. Thus, the highly precise value of absolute density is estimated by using the correct temperature, and the precise plasma chemistry will be understood and controlled. The temperature of neutral radicals is affected by many plasma conditions, and provides us with a lot of important information from the standpoint of understanding the reaction chemistries. Donnely *et al.* have reported that the increase of the neutral temperature causes the neutral density to decrease. A reduction in gas density causes the electron temperature to increase, which will often attributed to the damage in the etching plasma.[42] In the VHF-CCP, the plasma density increase and the self-bias voltage decreases with increasing the excitation frequency as described in section 1.3. It is indicated that the energy of species will changed with the excitation frequency, and the energy makes effect on the plasma process such as radical composition, film quality, and so on. Therefore, it is important to measure the radical temperature for clarifying the plasma chemistry in the VHF-CCP.

1.4.2 Previous studies on the radical temperature

Many different techniques to measure radical temperatures in plasmas have been applied in the past. Part of techniques such as analysis of rotational and vibrational spectra in absorption,[43]-[47]emission,[42],[48]-[54] or fluorescence,[48] measurements of Doppler broadening in absorption[55]-[57] or fluorescence,[58]-[60] and measurements of species flux through an orifice [61],[62] are shown in **Table 1-3**. The most general technique is the analysis of the rotational and vibrational band shapes of the optical emission and Fourie transform infrared spectroscopy. For example, the rotational and vibrational temperatures of CF, CN, CO, C_2, and SiF radicals in ICP CF_4 plasma are in the range of 1250 to 2300 K and 1750 to 5950 K, respectively.[53] However, a demerit of this method is that the rotational distribution of the upper electronic level is measured, which is not a good representation of the population of the different rotational levels in the ground electronic state. It is reported that rotational temperatures measured by

Table 1-3 various techniques for measurement of radical temperature.

Methods		species	references
rotational and vibrational spectra	Absorption	SiH_3, N_2O, CF_4, CF_2, CF_3	[43]-[47]
	Optical emission	N_2,SiF, CF, CO, C_2 CN	[42],[48]-[54]
	Fluorescence	CCl	[48]
Doppler broadening	Absorption	CF_4, Si	[55]-[57]
	Fluorescence	Ar^+, SiH_2	[58]-[60]
Mass spectroscopic		Cl_2, CF_4	[61],[62]

optical emission from trace amounts of N_2 in a CCl_4 discharge were in agreement with CCl radical temperatures determined by laser-Induced fluorescence. This fact suggests that the actinometric method using OES for determining plasma temperatures may be valid. However, the technique did not corresponded so well near a cooled electrode, due to the effect of chlorocarbon deposition.[48]

Kiehlbach *et al.* reported modeling and experimental results the gas temperatures ranging from 1200 to 2100 K in the CF_4/O_2 plasma abatement. Their model showed that the heating by the electron impact dissociation (Frank-Condon heating) and by the charge exchange and elastic collisions between ion and neutral were the most dominant heating mechanism in this plasma.[54] Donnelly *et al.* estimated temperatures from 650 to 1250 K from N_2 emission spectra in the Cl_2 ICP. They reported the heating was attributed primarily to the energy released by electron-impact dissociation.[42]

Singh *et al.* used the mass spectrometer sampling through an orifice in CF_4 ICP to estimate neutral temperatures in the range of 450 - 930 K.[62] The measurement of species flux through an orifice can provide the neutral translational temperature near a surface and it is fairly straightforward in an inert gas such as argon. However, application of this technique in reactive gases requires some assumptions regarding that the measured neutral density is accurate because the temperature is estimated by the neutral density ratio with plasma on and off.

Among these techniques, the measurement of Doppler broadening is the most

powerful method to directly measure the translational temperature of selected species. Tanaka *et al.* reported that the absolute density and the translational temperature of Si atoms in the RF (13.56MHz) SiH_4/Ar plasma were measured by using the ultraviolet absorption spectroscopic technique employing a ring dye laser. The translational temperatures varied from 380 K to 700 K with increasing SiH_4 flow rate ratio from 0 to 100 %.[57] In this method, the estimation of temperature is easy and accurate because the Doppler broadening of a single line is measured. However, there has never been reported on the dependence of the temperature of radicals on the excitation frequency in addition to their absolute densities in the VHF plasma.

1.5 Previous studies on the plasma chemistry using SiH_4 and SiF_4 gases

As described in section 1.3, VHF-CCP has been widely employed for the deposition of a-Si:H and poly-Si films. SiH_4/H_2 plasma is mainly employed for the formation of these films. For the formation of poly-Si films by addition of SiF_4, it is reported that fluorine-related radicals play an important role in the formation of films with preferential orientation and large-grain texture.[63] In manufacturing ultra-large-scale integration circuits (ULSIs), fluorine-doped silicon oxide (SiOF) thin films are also deposited by using both gases for interlayer insulating films. By addition of F atom into SiO_2 films, the dielectric constant of thin films are reduced in compared with SiO_2 films.[64] SiH_4/N_2 plasma is employed for formation of silicon nitride (SiN) films for passivation layer of Organic Light Emitting Devices (OLED) and gate insulating films of ULSIs, and the SiF_4/N_2 plasma is employed for formation of fluorine-doped silicon nitride (SiNF) thin films gate insulating films.[7],[65]-[67] Moreover for etching, highly reactive fluorine atoms and ions produced from the plasma interact with the Si substrate and produce volatile reaction products, such as the SiF_2 radical and the SiF_4 molecule.[52],[68] These products, in turn, diffuse back into the plasma where they are dissociated and ionized by electrons, and the resulting by-products are transported and re-deposited onto the substrate. Hebner *et al.* reported that the etch rate of 500 nm/min

Table 1-4 various techniques for measurement of radical density.

Methods	species	references
OES	SiH, Si	[70],[71]
LIF	SiH_2, SiH, Si SiF_2, SiF	[60],[70],[72]-[78] [88]-[94]
UVAS	Si SiF_2	[56],[57],[79]-[81] [95],[96]
IRLAS	SiH_3, SiH_2, SiH SiF, SiF_2	[43],[79],[82],[83] [97]-[100]
CRDS	SiH_3, SiH, Si	[86],[87]

translates into the etch by-product gas flow from the surface of approximately 40 sccm for an 8 inch diameter wafer.[69] The value of 40 sccm makes significant effects on the process, so the behavior of etching products can not be negligible.

The diagnostics of SiH_4 plasma has been frequently performed for the formation of a-Si:H and poly-Si films as shown in **Table 1-4**. Optical methods do not disturb the plasma. Optical emission spectroscopy (OES)[70],[71] and laser-induced fluorescence (LIF)[60],[70],[72]-[78] are applicable for measuring Si, SiH, and SiH_2 radicals. Ultraviolet absorption spectroscopy and vacuum ultraviolet absorption spectroscopy use the incoherent light source and the measuring devices are simple compared with measuring methods by using laser light sources such as infrared diode laser absorption spectroscopy (IRLAS) and LIF. On the other hand, Tanaka *et al.* reported that the absolute density and the translational temperature of Si atoms in the RF (13.56MHz) SiH_4/Ar plasma were measured by using UVAS employing a ring dye laser.[57]

The composition of gas species in plasma is obtained by measuring absolute densities of each gas species. Therefore, absolute density measurements of the radicals are essential to evaluate the chemical kinetics in the plasma. IRLAS is a powerful tool for absolute density measurements. In this method, the values obtained by measurement are directly converted to absolute densities. On the other hand, OES and LIF must be combined with other techniques for the calibration to obtain absolute values. With these advantages of IRLAS, previous studies on the SiH_x (x = 1-3) radicals by IRLAS have

provided important information on the SiH_4 plasma.[43],[79],[82],[83] The density of SiH_3 radical was very large in comparison with that of SiH_x (x=0-2) radical and the contribution of SiH_3 radical to the film formation was the dominant in the RF SiH_4 plasma. This was also reported by the radical separation technique using the long lifetime of SiH_3 radical.[84] Moreover, the gas phase interaction is a critical step for characterizing the network structure, that is, the quality of a-Si:H films.[85]

Ring down cavity spectroscopy is a very sensitive techniques for absolute density measurements.[86],[87] The advantages of this technique is easy for absolute density measurement without calibration and very sensitive due to multiple reflection using high reflectivity mirrors.

The diagnostics of SiF_4 plasma have hardly been reported systematically. The detection of SiF and SiF_2 radicals has been developed using laser-induced fluorescence,[88]-[94] ultraviolet absorption spectroscopy,[95],[96] and infrared absorption spectroscopy techniques.[97]-[100] The spatial distribution of SiF_2 and SiF_4 densities in ECR plasma has been only reported systematically in the SiF_4 plasma.[94] It is important to clarify the radical composition in the SiF_4 plasma, and hereby the precise control of SiF_4 based plasma process will be performed. Therefore, it is necessary to measure the radical density and radical temperature in the SiF_4 plasma.

The Si atom in SiH_4 and SiF_4 based plasma processes play an important role for the film formation, because the Si atom is one of very reactive species with the high loss probability in the gas phase and surface. For example, Yamamoto *et al* reported that the contribution of Si atom to the thin-film formation was about 3.3 times as large as that of SiH_3 radical in the ECR SiH_4/H_2 plasma.[79] Therefore, the contribution of Si atom to the thin film formation is very large. In the UVAS, the measuring devices using incoherent light source is simple compared with that using laser light sources such as IRLAS and LIF. The radical temperature of Si atom can be also measured by UVAS employing a ring dye laser. The measurement of Si atom is indispensable because it is easy to measure the absolute density and translational temperature of Si atoms by UVAS, thereby these results will give a lot of important information of plasma chemistry and effect on the Si contained-plasma process.

1.6 Purpose and composition of this thesis

The purpose of the research work presented in this thesis is to clarify the effect of excitation frequency on the contribution of the thin-film formation in the VHF-CCP employing SiF_4 or SiH_4 gases. For this purpose, the density and the temperature of the neutral radicals are systematically measured by ultraviolet absorption spectroscopy (UVAS), infrared diode laser absorption spectroscopy (IRLAS), laser-induced fluorescence (LIF). In this thesis, the behavior of Si atom was much focused on, because the absolute density and radical temperature of Si atom can be measured easily and the radical temperature gives a lot of important information of plasma chemistry.

The composition of this thesis is as follows:

Chapter 2 The principle and procedures for plasma diagnostics are described. Ultraviolet absorption spectroscopy (UVAS), infrared diode laser absorption spectroscopy (IRLAS), laser-induced fluorescence (LIF), actinometric optical emission spectroscopy (AOES), microwave interferometer, double probe, and pyrometer were used in this study. Experimental apparatus is also described in this chapter.

Chapter 3 The densities of Si, SiF, SiF_2 radicals and SiF_4 molecule in the VHF 60 MHz SiF_4 CCP by IRLAS, LIF, and UVAS were measured and clarified the radical composition. The production and loss processes of these species are discussed from these results and electron density and electron temperature. Optical emission of Ar and He were also measured as an actinometer. The spatial distribution of SiF and SiF_2 radicals, and SiF_4 molecule densities were measured by IRLAS and LIF, respectively. Measuring spatial distribution of gas species is useful for the clarification of film formation mechanisms and improvement of uniform film deposition and etching.

Chapter 4 The absolute density and translational temperature of Si atom and SiF_4 molecule in VHF 27 or 60 MHz SiF_4 CCP by UVAS and IRLAS are measured. The production and loss processes of Si atom are discussed on the basis of these measured results together with electron density and electron temperature. Moreover, the mechanism of translational temperature of Si atom is also discussed focusing on the effect of the excitation frequency. The effect of the excitation frequency on the density

and translational temperature of Si atom are discussed.

Chapter 5 The behaviors of absolute densities and translational temperatures of Si atoms in VHF SiH_4 CCP diluted with Ar, N_2, and H_2 gases were investigated by using UVAS with a ring dye laser and a hollow cathode lamp. The effects of the excitation frequency and dilution gas on the absolute densities and translational temperatures of Si atoms are discussed.

Chapter 6 In order to clarify correlations between the behavior of Si atom and the deposition rate, the estimation of the contribution of Si atom to the film deposition is calculated by using the flux of Si atom and SiH_3 radical to the substrate. Moreover, the effect of excitation frequency is investigated for the film deposition.

Chapter 7 The results in the present study and prospects for future are summarized.

Reference for chapter 1

[1] L. B. Rothman, J. Electrochem. Soc., **127,** 2216 (1980).

[2] J. A. Lange, J. Vac. Sci. Technol., **B6**, 1963 (1988).

[3] M. J. Shapiro, S. V. Nguyen, T. Matsuda, and D. Dobuzinsky, Thin Solid Films, 270, **503** (1995).

[4] T. Usami, K. Shimokawa, and M. Yoshimaru, Jpn. J. Appl. Phys., **33**, 408 (1994).

[5] T. Sakurai, IEEE Trans. Electron Devices, **40**, 118 (1993).

[6] Y. S. Kim, P. T. C. Wei, G. R. Tynan, R. Charatan, and D. Hemker, Jpn. J. Appl. Phys., **37**, 327 (1998).

[7] Y. Wu and G. Lucovsky, IEEE Electron Device Lett., **19** 367 (1998).

[8] K. Muraoka, K. Kurihara, N. Yasuda, and H. Satake, J. Appl. Phys., **94** 2038 (2003).

[9] W. E. Spear and P. G. Comber, Solid State Commun., **17**, 1193 (1975).

[10] D. L. Staebler and C. R. Wronski, Appl. Phys. Lett., **31**, 292 (1977).

[11] C. H. J. Van den Brekel and L. J. M. Bollen, J. Cryst. Growth., **54**, 310 (1981).

[12] M. K. Hatalis and D. W. Greve, J. Appl. Phys., **63**, 2260 (1987).

[13] R. B. Iverson and R. Reif, J. Appl. Phys., **62**, 1675 (1987).

[14] Y. Masaki, P. G. LeComber, and A. G. Fitzgerald, J. Appl. Phys., **74**, 129 (1993).

[15] H. Kuriyama, T. Nohda, Y. Aya, T. Kuwahara, K. Wakisaka, S. Kiyama, and S. Tsuda, Jpn. J. Appl. Phys., **33**, 5657 (1994).

[16] K. Shimizu, O. Sugiura, and M. Matsumura, IEEE Trans. Electron Decices., **40**, 112 (1993)

[17] T. Sameshima, M. Hara, and S. Usui, Jpn. J. Appl. Phys., **28**, 1789 (1989).

[18] A. T. Voutsas, Jpn. J. Appl. Phys., **37**, 388 (1998).

[19] M. Hori and T. Goto, Appl. Surf. Sci., **192**, 135 (2002).

[20] S. Miyake, *Ouyou Buturi*, **70**, 460 (2001).

[21] H. Sugai, *Ouyou Buturi*, **70**, 398 (2001).

[22] M. Surenda and D. B. Graves, Appl. Phys. Lett., **59**, 2091 (1991).

[23] M. J. Colgen, M. Meyyappan, and D. E. Murnick, Plasma Sources Sci. Technol., **3**, 181 (1993).

[24] M. Fivaz, S. Brunner, W. Schwarzenbach, A. A. Howling, and Ch. Hollenstein, Plasma Sources Sci. Technol., **4**, 373 (1995).

[25] C. Benecking, J. Appl. Phys., **68**, 4461 (1990).

[26] T. Kitamura, N. Nakano, T. Makabe, and Y. Yamaguchi, Plasma Sources Sci. Technol., **2**, 40 (1993).

[27] M. Moisan, C. Barbeau, R. Claude, C. M. Ferreira, J. Margot, J. Paraszczak, A. B. Sa, G. Sauve, and M. R. Wertheimer, J. Vac. Sci. Technol., **B9**, 8 (1991).

[28] K. M. Kalpakjian, M. A. Lieberman, and W. G. Oldham, J. Vac. Sci. Technol., **B12**, 1351 (1994).

[29] A. Koshiishi, M. Tomoyasu, Y. Tahara, and M. Kojima, *Proc. 19th Symposium on Dry Process*, Tokyo, 1998, p. 229.

[30] A. A. Howling, J. L. Dorier, Ch. Hollenstein, U. Kroll, and F. Finger, J. Vac. Sci. Technol., **A10**, 1080 (1992).

[31] M. Takai, T. Nishimoto, T. Nakagi, M. Kondo, and A. Matsuda, J. Non-Crystalline Solid, **266-269**, 90 (2000).

[32] F. Finger, U. Kroll, V. Viret, A. Shah, W. Beyer, X. -M. Tang, J. Weber, A. Howling, and Ch. Hollenstein, J. Appl. Phys., **71**, 5665 (1992).

[33] M. Heintze, R. Zedlitz, and G. H. Bauer, J. Phys., **D26**, 1781 (1993).

[34] F. Finger, P. Hapke, M. Luysberg, R. Carius, H. Wagner, and M. Scheib, Appl. Phys. Lett., **65**, 2588 (1994).

[35] J. Meier, R. Fluckiger, H. Keppner, and A. Shah, Appl. Phys. Lett., **65**, 860 (1994).

[36] D. L. Flamm, J. Vac. Sci. Technol., **A4**, 729 (1986).

[37] J. Dutta, U. Kroll, P. Chabloz, A. Shah, A. A. Howling, J.-L. Dorier, and Ch. Hollenstein, J. Appl. Phys., **72**, 3220 (1992).

[38] S. Oda, Plasma Sources Sci. Technol., **2**, 26 (1993).

[39] E. Abdel-Fattah and H. Sugai, Appl. Phys. Lett., **83**, 1533 (2003).

[40] R. C. Reid, J. M. Prausnitz, and T. K. Sherwood, *The Properties of Gases and Liquids* (McGraw-Hill, New York, 1977).

[41] B. Chapman, Glow Discharge Processes, *Sputtering and Plasma Etching* (wiley, New York, 1980).

[42] V. M. Donnelly and M. V. Malyshev, Appl. Phys. Lett., **77**, 2467 (2000).

[43] N. Itabashi, K. Kato, N. Nishiwaki, T. Goto, C. Yamada, and E. Hirota, Jpn. J. Appl. Phys., **28**, L325 (1989).

[44] T. A. Cieiand and D.W. Hess, J. Appl. Phys. **64**, 1068 (1988).

[45] M. Haverlag, F. J. de Hoog, and G. M. W. Kroesen, J. Vac. Sci. Technol., **A9**, 327 (1991).

[46] M. Magane, N. Itabshi, N. Nishiwaki, T. Goto, C. Yamada, and E. Hirota, Jpn. J. Appl. Phys., **29**, L829 (1990).

[47] K. Maruyama, A. Sakai, and T. Goto, J. Phys., **D26**, 199 (1993).

[48] G. P. Davis, and R. A. Gottscho, J. Appl. Phys., **54**, 3080 (1983).

[49] M. Oshima, Jpn. J. Appl. Phys., **17**, 1157 (1978).

[50] A. Chelouah, E. Marode, G. Hartmann, and S. Achat, J. Phys., **D27**, 940 (1994).

[51] R. A. Potter and W. R. Harshbarger, J. Electrochem. Soc., **126**, 460 (1979).

[52] E. M. van Veldhuizen, T. H. J. Bisschops, E. J. W. van Vliembergen, and H. M. C. van Wolput, J. Vac. Sci. Technol., **A3**, 2205 (1985).

[53] B. A. Cruden, M. V. V. S. Rao, S. P. Sharma, and M. Meyyappan, J. Appl. Phys., **91**, 8955 (2002).

[54] M. W. Kiehlbauch and D. B. Graves, J. Appl. Phys., **89**, 2047 (2001).

[55] M. Haverlag, E. Stoffels, W. W. Stoffels, G. M. W. Kroesen, and F. de Hoog, J. Vac. Sci. Technol., **A14**, 380 (1996).

[56] M. Hiramatsu, M. Sakakibara, M. Mushiga, and T. Goto, Meas. Sci. Technol., **2**, 1017 (1991).

[57] T. Tanaka, M. Hiramatsu, M. Nawata, A. Kono, and T. Goto, J. Phys., D **27**, 1660 (1994).

[58] G. A. Hebner, J. Appl. Phys., **80**, 2624 (1996).

[59] T. Nakano, N. Sadeghi, and R. A. Gottscho, Appl. Phys. Lett., **58**, 458 (1991).

[60] A. Kono, S. Hirose, K. Kinoshita, and T. Goto, Jpn. J. Appl. Phys., **37**, 4588 (1998).

[61] V. M. Donnelly, J. Appl. Phys., **79**, 9353 (1996).

[62] H. Singh, J. W. Coburn, and D. B. Graves, J. Vac. Sci. Technol., **A14**, 380 (1996).

[63] K. Nakahata, K. Ro, A. Suematsu, T. Kamiya, C. M. Fortmann, and I. Shimizu, Jpn. J. Appl. Phys., **39**, 3294 (2000).

[64] K. Koyanagi, K. Kishimoto, T. Huo, A. Matsumoto, N. Okada, N.Sumihiro, and H. Gomi, Jpn. J. Appl. Phys., **39**, 1091 (2000).

[65] H. Ohta, A. Nagashima, M. Hori, and T. Goto, J. Appl. Phys., **89**, 5083 (2001).

[66] W. Huang, X. Wang, M. Sheng, L. Xu, F. Stubhan, L. Luo, T. Feng, X. Wang, F. Zhang, and S. Zou, Materials Science and Engineering, **B98,** 248 (2003).

[67] H. Ohta, M. Hori, and T. Goto, J. Appl. Phys., **90**, 1955 (2001).

[68] G. Cunge, P. Chabert, and J. P. Booth, Plasma sources Sci, Technol., **6**, 349 (1997).

[69] G. A. Hebner, Appl. Surf. Sci., **192**, 161 (2002).

[70] Y. Takubo, Y. Takasugi, and M. Yamamoto, J. Appl. Phys., **64**, 1050 (1988).

[71] F. J. Kampas and R. W. Griffith, J. Appl. Phys., **52**, 1285 (1981).

[72] A. Kono, N. Koike, K. Okuda, and T. Goto, Jpn. J. Appl. Phys., **32**, L543 (1993).

[73] Y. Matsumi, T. Hayashi, H. Yoshikawa, and S. Komiya, J. Vac. Sci. Technol., **A4**, 1786 (1986).

[74] H. Nomura, K. Akimoto, A. Kono, and T. Goto, J. Phys., **D28**, 1977 (1995).

[75] Y. Nozaki, K. Kongo, T. Miyazaki, M. Kitazoe, K. Horii, H. Umemoto, A, Masuda, and H. Matsumura, J. Appl. Phys., **88**, 5437 (2000).

[76] N. Abramzon, K. E. Martus, and K. Becker, J. Chem. Phys., **113**, 2250 (2000).

[77] A. Kono, N. Koike, H. Nomura, and T. Goto, Jpn. J. Appl. Phys., **334**, 307 (1995).

[78] A. Kono, S. Hirose, and T. Goto, Jpn. J. Appl. Phys., **38**, 4389 (1999).

[79] Y. Yamamoto. H. Nomura, T. Tanaka, M. Hiramatsu, M. Hori, T. Goto, Jpn. J. Appl. Phys., **33**, 4320 (1994).

[80] M. Sakakibara, M. Hiramatsu, and T. Goto, J. Appl. Phys., **69**, 3467 (1991).

[81] Y. Yamamoto. S. Suganuma, M. Ito, M. Hori, T. Goto, Jpn. J. Appl. Phys., **36**, 4664 (1997).

[82] H. Nomura, A. Kono, and T. Goto, Jpn. J. Appl. Phys., **33**, 4165 (1994).

[83] N. Itabashi, Dr. Thesis, Nagoya University (1991).

[84] A. Matsuda and K. Tanaka, J. Appl. Phys., **60**, 2351 (1986).

[85] G. Ganguly and A. Matsuda, J. Non-Cryst. Solids, **164/166**, 31 (1993).

[86] W. M. M. Kessels, J. P. M. Hoefnagels, M. G. H. Boogaarts, D. C. Schram, and M. C. M. van de Sanden, J. Appl. Phys., **89**, 2065 (2001).

[87] W. M. M. Kessels, A. Leroux, M. G. H. Boogaarts, J. P. M. Hoefnagels, M. C. M. van de Sanden, and D. C. Schram, J. Vac. Sci. Technol., **A19**, 467 (2001).

[88] G. A. Hebner, Appl. Surf. Sci., **192**, 161 (2002).

[89] G. Cunge, P. Chabert, and J. P. Booth, Plasma Sources Sci. Technol., **6**, 349 (1997).

[90] Y. Matsumi, S. Toyoda, T. Hayashi, M. Miyamura, H. Yoshikawa, and S. Komiya, J. Appl. Phys., **60**, 4102 (1986).

[91] C. W. Watson and K. G. McKendrick, Chem. Phys., **187**, 87 (1994).

[92] S. Vanhaelemeerch, J. Van Hoeymissen, D. Vermeylen, and J. Peeters, J. Appl. Phys., **70**, 3892 (1991).

[93] A.C. Stanton, A. Freedman, J. Worthhoudt, and P. P. Gasper, Chem. Phys. Lett., **122**, 190 (1985).

[94] M. Nakamura, M. Hori, T. Goto, M. Ito, and N. Ishii, Jpn. J. Appl. Phys., **40**, 4730 (2001).

[95] J. P. Booth, G. Cunge, F. Neuilly, and N. Sadeghi, Plasma Sources Sci. Technol., **7**, 423 (1998).

[96] V. M. Khanna, G. Besenbruch, and J. L. Margrave, J. Chem. Phys., **46**, 2310 (1967).

[97] T. Tanaka, M. Tamura, and K. Tanaka, J. Mol. Struct., **413-414**, 153 (1997).

[98] K. Tanaka, Y. Akiyama, and T. Tanaka, J. Mol. Spectrosc., **137**, 55 (1989).

[99] G. L. Caldow, C. M. Deeley, P. H. Turner, and I. M. Mills, Chem. Phys. Lett., **82**, 434 (1981).

[100] K. Sugawara, F. Ito, T. Nakanaga, and H. Takeo, Chem. Phys. Lett., **232**, 561 (1995).

Chapter 2

Experimental apparatus and plasma diagnostics techniques

2.1 Experimental Apparatus

Figure 2-1 shows the cross-sectional view of the VHF-CCP chamber. The plasma chamber is rectangular parallelepiped, with an internal side of 54 cm in length for laser pass direction, which is specially designed for the IRLAS without White-type multiple reflection cell (single-path IRLAS) and LIF measurements.

The VHF power with the excitation frequency of 27 MHz or 60 MHz was applied to the upper electrode. The electrode was 25 cm in diameter. The electrode gap was 2.5 cm. The plasma chamber was configured for an 8-inch wafer. The Si wafer was placed on a substrate holder with water backside cooling during measurements for keeping the distribution of substrate temperature uniformly.

Process gases were supplied into the plasma chamber through a showerhead. Therefore, the plasma processes are performed on the 8-inch wafer with high-uniformity. The base pressure was of the order of 10^{-6} Torr. The chamber was exhausted by two turbomolecular pumps (1200 *l*/s each) and a rotary pump.

The radical traps were set around the beam pass windows to prevent radicals generated in the plasma from depositing on the beam pass windows. The deposition of radicals on the windows causes the decrease of laser intensity that leads to the decrease of the sensitivity of the measurements.

The optical system for UVAS, IRLAS, and LIF used in this study is shown in **Figure 2-2.** The guiding laser system consisted of eight small fixed mirrors and a rotational mirror. The laser beam was first reflected by the rotational mirror. By rotating the mirror, the laser beams were directed to one of the fixed mirrors, thereby passing through the

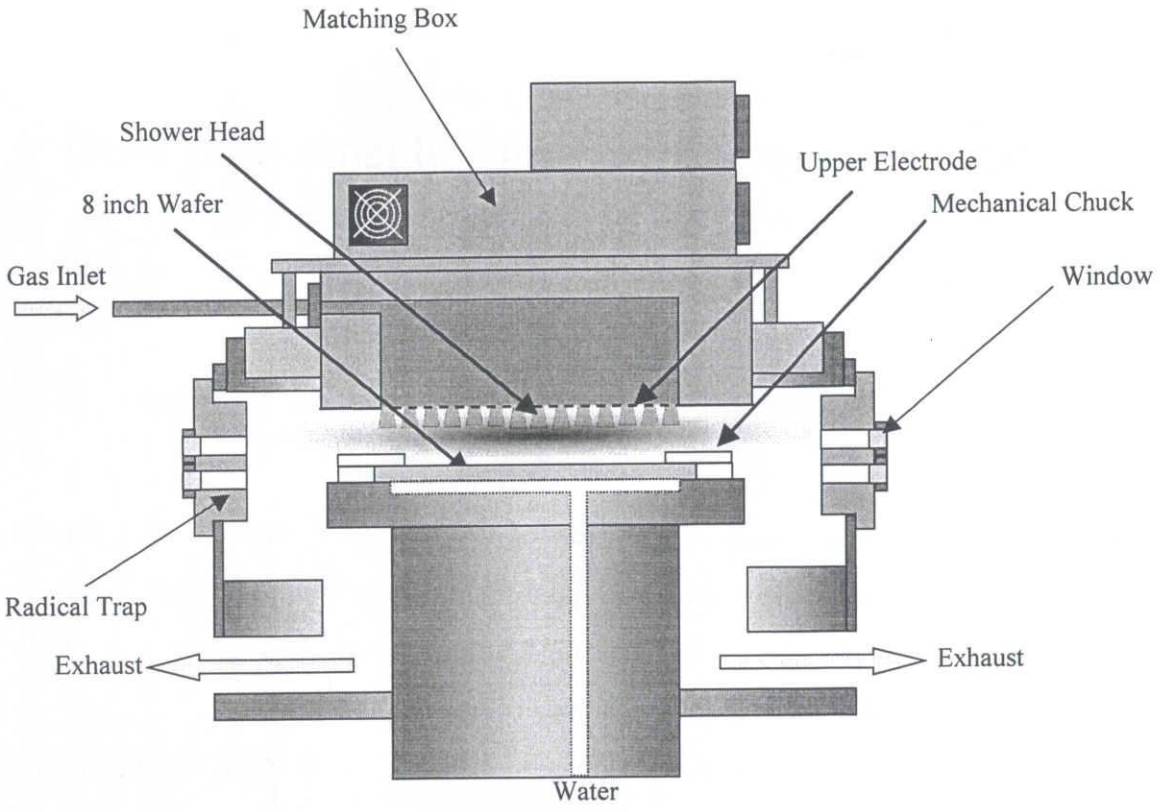

Figure 2-1 Very high frequency capacitively coupled plasma apparatus.

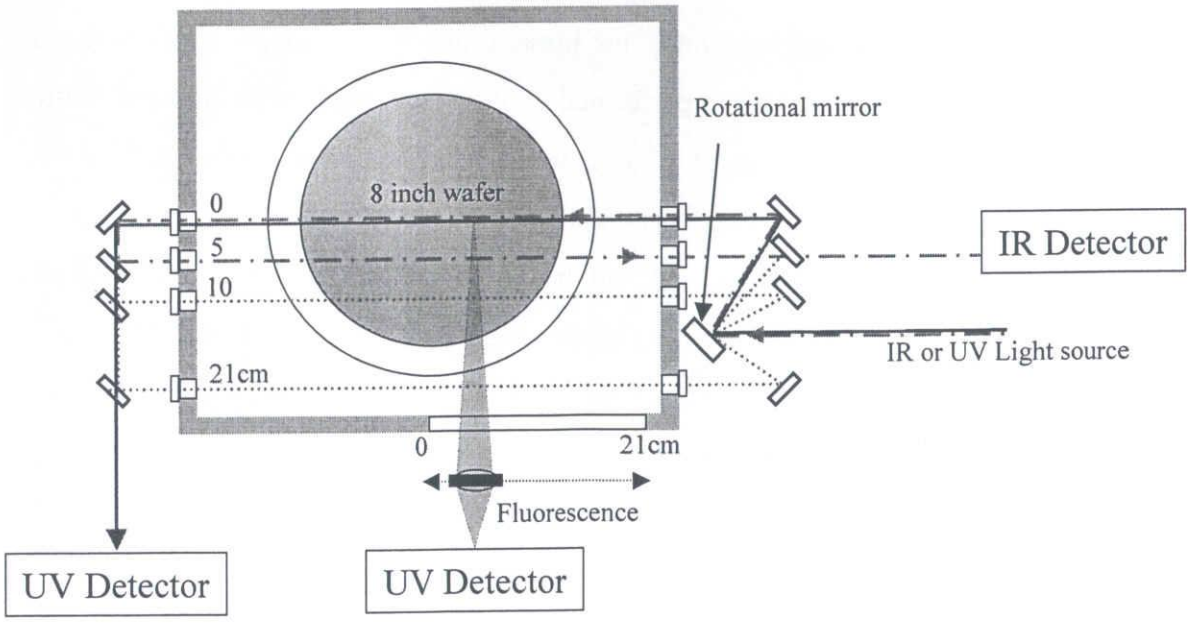

Figure 2-2 Optical system for IRLAS, UVAS, and LIF.

plasma chamber 1 cm above the substrate. The entrance and exit windows made by NaCl for the infrared laser beam and quartz for the ultraviolet light was attached at the chamber wall. The diameter of the laser beam was about 3 mm. The location of the beam path could be varied anywhere from the center of the chamber to the vicinity of the chamber wall. In the IRLAS and UVAS measurement, the IR or UV light source was detected by the IR or UV detector through the chamber. In the LIF measurement, the fluorescence was collected with a lens from the direction perpendicular to the laser beam axis and was focused on the UV detector.

Theory

[Electron density]

Figure 2-3 shows the basic homogeneous model of the CCP.[1],[2] The plasma is generated between the electrodes *a* and *b*. The electrodes are separated by a distance l and each has a cross sectional area A. The plasma density between the electrodes is n_g. The voltage and sinusoidal current between the electrodes are $V_{rf}(t)$ and $I_{rf}(t)$, respectively. It is assumed $n_e = n_i = n$ due to quasineutrality in the bulk plasma region except within the oscillating sheaths near the electrodes. The instantaneous sheath thickness is $s_a(t)$ and its time-averaged value is s_0.

The electric field within sheath a is given by Poisson's equation,

$$\frac{dE}{dx} = \frac{en}{\varepsilon_0} \qquad x \le s_a(t), \tag{2-1}$$

which on integration yields

$$E(x,t) = \frac{en}{\varepsilon_0}[x - s_a(t)]. \tag{2-2}$$

The displacement current flowing through sheath a into the plasma is

$$I_{rf}(t) = \varepsilon_0 A \frac{\partial E}{\partial t}. \tag{2-3}$$

Substituting eq. (2-2) in eq. (2-3), we obtain

$$I_{rf}(t) - enA\frac{ds_a}{dt}. \tag{2-4}$$

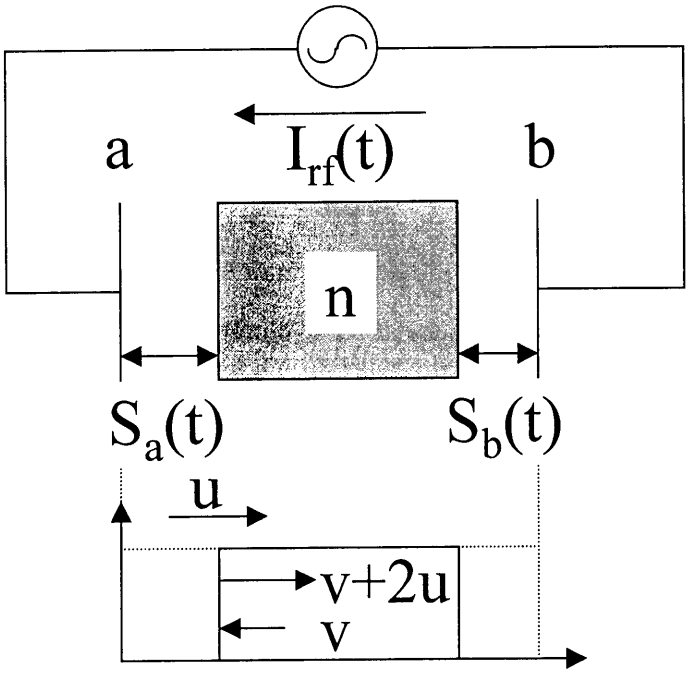

Figure 2-3 Homogeneous model.

From eq. (2-4), the sheath boundary s_a oscillates linearly with the applied current. Setting $I_{rf} = I_1 \cos \omega t$, we integrate eq. (2-4) to obtain

$$s_a = s_0 - s_0 \sin \omega t, \tag{2-5}$$

where

$$s_0 = \frac{I_1}{en\omega A}, \tag{2-6}$$

is the sinusoidal oscillation amplitude about the dc value s_0. The voltage across the sheath is given by

$$V_{ap}(t) = \int_0^{s_a} E \, dx = -\frac{en}{\varepsilon_0} \frac{s_a^2}{2}. \tag{2-7}$$

Substituting eq. (2-5) in eq. (2-7), we obtain

$$V_{ap}(t) = -\frac{en}{2\varepsilon_0} s_0^2 (1 - \sin \omega t)^2. \tag{2-8}$$

Similarly for sheath b, in the addition to the relation of $s_a + s_b = 2s_0$, we obtain

$$V_{bp}(t) = -\frac{en}{2\varepsilon_0} s_0^2 (1 + \sin \omega t)^2. \tag{2-9}$$

Although V_{ap} and V_{bp} are nonlinear as described in eq. (2-8) and eq. (2-9), the combined voltage $V_{ab} = V_{ap} - V_{bp} = V_{rf}$ across both sheaths is

$$V_{rf} = \frac{ens_0}{\varepsilon_0}(s_b - s_a) = \frac{2ens_0^2}{\varepsilon_0} \sin \omega t, \tag{2-10}$$

which is a linear voltage response. I and V are defined by current density from eq. (2-6) and amplitude of voltage from eq. (2-10), we obtain

$$I = en\omega s_0, \tag{2-11}$$

$$V = \frac{2en}{\varepsilon_0} s_0^2. \tag{2-12}$$

Next, it is considered about the power transferred to the electron by the sheath. Electron reflecting from the large accelerating fields of a moving high-voltage sheath can be approximated by assuming the reflected velocity is $v + 2u$ which occurs in an elastic collision of a ball with a moving wall to right side as shown in **Fig. 2-3**. v is the reflected electron velocity parallel to the time-varying electron sheath velocity u. On the

other hand, the electron with the velocity of $v-2u$ is reflected by the collision with the moving wall to left side. Here, the oscillation velocity at the sheath edge is $\frac{\mathrm{d}s_a}{\mathrm{d}t}=-\omega s_0\cos\omega t$, and this amplitude is ωs_0. The power density transferred to the electron was estimated by the stochastic average of the electron velocity assuming the Maxwellian distribution function,

$$P_{abs}=2mu_0^2\int_0^\infty vf(v)\mathrm{d}v=2mu_0^2\frac{1}{4}n\bar{v}=\frac{1}{2}mu_0^2n\bar{v}, \tag{2-13}$$

$$u_0=\omega s, \tag{2-14}$$

$$\bar{v}=\left(\frac{8eT_e}{\pi m}\right)^{\frac{1}{2}}. \tag{2-15}$$

The power absorbed by the plasma is equal to the sum with the collisional energy loss and the kinetic energy loss to the wall by electrons and ions,

$$P_{abs}=nu_BE_T. \tag{2-16}$$

$u_B=\left(\frac{eT_e}{M}\right)^{\frac{1}{2}}$, $E_T=E_c+E_e+E_i$ is the sum of collisional energy loss by electrons and ions,

$$n=\frac{mV\varepsilon_0\bar{v}^2}{4eu_BE_T}\omega^2. \tag{2-17}$$

Here, V, u_B, E_T, and v are a function of the electron temperature. The electron temperature is a function of the excitation frequency. Therefore, the electron density is a function of the excitation frequency and proportional to the square of the frequency.

[Sheath thickness]

The sheath thickness is expressed by

$$s=\left(\frac{2\varepsilon_0V}{en_s}\right)^{\frac{1}{2}}, \tag{2-18}$$

where n_s is the density at the plasma-sheath edge. Substituting eq. (2-17) in eq. (2-18), we obtain

$$s = \sqrt{\frac{2u_B E_T}{m\bar{v}^2}}\omega^{-1}. \tag{2-19}$$

Therefore, the sheath thickness is a function of the excitation frequency.

[Electron energy distribution function]

A cut off - density N_c, that is the density which the electron plasma frequency coincides with the excitation frequency, is expressed as follows,

$$\omega_{pe}[\mathrm{Hz}] = 8.98\sqrt{N_c[\mathrm{m}^{-3}]}, \tag{2-20}$$

where ω_{pe} is the plasma frequency.

Generally, in the range of $N_e > N_c$, when an electromagnetic wave is exposed to the plasma, the wave will be reflected at the plasma surface and possibly penetrate into the plasma only in skin depth (skin effect). Therefore, the wave heats the electrons at the plasma surface (surface heating). On the other hand, in the range of $N_e < N_c$, the wave penetrates into the bulk plasma, the electrons are heated in the whole plasma (bulk heating).

The transition of electron heating mode from bulk heating (high T_e, low N_e) to surface heating (low T_e, high N_e) is discussed at relatively high pressures (0.1~3 Torr) in the RF CCP.[3] In the RF discharges, the bulk heating mode corresponds to the α mode discharge having low electron density with high electron temperatures (~4 eV). On the other hand, the surface heating mode corresponds to the γ mode discharge or the discharge mode driven by the RF oscillating sheath, both having high electron density with low electron temperatures (0.3~1eV).[4] In the non-local regime, where the electron energy relaxation length is larger than the plasma length,[5] the majority of the electrons in the plasma bulk region are confined in the ambipolar dc potential well (φ_W) as shown in **Fig. 2-4(a)**. In the bulk heating case, all electrons are directly and continuously heated in the bulk region as shown in **Fig. 2-4 (b)**, thus the electron temperature becomes high. In the surface heating case, however, only a small group of high-energy electrons is accessible to the heating zone of the plasma surface due to the high potential barrier. After being heated there, the hot electrons return to the bulk region, where they produce cold electrons with ionization to compensate the diffusion loss in the

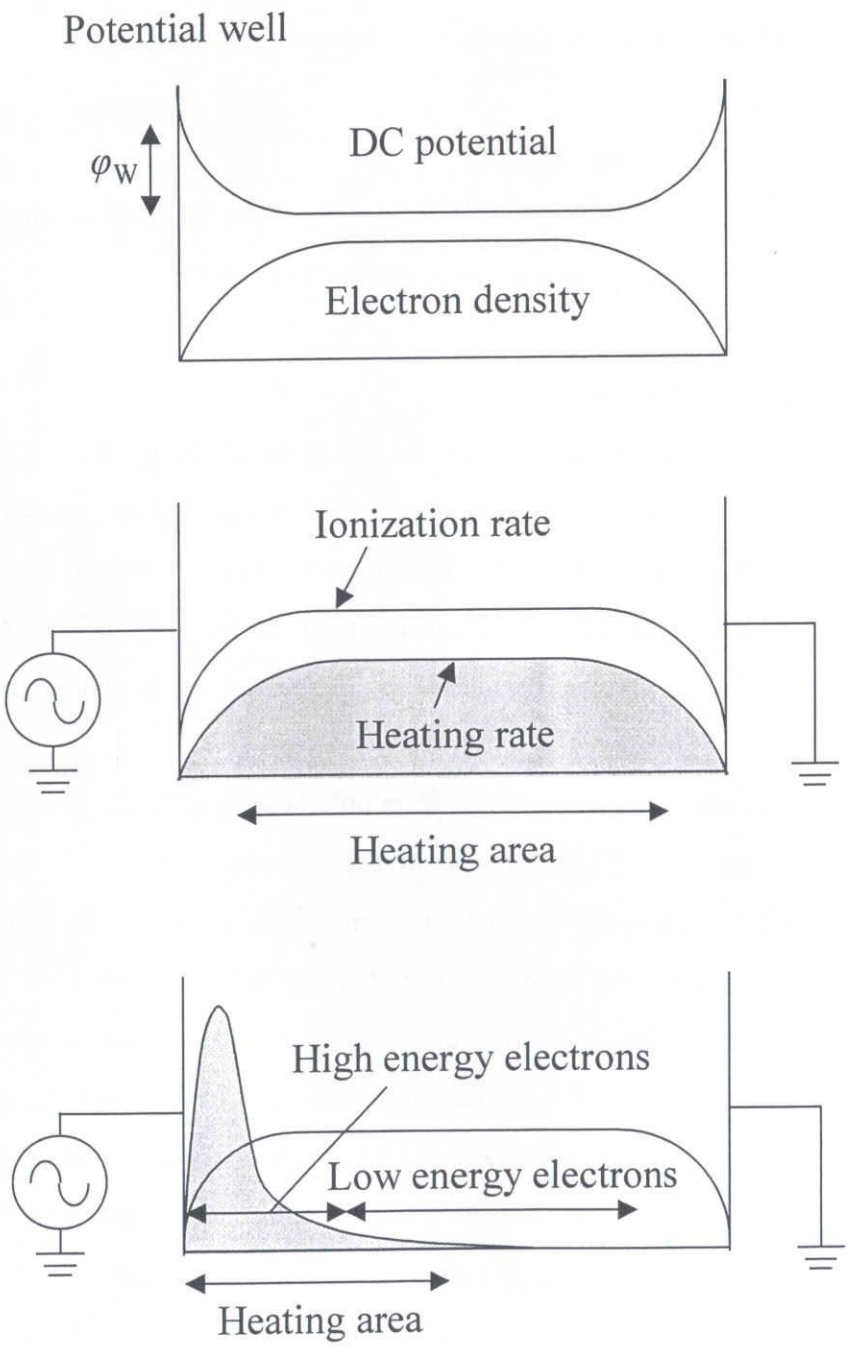

Figure 2-4 Schematic illustrations of heating mode.
(a) the distributions of the ambipolar potential well and the electron density (b) bulk heating (c) surface heating.

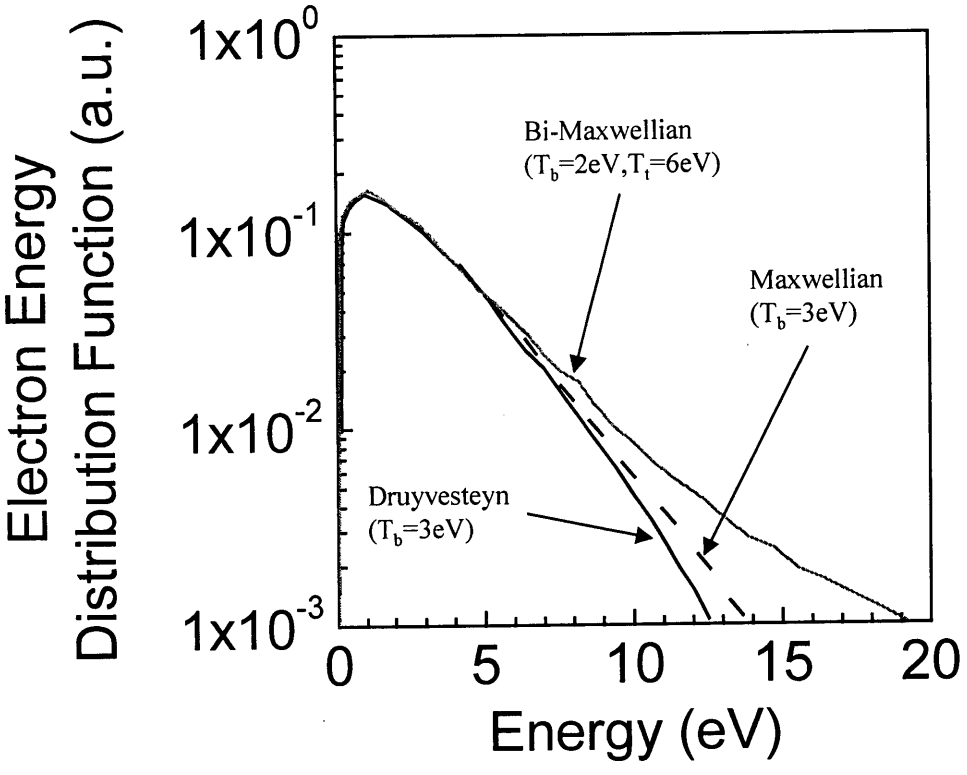

Figure 2-5 Electron energy distribution function.

steady-state. The majority of electrons remain relatively cold in the bulk region since no external heating source exists there as shown in **Fig. 2-4 (c)**. Thus, the electron energy distribution in the bulk region can be expressed as a bi-Maxwellian distribution as shown in **Fig. 2-5**. When the power is locally deposited to a high-energy fraction of energy space, the electron energy distribution function (EEDF) becomes a bi-Maxwellian type with a lower bulk temperature (T_b) and a higher tail temperature (T_t). When the power is deposited to the entire region of energy space, the EEDF becomes a single temperature type with a higher T_b (Druyvesteyn distribution).

Here, the absorbed power of electrons by the bulk heating is expressed as follows,[6]

$$P_{ohm} = \frac{e^2}{m}\frac{\nu}{\nu^2+\omega^2}\frac{E_0^2}{2}, \tag{2-21}$$

where ω is the angular frequency, ν is the electron collision frequency, and E_0 is the electric field. In the case of $\nu/\omega \ll 1$ with increasing the excitation frequency, the contribution of the bulk heating becomes small. On the other hand, the stochastic heating is assumed to be dominant due to the surface heating, the absorbed power of electron by the stochastic heating is given by eq. (2-13). This absorbed power by the stochastic heating increases with increasing the excitation frequency, that is, the contribution of the surface heating becomes large. Therefore, the EEDF becomes the bi-Maxwellian type with increasing the excitation frequency. Here, T_e measured by the Langmuir probe expresses the low-energy part of the EEDF and gives the bulk temperature. Accordingly, the bulk electron temperature becomes low with increasing the excitation frequency. However, Abdel-Fattah *et al.* reported that the surface heating is not explained enough by the stochastic heating.[7] Therefore, it is necessary to find the kinetic theory of surface heating localized strongly for the EEDF of VHF-CCP.

[Ion energy distribution function]

The ion energy distribution function is reported by models.[8],[9] A simple theory of the ion motion through the sheath leads to an expression for the ion energy distribution function (IEDF) assuming collision less positive ion sheath with the thickness d_s,

$$f(\varepsilon)=\frac{2N_e}{\omega_{RF}\Delta\varepsilon}\left[1-\frac{4}{\Delta\varepsilon^2}\left(\varepsilon-e\langle V_p\rangle\right)^2\right]^{-\frac{1}{2}}, \tag{2-22}$$

where the energy splitting $\Delta\varepsilon$ is given by

$$\Delta\varepsilon=\frac{4eV_{RF}}{3\omega_{RF}d_s}\sqrt{\frac{2e\langle V_p\rangle}{m_i}}. \tag{2-23}$$

$\langle V_p\rangle$ is the average plasma potential, V_{RF} is the RF voltage, N_e is the electron density, and m_i is the mass of ion. $\Delta\varepsilon$ decrease with increasing the excitation frequency as a consequence of the time averaging of the potential. The decrease is proportional to ω_{RF}^{-1}. Therefore, the distribution of ion energy decreases with increasing the excitation frequency and the change of the excitation frequency will much affect the film property.

As a result, the plasma density increases approximately in proportion to the square of the excitation frequency from eq. (2-17). VHF-CCP can operate at high plasma density under low-pressure condition. The sheath thickness decreases with inverse of the excitation frequency from eq. (2-19). Therefore, a higher frequency operation enables an increase in ion directionality and a reduction in ion bombardment on the substrate. Moreover, the EEDF becomes the bi-Maxwellian type with increasing the excitation frequency and the bulk electron temperature becomes low. Accordingly, VHF-CCP has much advantage in the plasma processes.

2.2 Plasma diagnostics techniques

2.2.1 Ultraviolet absorption spectroscopy

Several techniques such as absorption spectroscopy, laser induced fluorescence spectroscopy and mass spectroscopy have been applied for radical measurements. The absolute density in the ground-state can be easily derived from the measured absorption intensity using absorption spectroscopy. In this study, UVAS using a ring dye laser and hollow cathode lamp as a light source was used for measuring Si atom density.

[Ring dye laser]

The ring laser (Coherent, Model 899-21) produced tunable single-frequency radiation. The cw argon ion laser (Coherent, INNOVA, Sabre DBW-15) was used to optically pump the dye (Rhodamine 6G). The ring dye laser was equipped with the angle tuned intracavity frequency doubler (Coherent, Model 8500), producing UV radiation at a linewidth of 1 MHz and a scan width up to 60 GHz. The wavelength of the laser was tuned to 288.2 nm for detecting Si atoms with the $3p^2{}^1D_2$ level through the transition of $3p^2{}^1D_2$ - $3p4s{}^1P_1$. The absorption profile of the 288.2 nm line was obtained directly by scanning the laser wavelength. The translational temperature and the absolute density of Si atoms were evaluated from the width of the absorption profile and the maximum absorption intensity, respectively.

[Hollow cathode lamp]

The light radiated from the Si hollow cathode lamp (Hamamatsu Photonics, Hollow Cathode Lamp L233) travels at 1cm above the Si substrate with a beam diameter about 3 mm in the chamber. UVAS using hollow cathode lamp as a light source is the most simple in these methods. The Si atom densities at the $3p^2{}^1D_2$ level through the transition of the $3p^2{}^1D_2$ - $3p4s{}^1P_1$ (288.2 nm) and $3p^2{}^3P_2$ level through the transition of $3p^2{}^3P_2$ - $3p4s{}^3P_2$ (251.6 nm) were measured.

The schematic block diagram of the experimental apparatus of UVAS using a ring dye laser and a hollow cathode lamp is shown in **Figure 2-6**. The output laser beam or the light of the hollow cathode lamp was detected by a photomultiplier (PMT) through the monochromator. The electric signal from the PMT was averaged 1280 times by a personal computer. The absorption intensity is obtained by subtracting the plasma emission and the background noise from the detected signal. The light is chopped and the absorption intensity is obtained by subtracting the signal without discharge from that with discharge.

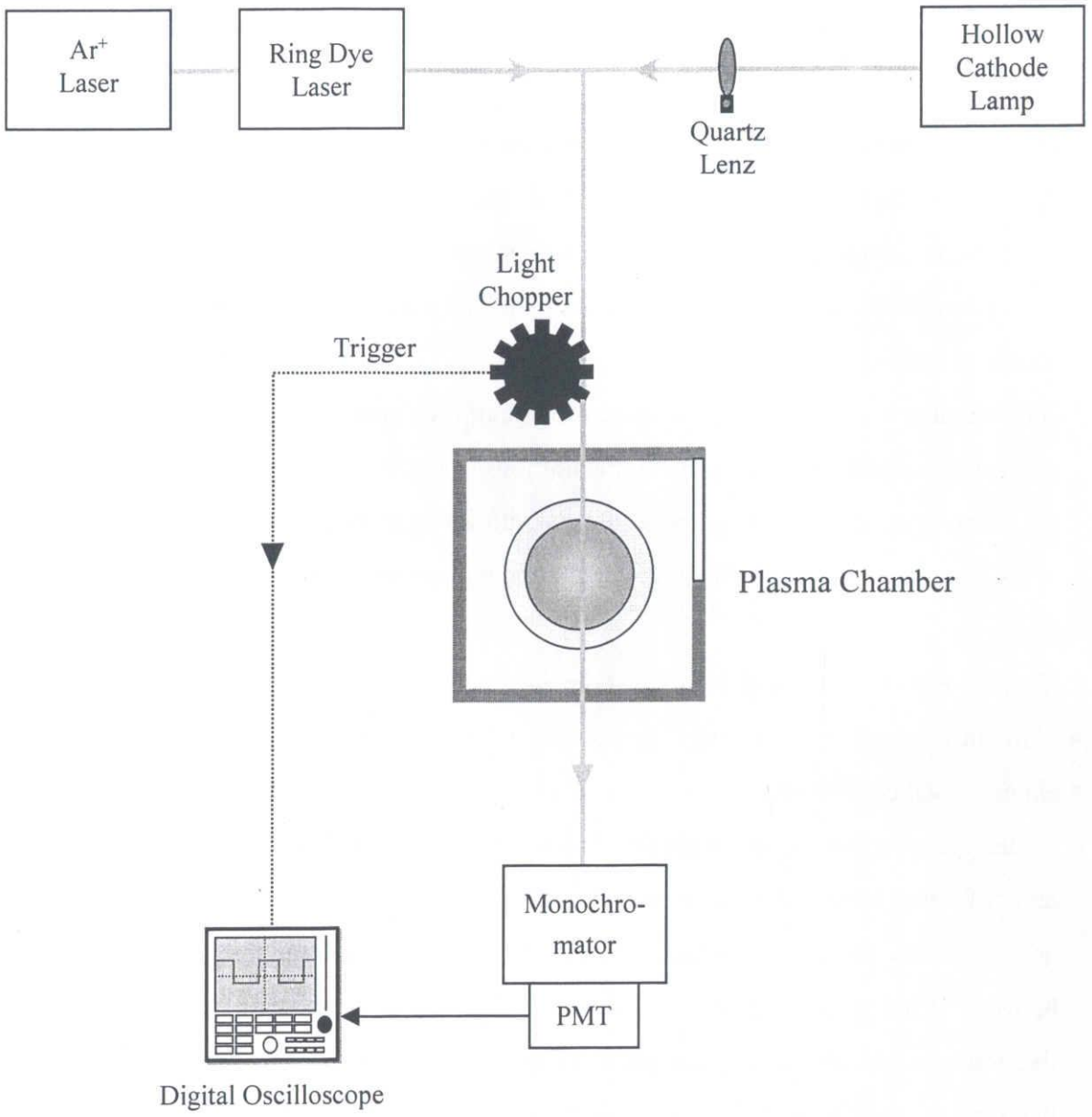

Figure 2-6 Schematic diagram of UVAS system.

Chapter 2

Theory

If the parallel light from a source passes through a absorption cell, such as plasma, the intensity of the transmitted light is given as following equation,[10]

$$I(\nu) = I_0(\nu)\exp[-k(\nu)L], \tag{2-24}$$

where ν is the frequency, $I(\nu)$ and $I_0(\nu)$ are the intensities of the transmitting light and the incident light, respectively. L and $k(\nu)$ are the absorption path length and the absorption coefficient as a function of frequency ν, respectively. The broadening of the absorption coefficient, that is, the broadening of the absorption line-profile is due to the causes as follows,

(1) Natural broadening due to the finite lifetime of the exited state.

(2) Doppler effect broadening due to the motions of the atoms.

(3) Lorentz broadening due to the collisions with foreign gases.

(4) Holtsmark broadening due to the collisions with other absorption atoms of the same kind.

(5) Stark effect broadening due to the collisions with electrons and ions.

In this study, the Doppler broadening should be taken into account in the experimental conditions.

Here, it is considered that a parallel beam of the light of frequency ν passed through a layer of atoms bounded by the planes at the length of dL. It is supposed that there are N_l normal atoms per cm^3 of which dN_l are capable of absorbing the frequency range between ν and ν+dν, and N_u excited atoms of which dN_u are capable of emitting this frequency range. Neglecting the effect of spontaneous re-emission in view of the fact that it takes place in all direction, the decrease in energy of the beam is given by

$$-[I(\nu)]\mathrm{d}\nu = \mathrm{d}N_l\,\mathrm{d}L\rho(\nu)B_{lu}h\nu - \mathrm{d}N_u\,\mathrm{d}L\rho(\nu)B_{ul}h\nu, \tag{2-25}$$

where B_{lu} and B_{ul} are Einstein B coefficient from lower state l to upper state u and from l to u, respectively. h is Planck's constant, and $\rho(\nu)$ is the radiation energy density given by $I(\nu)=c\rho(\nu)$, (c: light velocity). Rewriting eq. (2-25),

$$-\frac{1}{I(\nu)}\frac{\mathrm{d}[I(\nu)]}{\mathrm{d}L}\mathrm{d}\nu = \frac{h\nu}{c}(B_{lu}\,\mathrm{d}N_l - B_{ul}\,\mathrm{d}N_u). \tag{2-26}$$

Recognizing that the left-hand term is $k(\nu)\mathrm{d}\nu$ as defined by eq. (2-24), eq. (2-26) is

$$k(v)\,\mathrm{d}v = \frac{hv}{c}(B_{\mathrm{lu}}\,\mathrm{d}N_{\mathrm{l}} - B_{\mathrm{ul}}\,\mathrm{d}N_{\mathrm{u}}), \tag{2-27}$$

and integrating over the whole absorption line, neglecting the slight variation in v throughout the line,

$$\int k(v)\,\mathrm{d}v = \frac{hv_0}{c}(B_{\mathrm{lu}}N_{\mathrm{l}} - B_{\mathrm{ul}}N_{\mathrm{u}}), \tag{2-28}$$

where v_0 is the frequency at the center of the line. Here, we use the Einstein A coefficient,

$$\int k(v)\,\mathrm{d}v = \frac{c^2}{8\pi v_0^2}\frac{g_{\mathrm{u}}}{g_{\mathrm{l}}}AN_{\mathrm{l}}\left(1-\frac{g_{\mathrm{l}}N_{\mathrm{u}}}{g_{\mathrm{u}}N_{\mathrm{l}}}\right)$$

$$\cong \frac{c^2}{8\pi v_0^2}\frac{g_{\mathrm{u}}}{g_{\mathrm{l}}}AN_{\mathrm{l}} \qquad (N_{\mathrm{u}} << N_{\mathrm{l}}), \tag{2-29}$$

where g_{l} and g_{u} are the statical weights of the lower and upper level, respectively. Therefore, by measuring $I_0(v)$ and $I(v)$, $k(v)$ is decided and we can estimate the density N_{l}.

[Ring dye laser]

When the light source is monochromatic, the absorption coefficient is given by the following equation assuming that Doppler broadening is dominant,

$$k_{\mathrm{v}} = k_0 \exp\left\{-\left[\frac{2(v-v_0)}{\Delta v_{\mathrm{D}}}\sqrt{\ln 2}\right]^2\right\}, \tag{2-30}$$

where k_0 is the maximum absorption coefficient at line center. Δv_{D} is the Doppler width, depending only on the translational temperature T and the atomic weight M according to the formula,

$$\Delta v_{\mathrm{D}} = \frac{2}{c}\sqrt{2R\ln 2}\,v_0\sqrt{\frac{T}{M}}, \tag{2-31}$$

where c is the velocity of light and R is the gas constant. Integrating eq. (2-30) and using eq. (2-29), we obtained

$$N_l = \frac{k_0}{A}\frac{g_l}{g_u}\frac{4\pi\Delta\nu_0}{\lambda_0^2}\sqrt{\frac{\pi}{\ln 2}}. \tag{2-32}$$

Therefore, by using the measured absorption profile, the translational temperature T is obtained directly from the Doppler broadening width $\Delta\nu_D$, and the atom density N_l at the lower level is obtained easily from the measured maximum absorption coefficient k_0.

[Hollow cathode lamp]

When the light source is incoherent light such as lamp, the intensity of measured light is the integrated value over the frequency,

$$I_0 = \int e_0 f_0(\nu)\,\mathrm{d}\nu, \tag{2-33}$$

$$I_a = \int e_0 f_0(\nu)\{1-\exp[-k_0 f_a(\nu)L]\}\,\mathrm{d}\nu, \tag{2-34}$$

where I_0 and I_a are the intensities of the incident light and the absorption, respectively, $f_0(\nu)$ is the emission line-profile function for the light source, e_0 is the emission intensity of the light source at a center frequency of $f_0(\nu)$, $f_a(\nu)$ is the absorption line-profile function, and k_0 is the absorption coefficient at the center frequency of $f_a(\nu)$. The absorption intensity $A(k_0L)$ is given by the following formula,

$$A(k_0L) = 1-\frac{I_a}{I_0} = \frac{\int f_0(\nu)\{1-\exp[-k_0 f_a(\nu)L]\}\,\mathrm{d}\nu}{\int f_0(\nu)\,\mathrm{d}\nu}. \tag{2-35}$$

From $A(k_0L)$ obtained by measurement, k_0 is determined by assuming the line-profile function $f_0(\nu)$ and $f_a(\nu)$. Then, the number density of state l, N_l, is estimated by using eq. (2-35) as

$$N_l = \frac{8\pi\nu_0^2}{c^2}\frac{g_l}{g_u}\frac{1}{A}k_0\int f_a(\nu)\,\mathrm{d}\nu. \tag{2-36}$$

2.2.2 Infrared diode laser absorption spectroscopy

Most of diatomic or polyatomic molecules and radicals in process plasmas have rotation-vibration spectra in the infrared region. IRLAS is very useful tool for the plasma diagnostics. In this study, IRLAS was used for measuring SiF_4 and SiH_4 densities.

The schematic block diagram of the experimental apparatus of IRLAS is shown in **Figure 2-7**. The tunable infrared diode lasers (Laser Photonics, L5615) were used for the infrared light source. The diode laser was cooled down to less than 80 K by a closed-cycle refrigerator with a helium compressor. The oscillation frequency of the laser was adjusted roughly by controlling the operation temperature and adjusted fine by controlling the operation current of the laser. The oscillation frequency was scanned by scanning the laser current. The laser beam, which contained only a single mode after filtered with a monochromator, was split into the three parts by beam splitters (BS). One was the main beam to diagnose the plasma and others were to determine the precise wavenumber of the observed spectrum. The absorption spectrum of the reference gases was used to determine the absolute value of the wavenumber. A confocal etalon of 25 cm in length provided an interference fringe pattern with the intervals of 0.01 cm^{-1}, which was used as a relative scale. The laser beam was detected by the Mercury-Cadmium-Telluride (MCT) infrared detector. The line width of the laser was much narrower than the width of the observed spectral lines and the stability of the laser frequency was enough for the spectral line measurement. The laser current was modulated at 5 kHz for phase-sensitive detection (PSD). The signal of the reference spectrum and the interference fringes were recorded by PSD using lock-in amplifiers at twice the source modulation frequency.

The absorption wavenumber of the SiF_4 molecule was 1032.1 cm^{-1} of the v_3 band.[11] To improve the S/N ratio, a double-path IRLAS measurement was used. The absorption wavenumber of the SiH_4 molecule was 983.6 cm^{-1} of the v_2 Q-branch.[12]

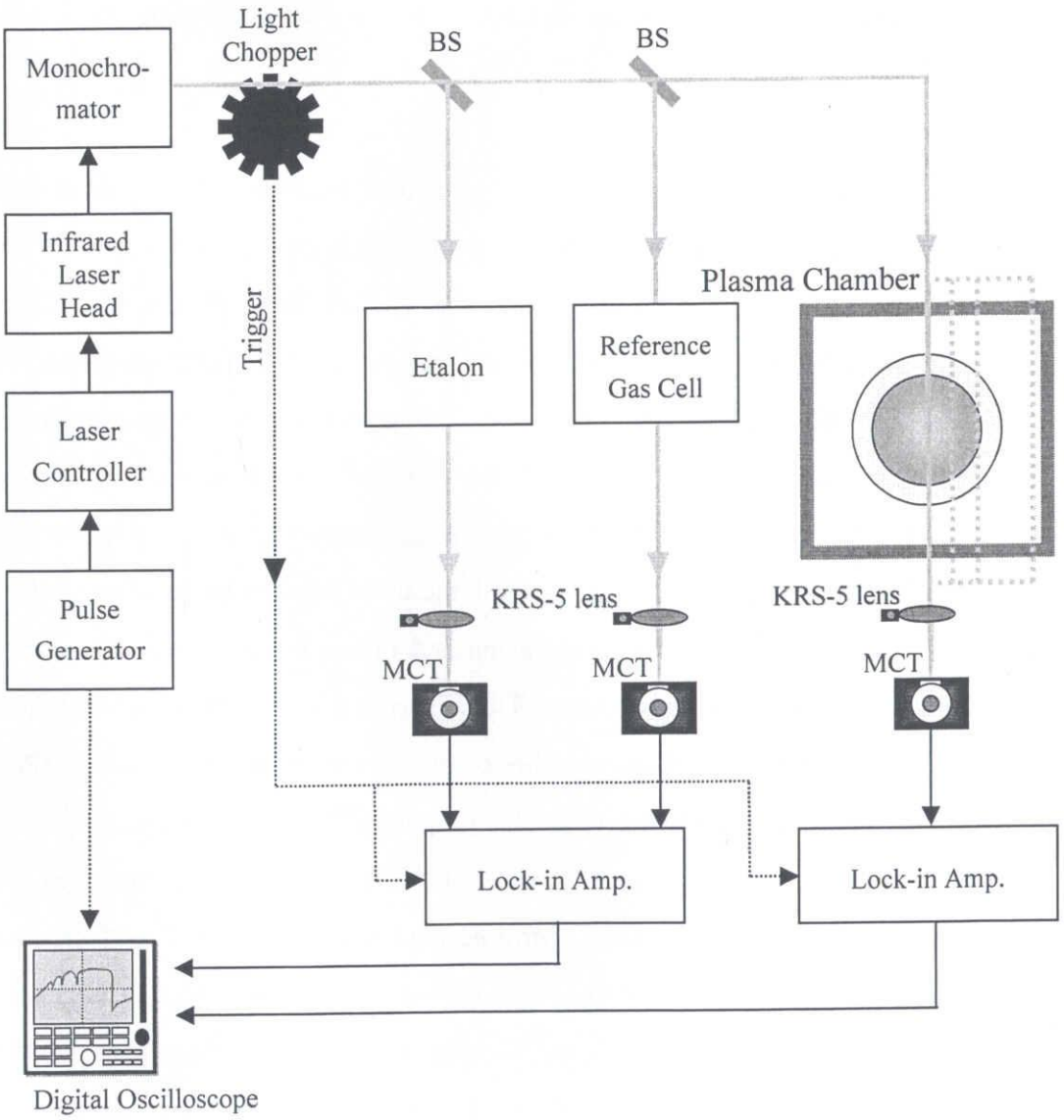

Figure 2-7 Schematic diagram of IRLAS system.

Chapter 2

Theory

The absorption coefficient $k(v)$ is derived from the following formula,

$$k(v) = -\frac{1}{L}\ln\left[\frac{I_0(v) - I_A(v)}{I_0(v)}\right], \tag{2-37}$$

where v is the wavenumber in cm^{-1}, L is the absorption path length in cm, $I_0(v)$ is the laser intensity without absorption, and $I_A(v)$ is the absorption intensity. At low pressures, $k(v)$ can be assumed to have a Doppler broadening line shape, which is given by

$$k(v) = k(v_c)\exp\left\{-\left(\frac{v - v_c}{\Delta v_D}\cdot 2\sqrt{\ln 2}\right)^2\right\}, \tag{2-38}$$

where v_c and $k(v_c)$ are the wavenumber and the absorption coefficient at the center of the absorption line profile, and Δv_D is the Doppler line width. Δv_D is given by

$$\Delta v_D = 2\frac{v_c}{c}\sqrt{2\ln 2 \cdot k_B N_A \frac{T}{M}}, \tag{2-39}$$

where c is the light velocity, k_B is the Boltzmann constant, N_A is the Avagadro's number, T is the translational temperature, and M is the molecular weight in atomic mass units. The translational temperatures are calculated from the full width at half maximum (FWHM) of each spectral profile.

The absolute density N_{total} is calculated from the absorption coefficient on the basis of the following equation,

$$N_{total} = \frac{1}{S_{line}}\int k(v)\,dv, \tag{2-40}$$

where S_{line} is the line strength. As the integrated absorption coefficient is derived using the following formula,

$$\int k(v)\,dv = \frac{1}{2}\sqrt{\frac{\pi}{\ln 2}}\Delta v_D \cdot k(v_c), \tag{2-41}$$

N_{total} could be determined by measured absorption coefficient $k(v_c)$ using eq.(2-38) as

$$N_{total} = \frac{v_c}{cS_{line}}\sqrt{2\pi k_B N_A}\sqrt{\frac{T}{M}}k(v_c). \tag{2-42}$$

If the line strength is unknown, it is determined by the relation between the line strength

and the band strength S_{band} as follows,

$$S_{line} = \frac{S_{band} \cdot g_l \cdot S_{r_l}^{r_h} \cdot \exp(-F_l ch/k_B T_r)}{Q}, \quad (2\text{-}43)$$

where g_l is the statistical weights for the lower state of transition, $S_{r_l}^{r_h}$ is the Hönl-London factor, F_l is the rotational term value for the lower state of transition, h is Plank constant, T_r is the rotational temperature, and Q is the partition function.

2.2.3 Laser induced fluorescence

LIF spectroscopy is a highly sensitive method with high time and spatial resolutions for detecting radicals, though it requires the calibration procedure if the absolute radical density is needed. In this study, LIF was used for measuring SiF and SiF_2 densities.

The schematic block diagram of the LIF measurement is shown in **Fig. 2-6**. The laser system used for the LIF measurements consisted of a pulsed dye laser (Quanta Ray PDL-2) pumped with a frequency doubled Nd:YAG laser (Quanta Ray DCR-3), with crystals for output wavelength conversion (Quanta Ray WEX-1). The dyes used for the SiF and SiF_2 detection were Rhodamine 610 and LDS 698, respectively. The repetition frequency of the laser pulse was 10 Hz. For LIF measurement, the excitation wavelengths of SiF and SiF_2 radicals were 288.05 nm [*X*-*B*(0,1)] and 225.35 nm [*X*-*A*(0,0,0 - 0,1,0)], respectively, and the fluorescence wavelengths of the SiF and SiF_2 radicals were 296.7 nm [*B*-*X*(1,1)] and 242.0 nm [*A*-*X*(0,1,0 - 0,9,0)], respectively.[13],[14] The ultraviolet laser for excitation wavelengths were synthesized by mixing second harmonic dye laser pumped with second harmonic YAG laser (532 nm) with 1064 nm YAG laser. The wavelength of pumped dye laser λ_{dye} should be tuned as follows to form the ultraviolet laser for radical excitation,

$$\lambda_{dye} = \frac{2}{\frac{1}{\lambda_{exe}} - \frac{1}{\lambda_{YAG}}}, \quad (2\text{-}44)$$

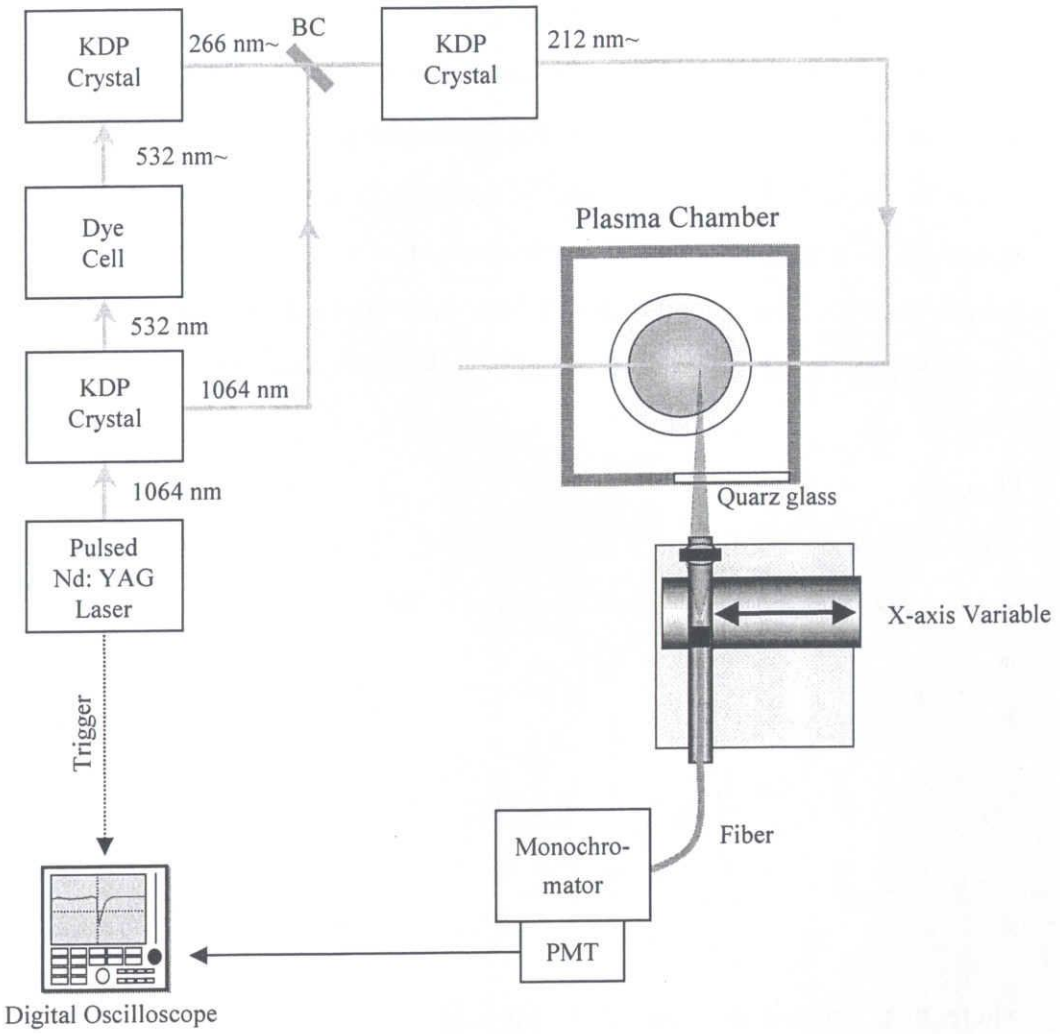

Figure 2-8 Schematic diagram of LIF system.

where λ_{exe} and λ_{YAG} are the wavelength of ultraviolet laser for radical excitation and that of Nd:YAG (1064 nm), respectively. The fluorescence was detected by using a photomultiplier tube (PMT). The electric signal from PMT was averaged 256 times by the digital oscilloscope. The optical system for LIF used is shown in **Fig. 2-2**. The ultraviolet laser beam was fixed at the center beam path, passed above the center of Si substrate. The entrance and exit windows made by quartz for the ultraviolet laser beam were attached at the chamber wall. The fluorescence was collected with an f = 150 mm lens from the direction perpendicular to the laser beam axis, was focused on the end of an optical fiber and was lead to the entrance slit of a 25-cm monochromator through the optical fiber. By moving the optical fiber parallel to the center laser beam path, the precise spatial distribution of relative radical densities could be determined.

Theory

Figure 2-9 shows diagrams of energy level. The rate equation of number density at each energy level in m level system is given as follows,[15]

$$\frac{dn_2}{dt} = B_{12}\rho n_1 - B_{21}\rho n_2 - (A_{21} + \sum_{i=3}^{m} A_{2i})n_2, \tag{2-45}$$

$$\frac{dn_i}{dt} = A_{2i}n_2 \qquad (i \geq 3), \tag{2-46}$$

$$n = \sum_{i=1}^{m} n_i, \tag{2-47}$$

where n_i is the number density in the i level, n is the ground-state density before excitation by laser, ρ is the energy density of laser beam for excitation, and A_{jk} and B_{jk} are the Einstein A and B coefficients for transitions from j to k level, respectively. The relations between Einstein A and B coefficients are expressed as follows,

$$g_j B_{jk} = g_k B_{kj}, \tag{2-48}$$

$$A_{jk} = \frac{8\pi h\nu^3}{c^3} B_{jk}, \tag{2-49}$$

where ν is the frequency of the radiation , h is the Planck constant, c is the speed of light, g_j and g_k is statistical weights in each levels. Here, the following relation is expressed by

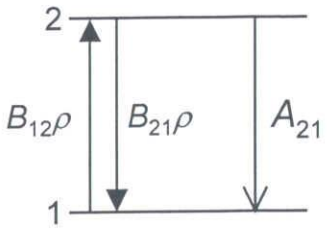

2 Level System

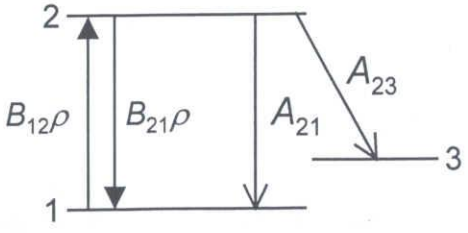

3 Level System

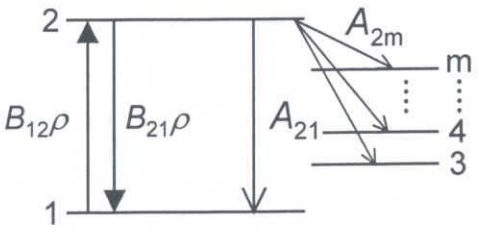

m Level System

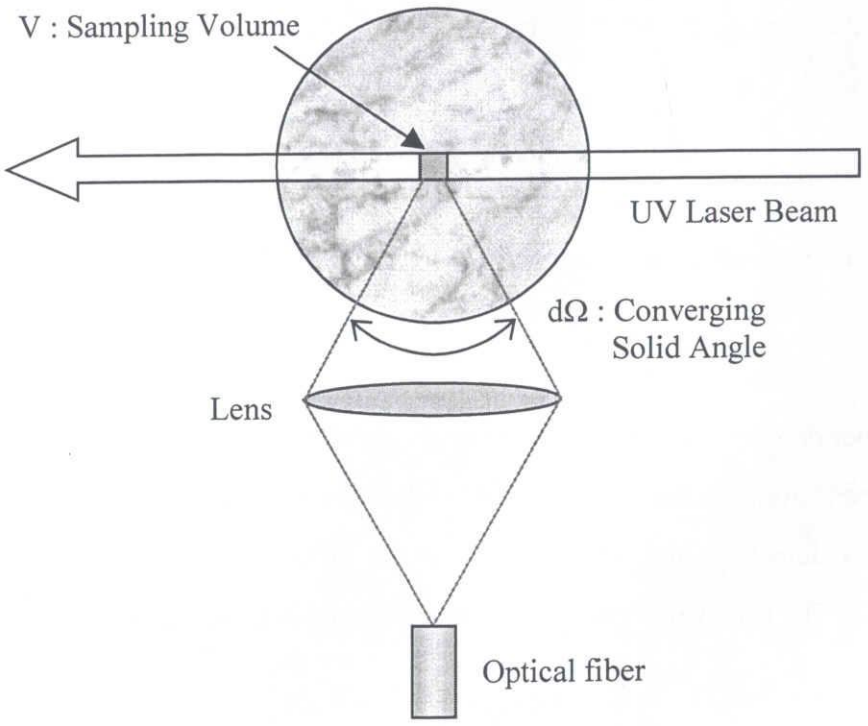

Figure 2-9 Diagrams of energy level.

assumption of 3 level system,

$$\sum_{i=3}^{m} n_i = n'_3, \tag{2-50}$$

$$\sum_{i=3}^{m} A_{2i} = A'_{23}. \tag{2-51}$$

The rate equation of number density at each energy level in m level system could be regarded as 3 level system and given from eqs. (2-45) ~ (2-47) as follows,

$$\frac{dn_2}{dt} = B_{12}\rho n_1 - B_{21}\rho n_2 - (A_{21} + A'_{23})n_2, \tag{2-52}$$

$$\frac{dn'_3}{dt} = A'_{23}\, n_2, \tag{2-53}$$

$$n = n_1 + n_2 + n'_3. \tag{2-54}$$

If the intensity of the laser beam for the excitation is sufficiently large, in which $\rho(B_{12} + B_{21}) \rangle\rangle (A_{21} + A'_{23})$, the ratio of the number densities at the ground state and excited state is equal to the ratio of the statistical weights at the ground state and the excited state immediately after laser irradiation. This relation is expressed as follows,

$$\frac{n_2}{n_1} = \frac{g_2}{g_1}, \tag{2-55}$$

$$n = n_1 + n_2. \tag{2-56}$$

From eqs. (2-55) and (2-56), we obtain

$$n_2 = \frac{g_2}{g_1 + g_2} n. \tag{2-57}$$

The number density at the excited-state is proportional to the density at the ground state, and independent with the laser intensity. When the laser irradiates continuously, all of the number density, which exist initially at the ground state, will finally transit at the 3~m levels. The time variation of the number density is given by

$$n_2(t) = \frac{g_2}{g_1 + g_2} n \exp\left(- \frac{g_2}{g_1 + g_2} A'_{23}\, t \right). \tag{2-58}$$

When the laser stops irradiating after the equilibrium state expressed by eq. (2-55), the time variation of the number density is given by

$$n_2(t) = \frac{g_2}{g_1 + g_2} n \exp\left(-\left(A_{21} + A'_{23}\right)t\right). \tag{2-59}$$

As the number of photons radiated per unit time and unit volume is $n_2 A'_{23}$, the number of photons detected with transition to i level is given by

$$\int A_{2i} n_2(t) \frac{d\Omega}{4\pi} V \, dt = C \int A'_{23} n_2(t) \, dt = Cn, \tag{2-60}$$

$$CA'_{23} = \frac{d\Omega}{4\pi} V A_{2i}. \tag{2-61}$$

Therefore, the signal intensity detected is in proportion of the ground-state density *n*. In the case of that laser beam for excitation is not sufficiently large, the signal intensity detected is in proportion of the ground-state density *n*, too.[8]

2.2.4 Actinometric optical emission spectroscopy

An AOES offers a way to monitor reactive species densities both *in situ* and nonintrusively in the discharge. Since OES does not require such as specialized laser equipment which is expensive and experimentally demanding, AOES which is one of the OES has been used widely as a simple method for diagnostics of the plasmas. In this study, AOES was used for the measurement of F atom density.

Theory

AOES requires the addition of a small amount of an inert gas such as argon to the feed gas of the plasma. The optical emission from the excited states of both the inert species (actinometer) and the species of interest are observed and compared. This comparison assumes that emission from the chosen excited states is proportional to the concentration of the same species in the ground state.

Valid actinometry requires that actinometer and measured species undergo the same excitation path (electron-impact), that the relaxation occurs exclusively by photoemission or by photoemission plus a parallel de-excitation pathway with a constant branching ratio, and that both species have similar cross-section functionality

with energy. The electron impact excitation of the ground state is

$$e + X \rightarrow X^* + e,$$

where X is the species of interest. Excitation is followed by the emission of a photon from the excited state,

$$X^* \rightarrow X + h\nu.$$

For actinometer gas, the same process occurs. The intensity of the emission form the excited state is

$$I_i = \Gamma_i k_i N_e [i], \tag{2-62}$$

where I_i is the intensity of emission from species i (either X or the actinometric gas), N_e is the electron density, $[i]$ is the concentration of species i, k_i is the excitation efficiency of species i, and Γ_i is the branching ratio for emission relative to all other de-excitation paths. The excitation rate coefficient is described by following equation,

$$k_i = \int_0^\infty v(\varepsilon)\sigma_i(\varepsilon) f(\varepsilon)\, d\varepsilon, \tag{2-63}$$

where ε is the electron energy, v is the electron velocity, $\sigma_i(\varepsilon)$ is the collision cross-section for the excitation of i, and $f(\varepsilon)$ is the electron energy distribution. Because the intensity of emission from species i depends on i, N_e, k_i, and Γ_i, changes in any of these factors will cause a proportionate change in I_i. Actinometry accounts for changes in the electron density by scaling the emission intensity of species X with the emission intensity of the actinometer as follows,

$$\frac{I_X}{I_A} = \frac{\Gamma_X k_X N_e [X]}{\Gamma_A k_A N_e [A]}. \tag{2-64}$$

Typically, the electron-impact excitation cross sections are chosen such that the excitation energy thresholds are comparable, therefore, the same group of electrons is responsible for the excitation of both species. For the ratio k_X / k_A to be approximately constant, the excitation cross sections $\sigma_i(\varepsilon)$ must also have similar functionalities. Γ_X / Γ_A is constant under conditions when collisional de-excitation is not important, which is usually true at low pressures; the time for emission is much faster than the time between molecular collisions. With these conditions met, the relative concentration of the reactive species can be determined from the ratio of emission intensities,

$$[X] \propto \frac{I_X}{I_A}[A]. \tag{2-65}$$

Thus the variation in [X] can be determined by AOES. The conditions of applicability are,

(1) The excitation cross sections have the same shape, particularly in the region close to the threshold.

(2) The population of excited levels from higher levels is negligible.

(3) Two-step excitation, e.g., via metastables, is negligible.

(4) There is no population of atomic levels via dissociation.

(5) Radiationless de-excitation (quenching) of excited levels is negligible.

Rare gases are considered to be suitable for use as the actinometer since they are chemically inert in plasma. In the case of application of AOES to the F atom density measurement, Ar gas has been commonly chosen as the actinometer. The measured emission lines of F atom and Ar atom were [3s($^2P_2$)-3p($^2P_2$)] transition at 703.7 nm for F atom with threshold energy of 14.5 eV, and [4s'(1/2)°-4P'(1/2)] transition at 750.4 nm for Ar atom with threshold energy of 13.5 eV, respectively. Although this technique is useful, there are some difficulties in the AOES technique. With accurate examination, both k_X and k_A are different functions of the electron energy as described above. The difference in the electron-energy dependence of k_X and k_A results in the poor reliability of AOES. The validity of AOES has been studies by several researchers.[16],[17] They have reported that the AOES measurement for the relative F atom density with Ar actinometer roughly gives correct results in plasmas.

2.2.5 Microwave interferometer

In this study, a 35 GHz microwave interferometer was used for measuring electron density.

Theory

The propagation measurement have been used to measure plasma density because the

propagation constant of a wave is dependent on the plasma frequency $\omega_p^2 = e^2 N_e/\varepsilon_0 m$. Here, N_e and ε_0 are the electron density and the permittivity of free space, respectively. The principle of its use is that the change in phase shift across a region with and without plasma can be measured. This in turn can be related to the change in the propagation constant and hence to the plasma frequency. The change in phase shift is

$$\Delta\varphi = k_0 \int_0^l \left[1 - \frac{\omega_p^2(x)}{\omega^2}\right]^{1/2} \mathrm{d}x - l, \tag{2-66}$$

where $k_0 = \omega/c$ is the free space propagation constant, and l is the distance across which the wave propagates. It is often possible to choose the diagnostics frequency sufficiently higher than the plasma frequency that square root can be expanded. The free space part of the phase shift the conveniently cancels leaving,

$$\Delta\varphi \approx k_0 \int_0^l \frac{\omega_p^2(x)}{2\omega^2} \mathrm{d}x = \frac{k_0 e^2}{2\varepsilon_0 m\omega^2} \int_0^l N(x)\mathrm{d}x. \tag{2-67}$$

In this approximation, we see that the line integral of the density can be directly measured in term of a phase shift.

2.2.6 Double probe

The probe technique is one of the most useful tools for diagnosing plasma. In this study, the electron temperature was measured by double probe.

Theory

A metal probe, inserted in a discharge and biased positively or negatively to draw electron or ion current, is one of the most useful tools for diagnosing plasma. These probes, introduced by Langmuir are usually called *Langmuir probes*. As with any other electrode, the probe is surrounded by a sheath. However, unlike large electrode surfaces that are used to control plasma, probes are usually quite small and under suitable conditions, produces only minor local perturbations.

Double probes are generally used if no well-defined ground electrode exists in the plasma. A schematic of a double probe is shown in **Figure 2-10 (a)**, with typical probe characteristic as shown in **Figure 2-10 (b)**. Since the two probes draw no net current they will both be negative with respect to the plasma. Current flows between the probes if the differential potential $V \neq 0$. As V becomes large, the more negative probe (in this case probe 2) essentially draws ion saturation current, which is just balanced by the net electron current to probe 1. The double probe system has the advantage that the net current never exceeds the ion saturation current, minimizing the disturbance to the discharge, but has a consequent disadvantage that only the high-energy tail of the electron distribution is collected by either probe. The distribution of these electrons may not be representative of the distribution of bulk electrons in the discharge.

Defining the ion and electron currents to probe 1 and 2 as I_{1i}, I_{1e}, I_{2i}, I_{2e}, then the condition that the system float is

$$I_{1i} + I_{2i} - I_{1e} - I_{2e} = 0 . \tag{2-68}$$

The loop current is

$$I_{2i} - I_{2e} - (I_{1i} - I_{1e}) = 2I . \tag{2-69}$$

Combining eq. (2-68) with eq. (2-69), we obtain

$$I = I_{1e} - I_{1i} = I_{2i} - I_{2e} . \tag{2-70}$$

For the electron current, we have

$$I_{1e} = A_1 J_{esat} e^{\frac{V_1}{T_e}}, I_{2e} = A_2 J_{esat} e^{\frac{V_2}{T_e}}, \tag{2-71}$$

where J_{esat} is the electron random current density and V_1 and V_2 are the probe potentials with respect to the plasma potential. Using $V = V_1 - V_2$ and substituting eq. (2-58) into eq. (2-68) we obtain

$$\frac{I + I_{1i}}{I_{2i} - I} = \frac{A_1}{A_2} e^{\frac{V}{T_e}}, \tag{2-72}$$

which generally plots as shown in **Fig. 2-10 (b)**. For $A_1 = A_2$, then $I_{1i} = I_{2i} = I_i$, such that eq. (2-70) simplifies to

$$I = I_i \tanh\left(\frac{V}{2T_e}\right). \tag{2-73}$$

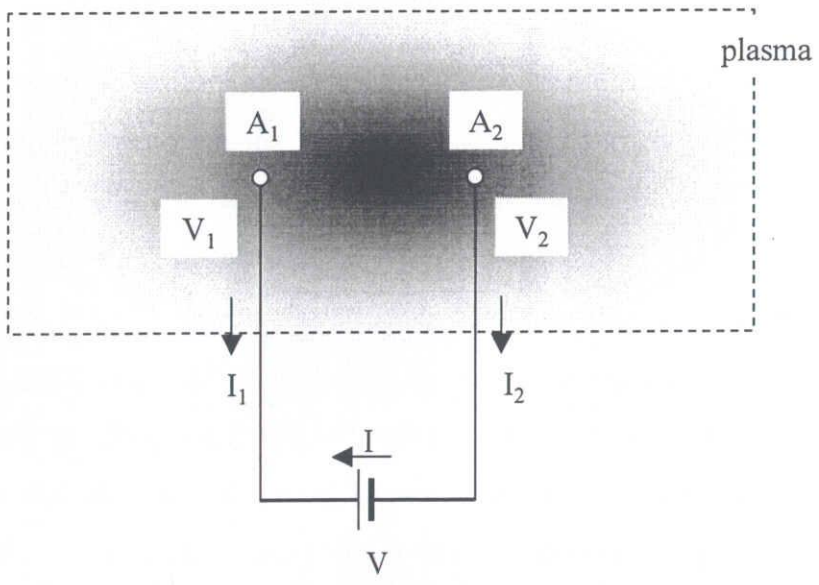

(a)

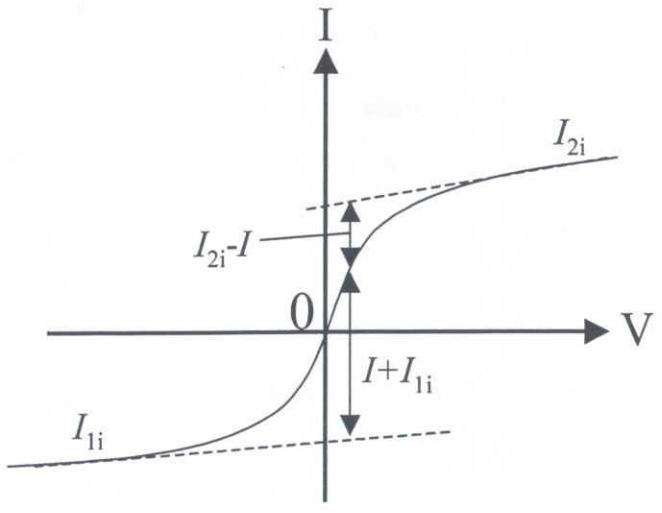

(b)

Figure 2-10 Schematic of double probe.
(a) Definition of voltage and currents,
(b) Typical current-voltage characteristic.

2.2.7 Pyrometer

In the plasma, we measured the electrode heating effect due to the charged species by using pyrometer. The pyrometer enabled us to measure the temperature of the Si surface in the range of 473-2273 K without any influence due to a heater under the substrate. In this study, the surface temperature of upper electrode was measured by the pyrometer (LEC Company Limited. KTL-P1).

Theory

The thermal energy is radiated as an electromagnetic wave from the matter. It is called thermal radiation. The pyrometer is used for measuring the temperature through the thermal radiation. The energy radiated from the matter depends on the absolute temperature of the matter and the wavelength. The thermal radiation energy is given by Planck's radiation law,

$$\rho(\lambda,T)=\frac{8\pi hc}{\lambda^5}\frac{1}{\exp\left(\frac{ch}{k_B T\lambda}\right)-1}, \tag{2-72}$$

where c is the speed of light, λ is the wavelength, h is the Planck constant, k_B is the Boltzmann constant, and T is the absolute temperature of matter.

Reference for chapter 2

[1] M. A. Lieberman and A. J. Lichtenberg: *Principles of Plasma Discharges and Materials Processing* (John Wiley & Sons, Inc. New York 1994).

[2] H. Sugai, *Ouyou Buturi*, **70**, 398 (2001).

[3] V. A. Godyak and R. B. Piejak, Phys. Rev. Lett., **65**, 996 (1990).

[4] H. Sugai, I Ghanashev, M. Hosokawa, K. Mizuno, K. Nakamura, H. Toyoda, and K. Yamauchi, Plasma Sources Sci. Technol., **10**, 378 (2001).

[5] S. V. Berezhnoi, I. D. Kaganovich, and L. D. Tsendin, Plasma Sources Sci. Technol., **7**, 268 (1998).

[6] H. Sugai, *plasma electronics* (ohmsha, Japan 2000).

[7] E. Abdel-Fattah and H. Sugai, Appl. Phys. Lett., **83**, 1533 (2003).

[8] D. Vender and R. W. Boswell, IEEE Trans. Plasma Sci., **18**, 725 (1990).

[9] M. Kratzer, R. P. Brinkmann, W. Sabisch, and H. Schmidt, J. Appl. Phys., **90**, 2169 (2001).

[10] A. C. G. Mitchell and M. W. Zemansky: *Resonance Radiation and Exited Atoms* (Cambridge, London 1961).

[11] M. Nakamura, M. Hori, T. Goto, M. Ito, and N. Ishii, Jpn. J. Appl. Phys., **40**, 4730 (2001).

[12] H.W.Kattenberg and A.Oskam, J. Molecule. Spectroscopy, **49**, 52 (1974).

[13] G. A. Hebner, J. Appl. Phys., **89**, 900 (2001).

[14] G. Cunge, P. Chabert, and J. P. Booth, Plasma Sources Sci. Technol., **6**, 349 (1997).

[15] C. Suzuki, DC Thesis, Nagoya University (1999).

[16] R. E. Walkup, K. L. Saenger, and G. S. Sewyn, J. Chem. Phys., **84**, 2668 (1986).

[17] H. M. Katsch, A. Tewes, E. Quandt, A. Goehlich, T. Kawetzki, and H. F. Döbele, J. Appl. Phys., **88**, 6232 (2000).

Chapter 3

Measurement of Si, SiF, SiF_2 radicals and SiF_4 molecule using very high frequency capacitively coupled plasma employing SiF_4

3.1 Introduction

In the fabrication of ultralarge scale integrated circuits (ULSIs), fluorine-based plasmas have been employed for plasma-assisted etching and the deposition of thin films. SiF_4-based gases have been employed for the deposition of thin films such as fluorine-doped silicon oxide (SiOF),[1] fluorine-doped silicon nitride (SiNF),[2] poly-Si[3] and so on. For etching, highly reactive fluorine atoms and ions produced from the plasma interact with the Si substrate and produce volatile reaction products, such as the SiF_2 radical and the SiF_4 molecule. These products, in turn, diffuse back into the plasma where they are dissociated and ionized by electrons, and the resulting by-products are transported and re-deposited onto the substrate. Therefore, the SiF_4 molecule and SiF_x (x = 0-3) radicals play an important role in these plasma processes.

So far, the detection of SiF and SiF_2 radicals in the reactive plasma has been developed using infrared absorption spectroscopy techniques,[4]-[7] laser-induced fluorescence[8]-[13] and ultraviolet absorption spectroscopy.[14],[15] The spatial distribution of SiF_2 and SiF_4 densities in high density electron cyclotron resonance (ECR) plasma has been reported.[16] However, there are few systematic reports on the behavior of species in SiF_4 plasma. It is important to clarify the production and loss process of species and the radical composition in the plasma for precisely controlling SiF_4 based plasma.

In the ULSIs fabrication, it is necessary to reduce of the production cost. The wafer size used in production today is 8-inch in diameter. Therefore, it is important to clarify the uniformity of plasma process and the spatial distribution of radical density.

In this chapter, the absolute line-integrated density of the SiF_4 molecule and the relative densities of SiF_2 and SiF radicals were measured by IRLAS and LIF, respectively. The absolute density of the Si atom was measured by UVAS. The relative density of the F atom was measured by AOES. Based on these results, the production and loss processes of Si, SiF and SiF_2 radicals together with SiF_4 molecules in VHF 60 MHz SiF_4 CCP are discussed.

3.2 Measurement of Si, SiF, SiF_2 radicals and SiF_4 molecule

The electron density (N_e) and electron temperature (T_e) at the center of electrode were measured. N_e was measured by a 35 GHz microwave interferometer and a double probe technique. The deference of value of N_e measured using the double probe or the 35 GHz interferometer is about 20%. In the following figures, the value of N_e measured using the 35 GHz interferometer was used. The plasma condition was maintained at a total pressure of 5.3 Pa and a SiF_4 flow rate of 90 sccm. **Figure 3-1** shows N_e and T_e as a function of VHF power. N_e increased from 3.8×10^{10} cm^{-3} to 1.7×10^{11} cm^{-3} with increasing VHF power from 0.5 kW to 2.5 kW. T_e slightly decreased from 3 eV to 2.3 eV and was inclined to saturate with increasing VHF power.

Figure 3-2 shows the SiF_4 molecule density as a function of N_e at the center of electrode measured by IRLAS. The N_e obtained in **Fig. 3-1** was used as the horizontal axis. Here, the SiF_4 density was measured by double-pass IRLAS to improve the S/N ratio. The plasma region was assumed to be 25 cm in diameter, the same size as the electrode. The absorption length in the plasma region were calculated from the size of the plasma where the laser beams passed. The density outside the plasma region was assumed to be the same as the density in the vicinity of the chamber wall. Therefore, the net density in the plasma region was estimated by subtracting the density outside the

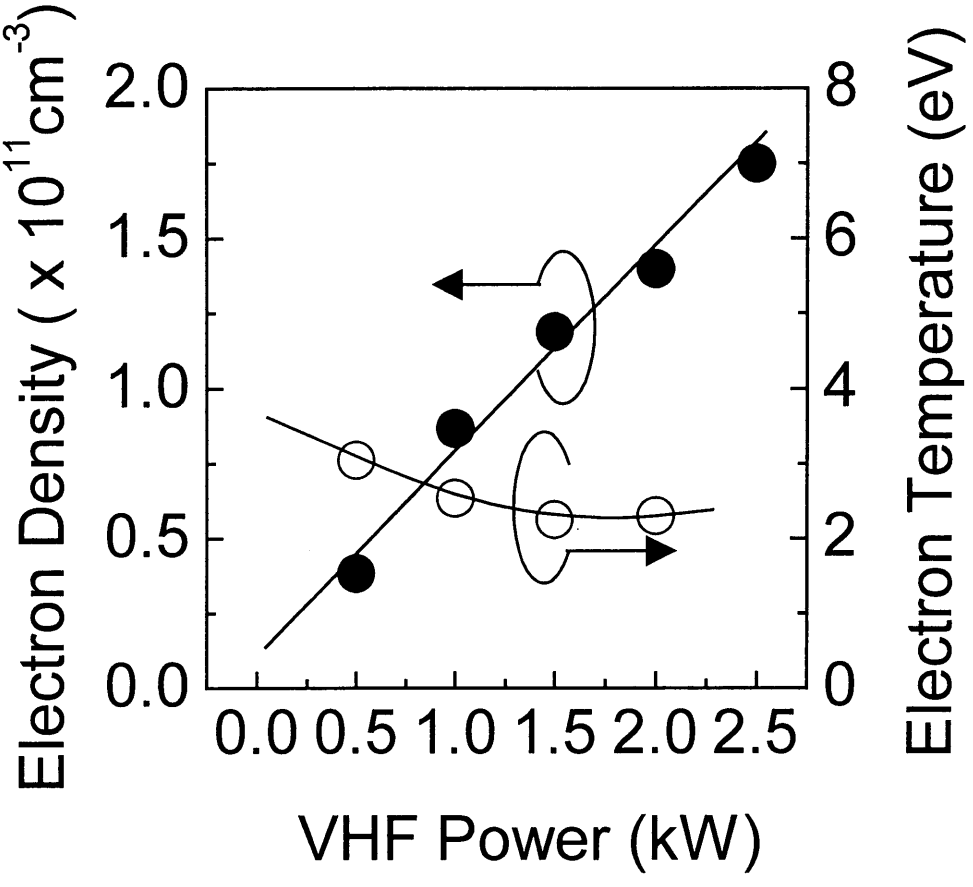

Figure 3-1 Electron density and electron temperature as a function of VHF power.

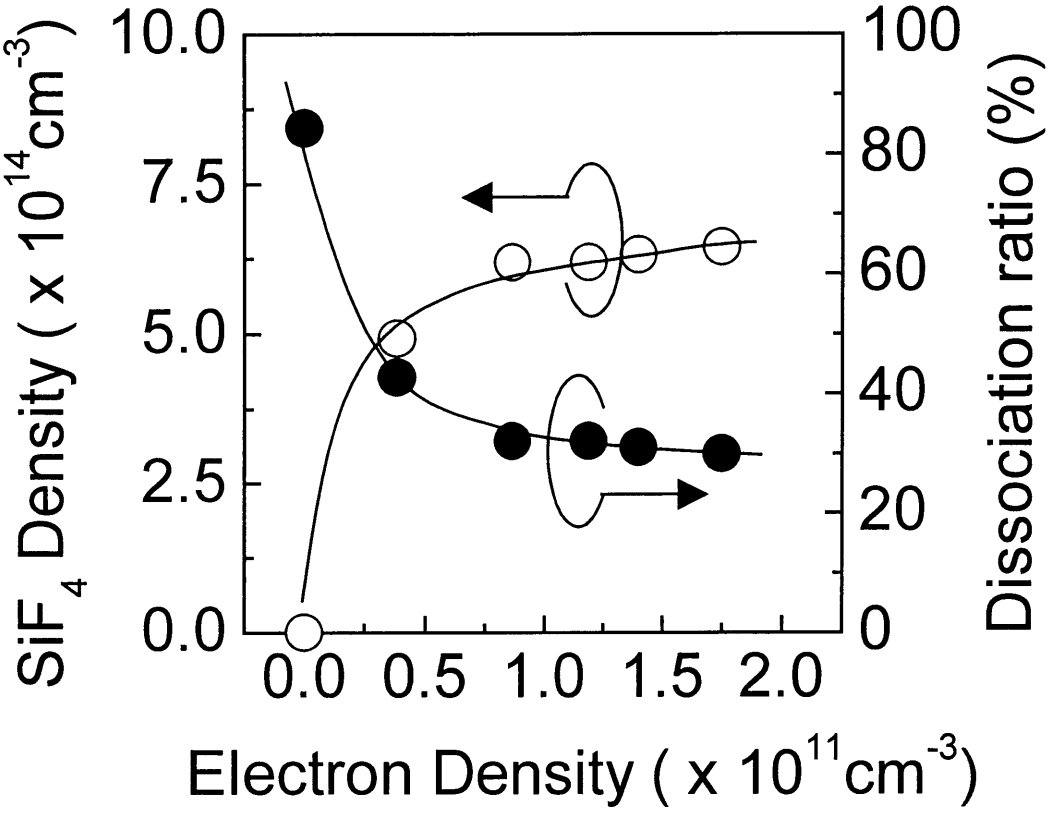

Figure 3-2 Absolute density of SiF_4 molecule and dissociation ratio of the SiF_4 molecule as a function of electron density.

plasma region from the total line-averaged density. The SiF_4 density decreased up to the N_e of 8.7×10^{10} cm^{-3} and saturated with further increase in N_e. The translational temperatures were calculated from the full width at half maximum of each spectral profile. The line-averaged translational temperature of the SiF_4 molecule at the center of the electrode was estimated to be about 400 K, and the temperature in the vicinity of the chamber wall outside the plasma region was estimated to be about 350 K. These temperatures did not change with varying VHF power. SiF_4 molecule densities in the vicinity of the chamber wall were twice those in the center of the electrode. From these results, the translational temperature of SiF_4 molecule at the plasma region was roughly estimated to be about 500 K by the superposition of each Gaussian distribution of the line-averaged translational temperatures within the plasma region and outside the plasma region. The SiF_4 molecule density estimated using 500 K agreed with that using 400 K within the experimental error value of about 12%. The dissociation ratio of the SiF_4 molecule was estimated to be about 63% at N_e of 8.7×10^{10} cm^{-3}.

Figure 3-3 shows SiF_2 radical density as a function of N_e measured by LIF. The SiF_2 density increased with increasing N_e from 3.8×10^{10} to 1.2×10^{11} cm^{-3} and slightly decreased with further increase in N_e above 1.2×10^{11} cm^{-3}. The production and loss processes of the SiF_2 radical can be expressed as follows. The major production process of the SiF_2 radical is assumed to be the electron impact dissociation of SiF_4 molecule,

$$R1: SiF_4 + e \xrightarrow{k_1} SiF_2 + \text{products} + e .$$

On the other hand, the loss process of the SiF_2 radical is considered to be diffusion to the wall, electron impact dissociation and reaction with the F_2 molecule and the F atom as follows,

$$R2: SiF_2 + e \xrightarrow{k_2} (\text{SiForSi}) + \text{products} + e .$$

$$R3: SiF_2 + F_2 \xrightarrow{k_3} SiF_3 + F .$$

$$R4: SiF_2 + F \xrightarrow{k_4} SiF_3^* \longrightarrow SiF_3 + h\nu .$$

The rate coefficients k_3 and k_4 were $(4.7 \pm 0.3) \times 10^{-13}$ cm^3s^{-1} and $(5 \pm 1) \times 10^{-13}$ cm^3s^{-1}, respectively.[12],[13] However, $R3$ and $R4$ were negligible because k_3 and k_4 are considerably small. Accordingly, the balance equation for the production and loss of the

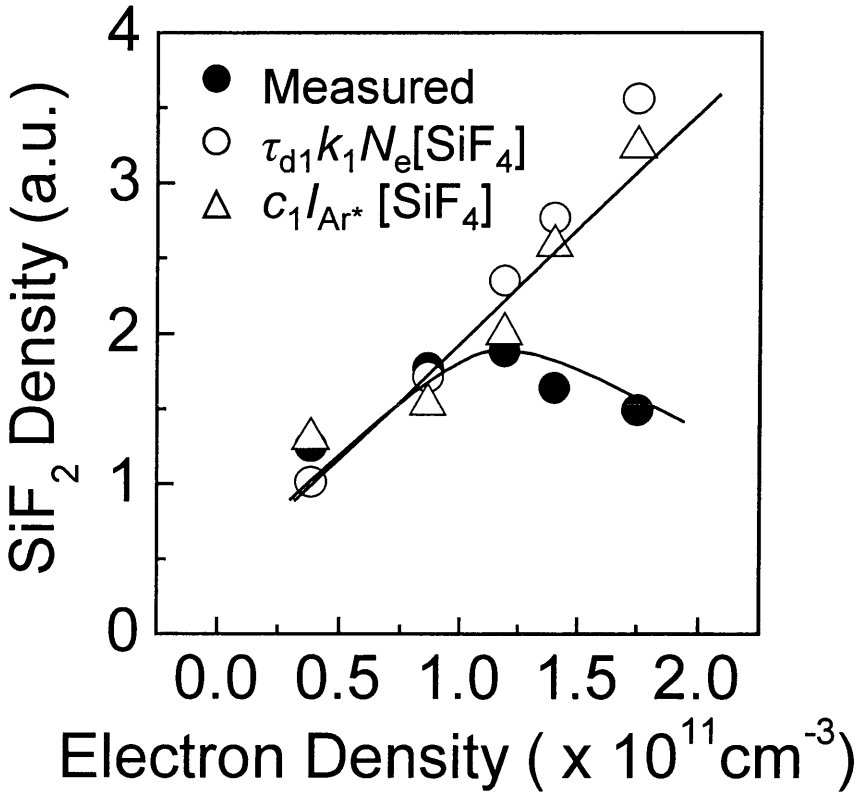

Figure 3-3 Relative density of SiF_2 radical as a function of electron density.

SiF_2 radical can be expressed by the following equation,

$$\frac{d}{dt}[SiF_2] = k_1 N_e [SiF_4] - k_2 N_e [SiF_2] - \frac{[SiF_2]}{\tau_{d1}}, \quad (3\text{-}1)$$

where N_e, $[SiF_2]$ and $[SiF_4]$ are the densities of electron, SiF_2 and SiF_4, respectively. k_1 and k_2 are the rate coefficients for reactions $R1$ and $R2$. τ_{d1} is the diffusion lifetime of the SiF_2 radical. τ_{d1} is a constant with the variation in N_e because the pressure was fixed.

The SiF_2 radical density in a steady state is then expressed by

$$[SiF_2] = \frac{k_1 N_e [SiF_4]}{k_2 N_e + \frac{1}{\tau_{d1}}}. \quad (3\text{-}2)$$

When diffusion loss is dominant, the SiF_2 density is expressed by the following equation from eq. (3-2),

$$[SiF_2] = \tau_{d1} k_1 N_e [SiF_4]. \quad (3\text{-}3)$$

The SiF_2 density is proportional to $k_1 N_e[SiF_4]$ because τ_{d1} is constant. Assuming the diffusion loss is dominant, the calculated density of SiF_2 radical is described by the open circle as shown in **Fig. 3-3**. Here, the emission intensity of Ar^* provides information on the production process of the SiF_2 radical. The rate equation of excited Ar^* atom density in the steady state is expressed by the following equation,

$$k_{Ar} N_e = \frac{[Ar^*]}{\tau_{Ar}[Ar]} \propto \frac{I_{Ar^*}}{[Ar]}. \quad (3\text{-}4)$$

where k_{Ar} is the excitation rate constant, τ_{Ar} is the radiative lifetime, and [Ar] and $[Ar^*]$ are the densities of the Ar atom in the ground and excited states, respectively. The Ar^* emission intensity I_{Ar^*} is proportional to $k_{Ar}N_e$. The emission threshold energy of Ar* is 13.5 eV, which corresponds to the threshold energy of 13.9 eV for SiF_4 dissociation that produces the SiF_2 radical.[17] Therefore, the generation rate of the SiF_2 radical is expressed by the following equation,

$$[SiF_2] \propto c_1 I_{Ar^*} \cdot [SiF_4], \quad (3\text{-}5)$$

where c_1 is a constant. The generation rate of the SiF_2 radical is described by the open triangle as shown in **Fig. 3-3**. The calculated density and the generation rate of the SiF_2

radical increased with increasing N_e. The calculated density corresponds to the measured density of SiF_2 radical at N_e ranging from 3.8×10^{10} to 1.2×10^{11} cm^{-3}. This suggests that the denominator in eq. (3-2) is almost constant regardless of the increase in N_e, and the SiF_2 radical is extinguished by diffusion to the wall. However, the measured density of the SiF_2 radical was smaller than the calculated density, and slightly decreased at N_e above 1.2×10^{11} cm^{-3}. This suggests that the denominator in eq. (3-2) increases at N_e above 1.2×10^{11} cm^{-3}. Here, when the electron impact dissociation is dominant in the loss process of the SiF_2 radical, the SiF_2 density is expressed by the following equation from eq. (3-2),

$$[SiF_2] \propto c_2 [SiF_4], \tag{3-6}$$

where c_2 is a constant. As shown in **Fig. 3-2**, SiF_4 density slightly decreased at N_e above 8.7×10^{10} cm^{-3}. Therefore, when the loss process of the SiF_2 radical is electron impact dissociation, the SiF_2 density slightly decreases. As shown in **Fig. 3-3**, the measured density slightly decreased. Thus, it is considered that the SiF_2 radical is mainly produced by the electron impact dissociation of the SiF_4 molecule, extinguished by diffusion to the wall at N_e below 1.2×10^{11} cm^{-3} and by electron impact dissociation at N_e above 1.2×10^{11} cm^{-3} resulting in the production of Si and SiF radicals according to *R*2.

Figure 3-4 shows SiF radical density as a function of N_e measured by LIF. SiF radical density increased linearly with increasing N_e. The production and loss processes of the SiF radical are expressed as follows. The major production process of the SiF radical is assumed to be electron impact dissociation of the SiF_4 molecule,

$$R5: SiF_4 + e \xrightarrow{k_5} SiF + \text{products} + e .$$

On the other hand, the loss process of the SiF radical is considered to be diffusion to the wall, electron impact dissociation and reaction with the SiF_4 and F_2 molecules as follows,

$$R6: SiF + e \xrightarrow{k_6} Si + F + e .$$

$$R7: SiF + SiF_4 \xrightarrow{k_7} SiF_2 + SiF_3 .$$

$$R8: SiF + F_2 \xrightarrow{k_8} SiF_2 + F .$$

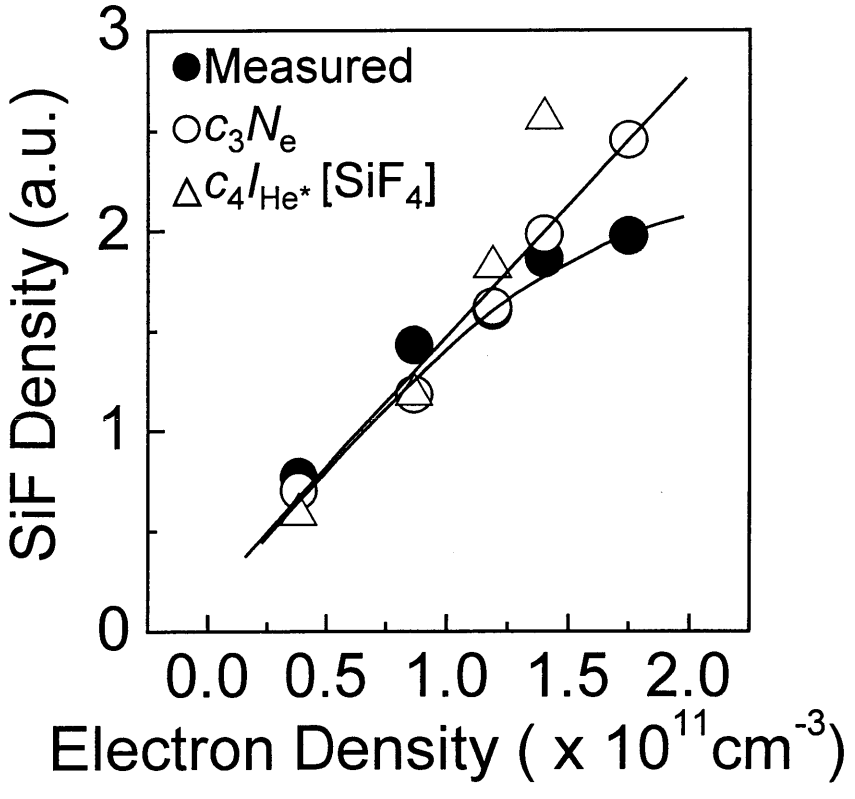

Figure 3-4 Relative density of SiF radical as a function of electron density.

The rate coefficients k_7 and k_8 were (2.8 ± 1.2) × 10^{-11} cm^3s^{-1} and (2.4 ± 1.2) × 10^{-11} cm^3s^{-1}, respectively.[18] However, *R*8 may be negligible because F_2 density is relatively small in comparison with SiF_4 density. Thus, the major loss process of the SiF radical is considered to be diffusion to the wall, electron impact dissociation and reaction with the SiF_4 molecule. Accordingly, the balance equation for the production and loss of the SiF radical can be expressed by the following equation,

$$\frac{d}{dt}[SiF] = k_5 N_e [SiF_4] - k_6 N_e [SiF] - k_7 [SiF][SiF_4] - \frac{[SiF]}{\tau_{d2}}, \quad (3\text{-}7)$$

where N_e, [SiF], and [SiF_4] are the densities of the electron, SiF and SiF_4, respectively. k_5 and k_6 are the rate coefficients for reactions *R*3 and *R*4. τ_{d2} is the diffusion lifetime of the SiF radical. τ_{d2} is constant with variation in N_e. The SiF radical density in the steady state is expressed by,

$$[SiF] = \frac{k_5 N_e [SiF_4]}{k_6 N_e + k_7 [SiF_4] + \frac{1}{\tau_{d2}}}. \quad (3\text{-}8)$$

Here, the production process of the SiF radical is also assumed to be the electron impact dissociation of the SiF_2 radical described above. From eq. (3-2), SiF_2 density is roughly estimated to be of the order of 10^{12} cm^{-3} using rate coefficient k_1 that is calculated to be 6.7 × 10^{-12} cm^3s^{-1} using the cross section from Ref. 22. The rate coefficient k_2 of the electron impact dissociation of the SiF_2 radical for the production of SiF radical was unknown. It is assumed to be of the order of 10^{-10}-10^{-11} cm^3s^{-1} at maximum. The SiF radical density ($k_2N_e[SiF_2]$) produced by the electron impact dissociation of the SiF_2 radical was estimated to be of the order of 10^{12} cm^{-3}. On the other hand, the numerator of eq. (3-8) was of the order of 10^{13} cm^{-3} using k_5 calculated by the cross section from Ref. [17]. Therefore, $k_2N_e[SiF_2]$ will be much smaller than the numerator of eq. (3-8), and the contribution of the electron impact dissociation of the SiF_2 radical to the production of the SiF radical will be much smaller than that of the SiF_4 molecule. In the higher electron density region, however, the SiF radical will be also produced from the SiF_2 radical with electron impact dissociation.

Each term of the denominator in eq. (3-8) was considered as follows. The reaction rate constant k_7 was (2.8 ± 1.2) × 10^{-11} cm^3s^{-1} and the SiF_4 density was of the order of 10^{14} cm^{-3} as shown in **Fig. 3-2**. Thus, the second term was estimated to be of the order of 10^3-10^4 s^{-1}. On the other hand, k_6 was unknown, and N_e was of the order of 10^{10}-10^{11} cm^{-3} as shown in **Fig. 3-1**. If the first term is larger than the second term, k_6 should be larger than 10^{-7} cm^3s^{-1} whose value is too large. It is considered that k_6 is generally of the order of 10^{-10}-10^{-11} cm^3s^{-1}. Thus, the first term will be much smaller than the second term. The third term is expressed by the following equation,[19]

$$\tau_d = \frac{p\Lambda_0^2}{D} + \frac{2l_0(2-\alpha)}{v\alpha}, \tag{3-9}$$

where p is the pressure and Λ_0 is the geometrical diffusion length determined by the chamber structure. In this study, the electrode gap of 2.5 cm is much smaller than the chamber length 54 cm. Therefore, Λ_0 is expressed by the following equation,

$$\Lambda_0 = \frac{L}{\pi}, \tag{3-10}$$

where L is 2.5 cm, l_0 is expressed by V/S with V and S being the volume and surface area of the chamber, respectively. v is the velocity of the SiF radical given by $(8kT/\pi m)^{1/2}$(T and m are the temperature and mass of the SiF radical, respectively, and k is the Boltzmann constant). α is the surface loss probability on the chamber wall, and α was assumed to be 0.0245 from Ref. [17]. D is the diffusion coefficient for the SiF radical in the SiF_4 molecule and is calculated to be 1306 cm^2·Torr·s^{-1} using the Chapman-Enskog theory with the Lennard-Jones intermolecular potential.[20], [21] The third term of the denominator in eq. (3-8) is estimated to be about 46.2 s^{-1}. Therefore, the value of the second term is much larger than that of the third term. Accordingly, the reaction of the SiF radical with the SiF_4 molecule in the gas phase becomes dominant as the loss process. Here, when the gas phase reaction for the loss process is dominant, SiF density is expressed by the following equation from eq. (3-8),

$$[\mathrm{SiF}] \propto c_3 N_e, \tag{3-11}$$

where c_3 is constant. The SiF density is proportional to N_e. The calculated density of the

SiF radical, whose reaction loss is dominant, is also described by the open circle as shown in **Fig. 3-4**. Here, the emission intensity of He^* provides information on the production process as described above. The emission threshold energy of He* is 23.07 eV, and the threshold energy of SiF_4 dissociation producing the SiF radical is 20.4 eV.[22] Therefore, the generation rate of the SiF radical is expressed by the following equation,

$$[\mathrm{SiF}] \propto c_4 I_{\mathrm{He}^*} \cdot [\mathrm{SiF_4}]. \tag{3-12}$$

This generation rate of the SiF radical is described by the open triangle as shown in **Fig. 3-4**. The calculated density and the generation rate of the SiF radical increased with increasing N_e. The calculated density corresponds well to the measured density of the SiF radical at the N_e ranging from 3.8×10^{10} to 1.4×10^{11} cm^{-3}. This suggests that the denominator in eq. (3-8) is almost constant regardless of the increase in N_e, and the SiF radical is dominantly extinguished by reaction with the SiF_4 molecule. However, the measured density of the SiF radical was smaller than the calculated density at N_e above 1.4×10^{11} cm^{-3}. It is considered that the SiF radical is furthermore extinguished by electron impact dissociation in the same way as the SiF_2 radical. Thus, the SiF radical is mainly produced by the electron impact dissociation of the SiF_4 molecule and extinguished by reaction with the SiF_4 molecule at N_e below 1.4×10^{11} cm^{-3} and by electron impact dissociation at N_e above 1.4×10^{11} cm^{-3} resulting in the production of the Si atom according to *R6*.

Figure 3-5 shows Si atom densities at the $3p^2{}^3P_2$ level (251.6 nm) and $3p^2{}^1D_2$ level (288.2 nm) as a function of N_e measured by UVAS employing a hollow cathode lamp as a light source. Assuming the absorption profile to be the Boltzmann distribution, the total density of the Si atom at the electronic ground state, that is composed of the $3p^2{}^3P$ and $3p^2{}^1D$ levels, can be estimated. Here, when the temperature of the Si atom is 600 K, the Si density ratio for the $3p^2{}^3P_0$: $3p^2{}^3P_1$: $3p^2{}^3P_2$: $3p^2{}^1D_2$ levels is given as 0.34 : 0.85 : 1 : 4.64×10^{-7} using the Boltzmann distribution. As shown in **Fig. 3-5**, the Si atom density at the $3P^2{}^3P_2$ level was about twice as large as that at the $3P^2{}^1D_2$ level at N_e of 3.8×10^{10} cm^{-3}. Accordingly, the total Si density at N_e of 3.8×10^{10} cm^{-3} was estimated by multiplying the density of the $3p^2{}^3P_2$ level by a factor of 2.7.[22], [23]

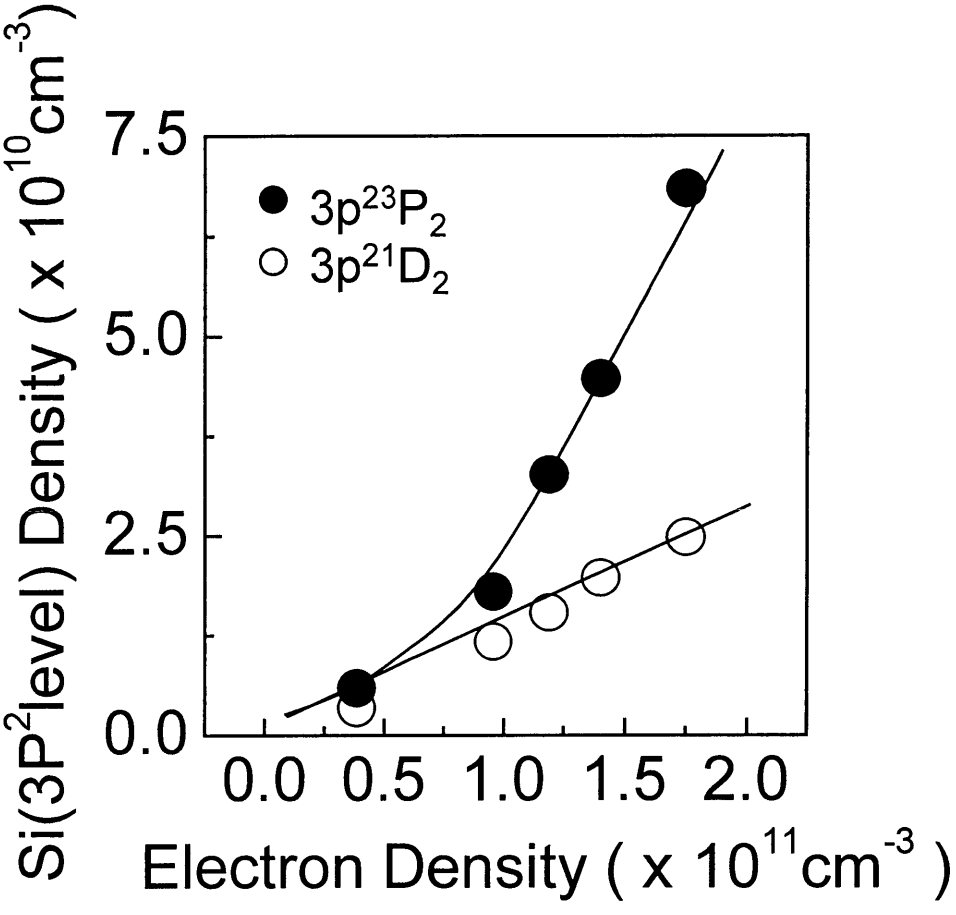

Figure 3-5 Absolute densities of Si atom at the $3p^{23}P_2$ level (251.6 nm) and $3p^{21}D_2$ level (288.2 nm) as a function of electron density.

Therefore, the total density of the Si atom was calculated as shown in **Figure 3-6**. The total density of the Si atom was found to be of the order of 10^{10}-10^{11} cm^{-3} and increased with increasing N_e. The production and loss processes of the Si atom can be expressed as follows. The major production process of the Si atom is assumed to be the electron impact dissociation of the SiF_4 molecule,

$$R9: SiF_4 + e \xrightarrow{k_9} Si + products + e .$$

Here, the production process of the Si atom is also assumed to be the electron impact dissociation of SiF and SiF_2 radicals as described above. The rate coefficients of the electron impact dissociation of SiF_2 and SiF radicals for the production of the Si atom were unknown. The production process of the Si atom was complicated since many parameters producing the Si atom were considered, especially in the higher electron density region. A simple model in which the Si atom is produced only by electron impact dissociation of the SiF_4 molecule is assumed in this study.

The major loss processes of the Si atom are diffusion to the wall and reaction with the SiF_4 and F_2 molecules as follows,

$$R10: Si + SiF_4 \xrightarrow{k_{10}} SiF_2 + SiF_3 .$$

$$R11: Si + F_2 \xrightarrow{k_{11}} SiF + F .$$

The rate coefficients k_{10} and k_{11} were (2.2 ± 1.4) × 10^{-11} cm^3s^{-1} and (2.9 ± 1.1) × 10^{-11} cm^3s^{-1}, respectively.[18] However, $R11$ was negligible because F_2 density was relatively small in comparison with SiF_4 density. Thus, the major loss process of the Si atom is diffusion to the wall and reaction with the SiF_4 molecule. Accordingly, the balance equation for the production and loss of the Si atom can be expressed by the following equation,

$$\frac{d}{dt}[Si] = k_9 N_e [SiF_4] - k_{10}[Si][SiF_4] - \frac{[Si]}{\tau_{d3}}, \qquad (3\text{-}13)$$

where N_e, [Si] and [SiF_4] are the densities of the electron, Si and SiF_4, respectively. k_9 and k_{10} are the rate coefficients for reactions $R9$ and $R10$. τ_{d3} is the diffusion lifetime of the Si atom. τ_{d3} and k_{10} are constant with the variation in N_e. The Si atom density in a steady state is expressed as,

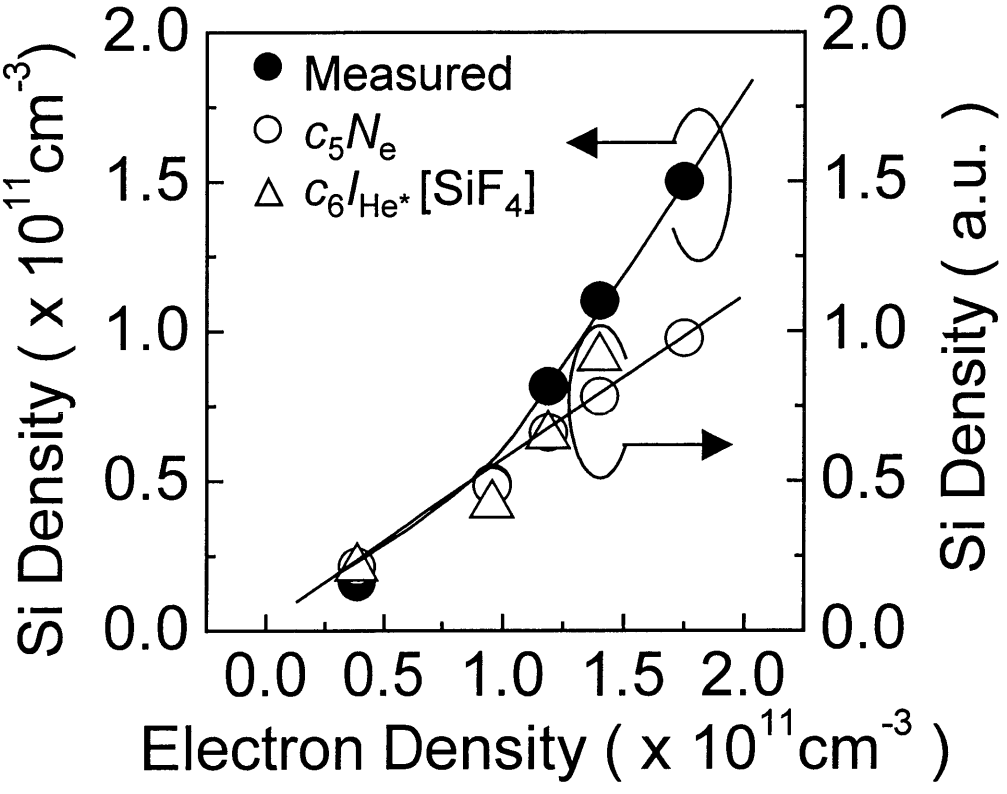

Figure 3-6 Total absolute density of Si atom as a function of electron density.

$$[\mathrm{Si}]=\frac{k_9 N_e[\mathrm{SiF_4}]}{k_{10}[\mathrm{SiF_4}]+\frac{1}{\tau_{d3}}}. \tag{3-14}$$

The first term of the denominator in eq. (3-14) is explained as follows. The reaction rate constant k_{10} was 2.2×10^{-11} cm^3s^{-1}, and SiF_4 density was of the order of 10^{14} cm^{-3} as shown in **Fig. 3-2**. Therefore, the first term of the denominator in eq. (3-14) was estimated to be of the order of 10^3-10^4 s^{-1}. On the other hand, the second term of the denominator in eq. (3-14) is given by eq. (3-9), with α of 0.063 from Ref. [17]. The diffusion coefficient for Si atoms in the SiF_4 molecule is calculated to be 1855 $cm^2 \cdot Torr \cdot s^{-1}$. The second term of the denominator in eq. (3-14) is estimated to be about 173 s^{-1}. Therefore, the value of the first term is much larger than that of the second term. Accordingly, the reaction with the SiF_4 molecule becomes dominant as the loss process. Here, when the reaction of the Si atom with the SiF_4 molecule is dominant as the loss process of the Si atom, Si density is expressed by the following equation from eq. (3-14),

$$[\mathrm{Si}] \propto c_5 N_e, \tag{3-15}$$

where c_5 is constant. Si density is proportional to N_e. The calculated density of the Si atom, where the reaction loss is dominant, is also described by the open circle as shown in **Fig. 3-6**. Here, the emission intensity of He^* also provides information on the production process as described above. The threshold energy of SiF_4 dissociation that produces the Si atom is 24.6 eV.[17] Therefore, the generation rate of the Si atom is expressed by the following equation,

$$[\mathrm{Si}] \propto c_6 I_{He} \cdot [\mathrm{SiF_4}]. \tag{3-16}$$

The generation rate of the Si atom is described by the open triangle as shown in **Fig. 3-6**. The calculated density and generation rate of the Si atom increased with increasing N_e. The calculated density of the Si atom corresponds to the measured density at N_e ranging from 3.8×10^{10} to 1.0×10^{11} cm^{-3}. This suggests that the denominator in eq. (3-8) is almost constant regardless of increasing N_e, and the Si atom is extinguished by the reaction with the SiF_4 molecule. However, the measured density of the Si atom was

larger than the calculated density at N_e above 1.0×10^{11} cm^{-3}. It is considered that the Si atom was produced by the electron impact dissociation of SiF_x (x = 1-3) radicals in addition to the SiF_4 molecule, resulting in the Si density being larger than the calculated density of the Si atom. Therefore, the Si atom is mainly produced by the electron impact dissociation of SiF_4 molecule at N_e below 1.0×10^{11} cm^{-3} and by the electron impact dissociation of SiF_x (x = 1-3) radicals in addition to the SiF_4 molecule at N_e above 1.0×10^{11} cm^{-3}, and it is extinguished by the reaction with the SiF_4 molecule.

Figure 3-7 shows the F atom density as a function of N_e measured by AOES. The F density increased linearly with increasing N_e. The F atom would be produced with the dissociation of SiF_x (x = 1-4) such as reactions R1, 2, 5 and 6. Therefore, it is considered that dissociation in the production of F atom increased with increasing N_e.

3.3 Spatial distribution

Figure 3-8 shows the spatial distribution of SiF_4 molecule densities as a function of N_e. The SiF_4 molecule density at the center of the electrode was lower than that in the vicinity of the chamber wall due to the electron impact dissociation. The SiF_4 molecule densities were almost flat in the plasma region at a relatively high electron density and tended to increase gradually from the plasma region towards the wall.

Figure 3-9 shows the spatial distribution of SiF_2 radical densities as a function of N_e. The distribution of SiF_2 radical densities was almost flat in the plasma region and decreased outside the plasma region. SiF_2 density increased with increasing N_e from 3.8×10^{10} to 1.2×10^{11} cm^{-3} and slightly decreased with increasing N_e above 1.2×10^{11} cm^{-3} as shown in **Fig. 3-3**. This behavior was also observed all over the electrode. **Figure 3-10** shows the spatial distribution of SiF radical densities as a function of N_e. The distribution of SiF radical densities was almost flat in the plasma region and decreased outside the plasma region as observed in the SiF_2 radical. However, SiF and SiF_2 radical densities tend to decrease slightly from the plasma boundary towards the center of the electrode. **Figure 3-11** shows the spatial distribution of the electron density and the

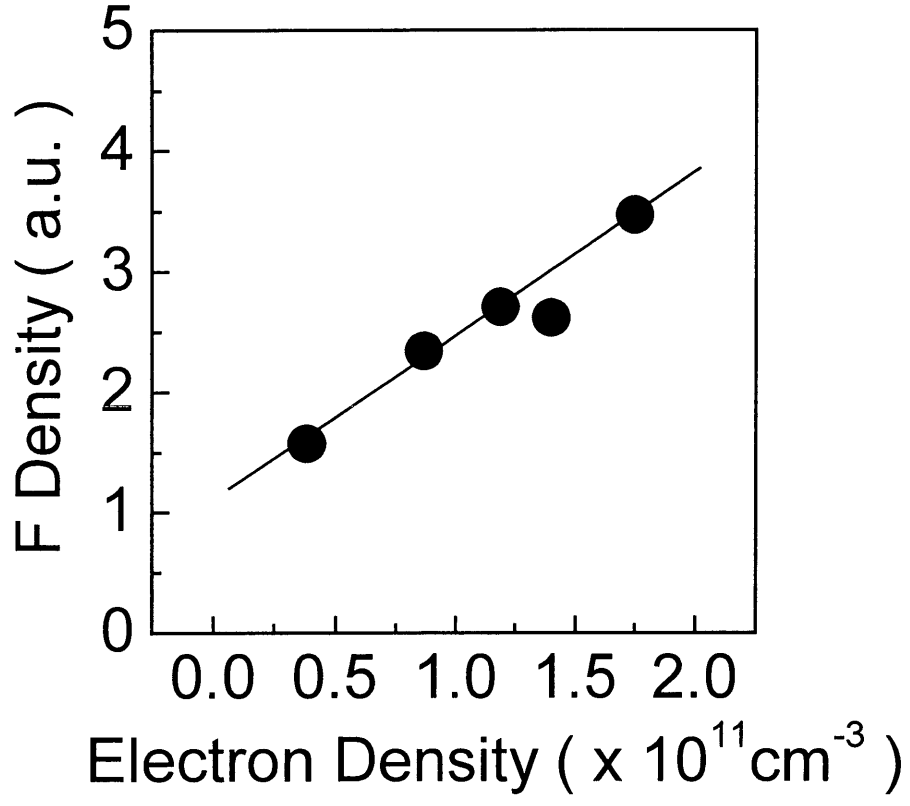

Figure 3-7 Relative density of SiF radical as a function of electron density.

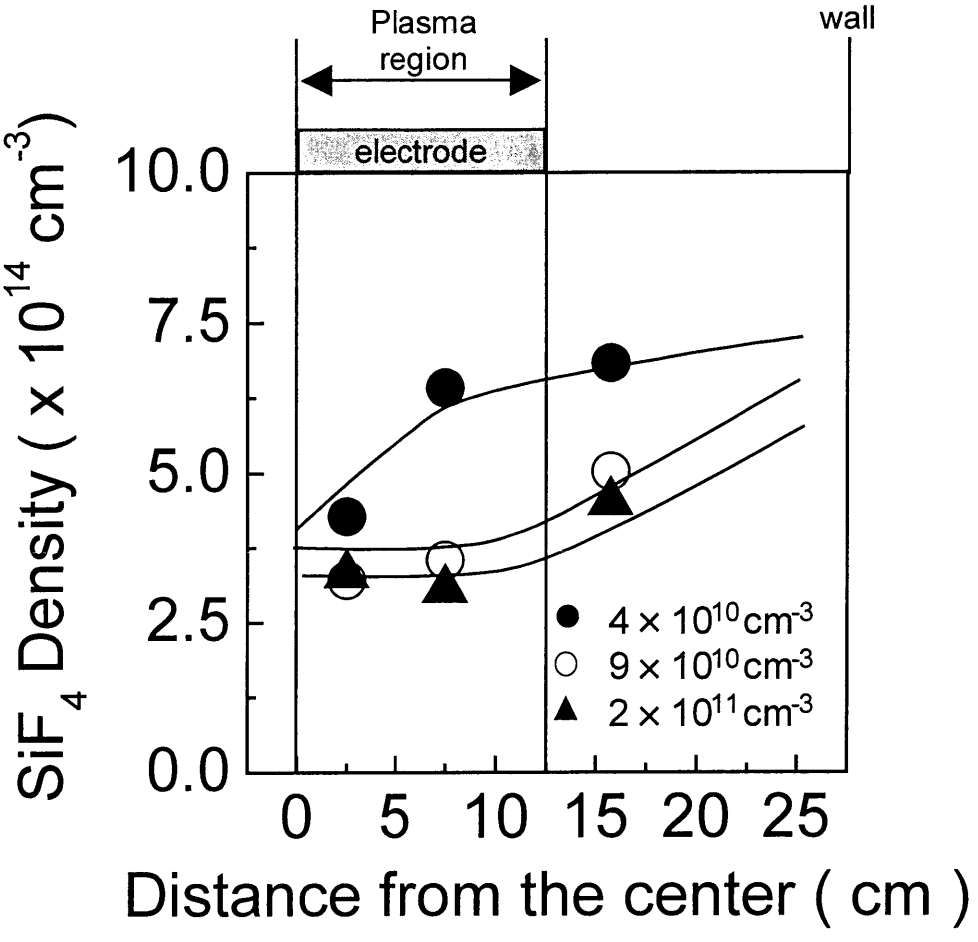

Figure 3-8 Spatial distribution of SiF_4 molecule density.

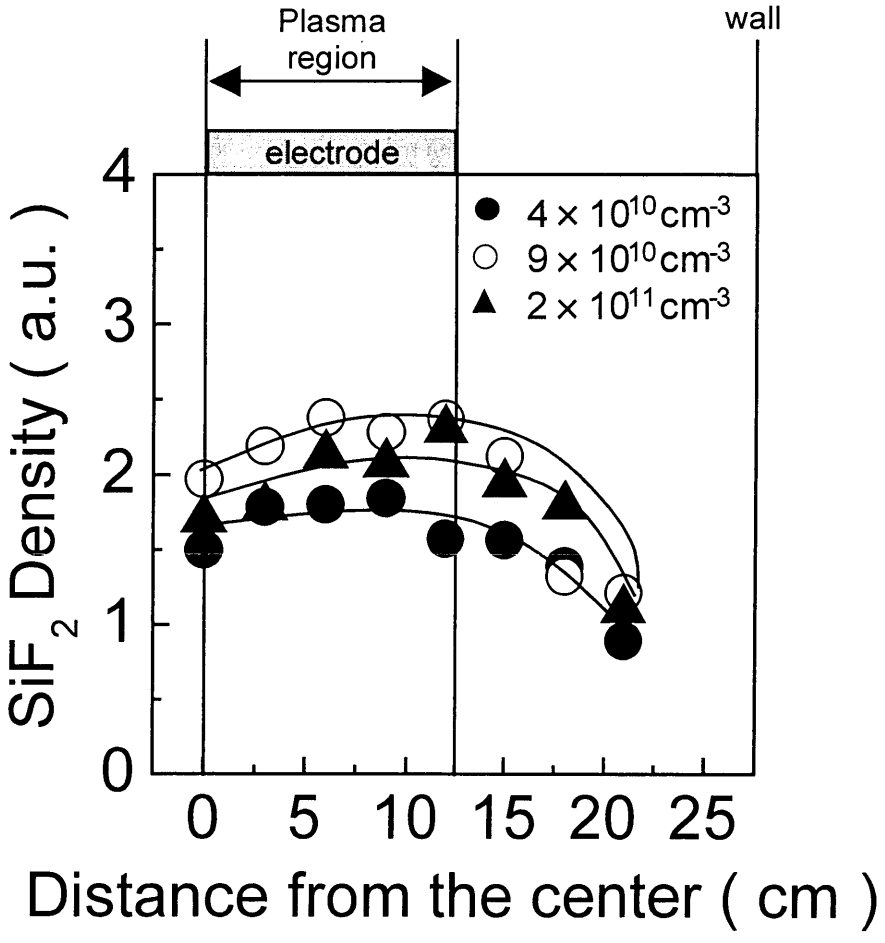

Figure 3-9 Spatial distribution of SiF_2 radical density.

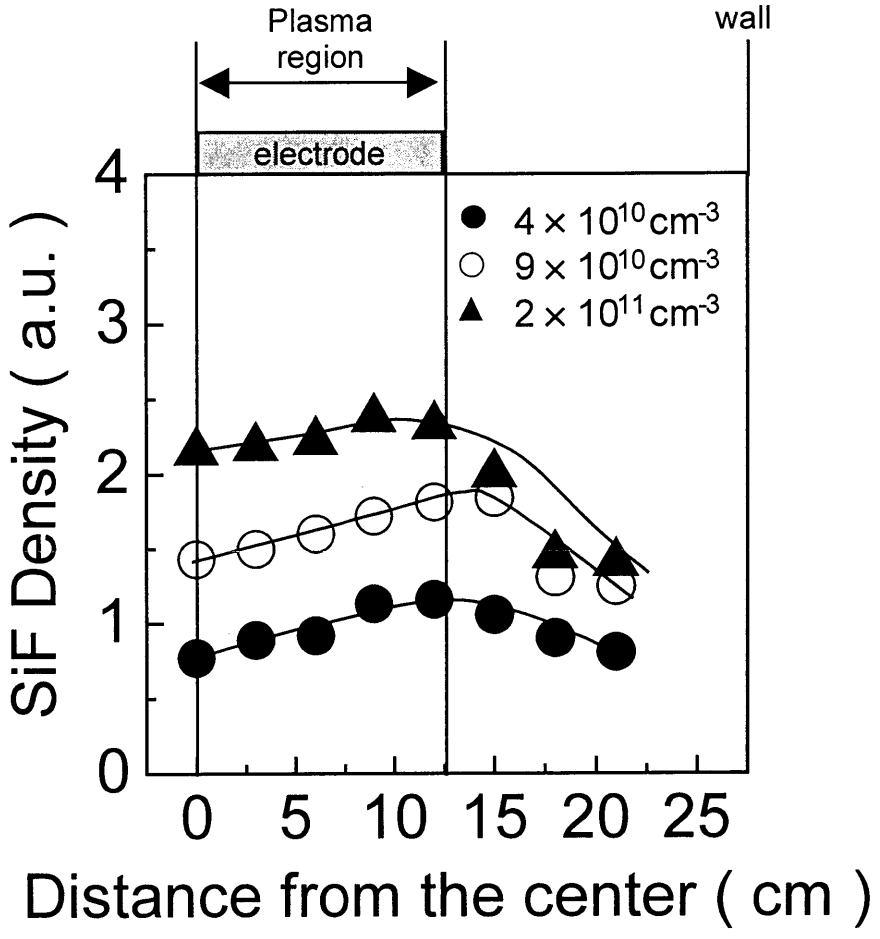

Figure 3-10 Spatial distribution of SiF radical density.

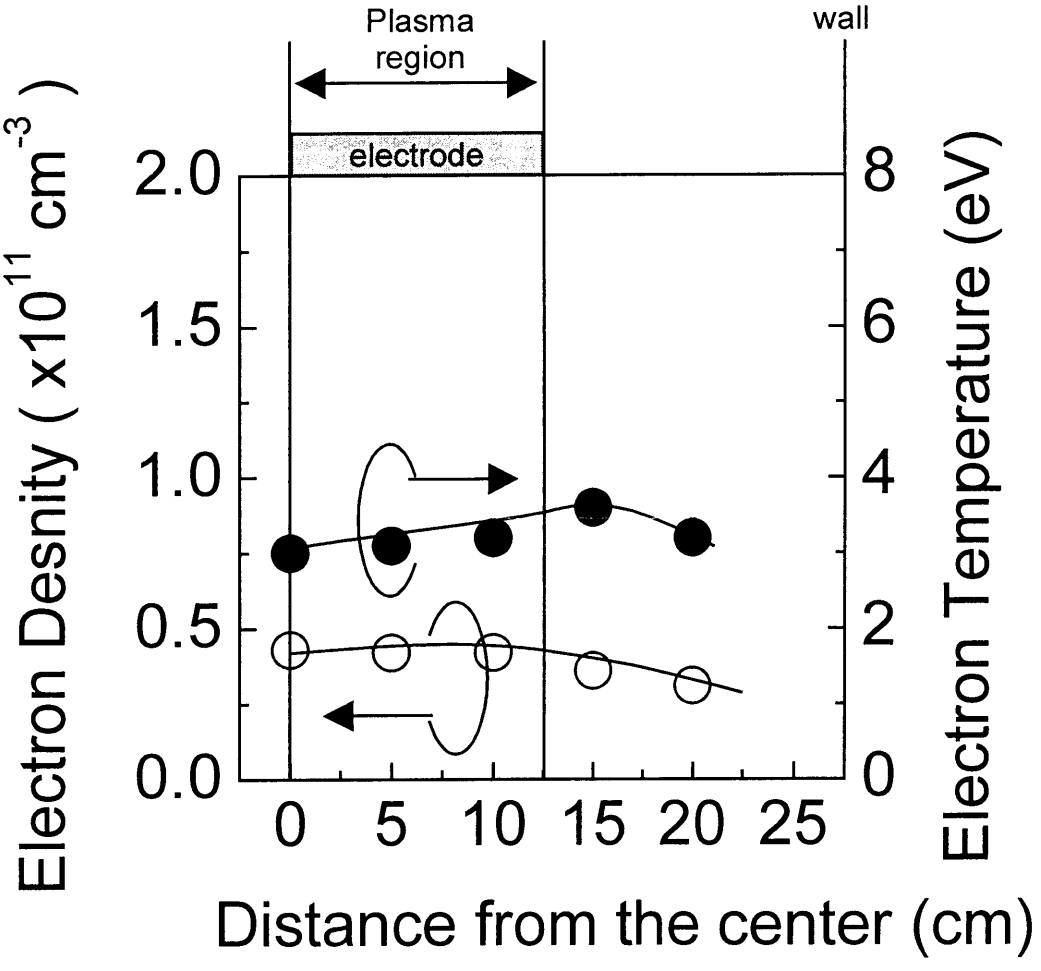

Figure 3-11 Spatial distribution of electron density and electron temperature.

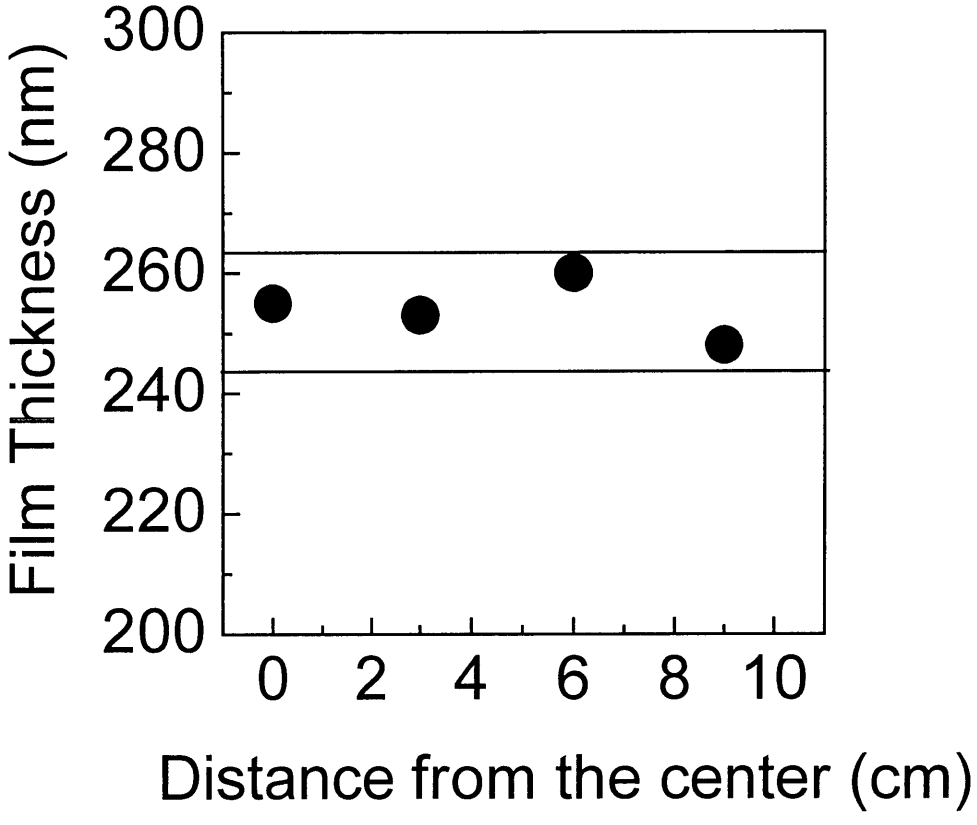

Figure 3-12 Uniformity of film thickness.

electron temperature. The condition is N_e of 3.8×10^{10} cm^{-3} at the center of the electrode and a pressure of 40 mTorr. The N_e is almost flat in the plasma region and decreased outside the plasma region, while the T_e was large at the plasma boundary region. Therefore, the production of SiF and SiF_2 radicals by electron impact dissociation was large, resulting that SiF and SiF_2 radical densities tend to decrease slightly from the plasma boundary towards the center of the electrode.

Figure 3-12 shows the film thickness. The deposition condition is VHF power of 1 kW, a pressure of 5.3 Pa, SiF_4 flow rate of 90 sccm, and deposition time of 15 minutes. The film thickness was between 248 and 260 nm, and was achieved the high uniformity deposition within 5 %. Therefore, it is clarified that VHF-CCP has an advantage for large area plasma process with high uniformity.

3.4 Summary

The densities of the Si, SiF and SiF_2 radical and the SiF_4 molecule in VHF 60 MHz SiF_4 CCP were measured as a function of N_e using LIF, IRLAS and UVAS techniques and the behavior of their radicals and the SiF_4 molecule was characterized using an internal plasma parameter of N_e. The SiF_4 density decreased with increasing N_e, and the dissociation ratio of SiF_4 was saturated at about 63 % at N_e of 8.7×10^{10} cm^{-3}. SiF_4 molecules are dissociated into SiF_x (x = 0-3) radicals by electron impact.

SiF_2 radical density decreased while Si and SiF densities increased with increasing N_e above 1.2×10^{11} cm^{-3}. The SiF_2 radical is mainly produced by electron impact dissociation of SiF_4 and extinguished by diffusion to the wall at N_e below 1.2×10^{11} cm^{-3} and by electron impact dissociation at N_e above 1.2×10^{11} cm^{-3}, resulting in the production of the Si atom and the SiF radical. SiF radical density increased linearly with increasing electron density. The SiF radical is mainly produced by electron impact dissociation of the SiF_4 molecule and extinguished by reaction with the SiF_4 molecule.

The total atom density of the Si atom was estimated to be of the order of 10^{10}-10^{11} cm^{-3}. The Si atom is mainly produced by electron impact dissociation of SiF_4 molecule

at N_e below 1.0×10^{11} cm^{-3} and by electron impact dissociation of SiF_x (x = 1-3) radicals in addition to the SiF_4 molecule at N_e above 1.0×10^{11} cm^{-3}

The spatial distribution of SiF, SiF_2 and SiF_4 densities was measured by LIF and IRLAS, showing an almost flat distribution inside the plasma region. Therefore, the film thickness was achieved the uniformity of 5 % in the diameter of 8 inchs.

The kinetics of species in SiF_4 plasma has been clarified quantitatively, providing important basic data on plasma processing.

References for chapter 3

[1] S. Lee and J. W. Park, J. Appl. Phys., **80**, 5260 (1996).

[2] H. Ohta, M. Hori, and T. Goto, J. Appl. Phys., **90**, 1955 (2001).

[3] T. Kamiya, K. Ro, C. M. Fortmann and I. Shimizu, Jpn. J. Appl. Phys., **38**, 5762 (1999).

[4] T. Tanaka, M. Tamura, and K. Tanaka, J. Mol. Struct., **413-414**, 153 (1997).

[5] K. Tanaka, Y. Akiyama, and T. Tanaka, J. Mol. Spectrosc., **137**, 55 (1989).

[6] G. L. Caldow, C. M. Deeley, P. H. Turner, and I. M. Mills, Chem. Phys. Lett., **82**, 434 (1981).

[7] K. Sugawara, F. Ito, T. Nakanaga, and H. Takeo, Chem. Phys. Lett., **232**, 561 (1995).

[8] G. A. Hebner, Appl. Surf. Sci., **192**, 161 (2002).

[9] G. Cunge, P. Chabert, and J. P. Booth, Plasma Sources Sci. Technol., **6**, 349 (1997).

[10] Y. Matsumi, S. Toyoda, T. Hayashi, M. Miyamura, H. Yoshikawa, and S. Komiya, J. Appl. Phys., **60**, 4102 (1986).

[11] C. W. Watson and K. G. McKendrick, Chem. Phys., **187**, 87 (1994).

[12] S. Vanhaelemeerch, J. Van Hoeymissen, D. Vermeylen, and J. Peeters, J. Appl. Phys., **70**, 3892 (1991).

[13] A.C. Stanton, A. Freedman, J. Worthhoudt, and P. P. Gasper, Chem. Phys. Lett., **122**, 190 (1985).

[14] J. P. Booth, G. Cunge, F. Neuilly, and N. Sadeghi, Plasma Sources Sci. Technol., **7**, 423 (1998).

[15] V. M. Khanna, G. Besenbruch, and J. L. Margrave, J. Chem. Phys., **46**, 2310 (1967).

[16] M. Nakamura, M. Hori, T. Goto, M. Ito, and N. Ishii, Jpn. J. Appl. Phys., **40**, 4730 (2001).

[17] T. Nakano and H. Sugai, J. Phys., D **26**, 1909 (1993).

[18] D. R. Harding and D. Husain, J. Chem. Soc. Faraday. Trans., **82**, 937 (1986).

[19] P. J. Chantry, J. Appl. Phys., **62**, 1141 (1987).

[20] R. C. Reid, J. M. Prausnitz, and T. K. Sherwood, *The Properties of Gases and Liquids* (McGraw-Hill, New York, 1977).

[21] R. A. Svehla, NASA Tech. Report No. R-132, Lewis Research Center, 1962.

[22] Y. Yamamoto, H. Nomura, T. Tanaka, M. Hiramatsu, M. Hori, and T. Goto, Jpn. J. Appl. Phys., **33**, 4320 (1994).

[23] Y Yamamoto, M. Hori, T. Goto and M. Hiramatsu, J. Vac. Sci. Technol., **A14**, 1999 (1996).

Chapter 4

Effect of excitation frequency on the translational temperature and absolute density of Si atoms in very high frequency capacitively coupled SiF_4 plasmas

4.1 Introduction

The Si atom is one of the most important species for SiF_4 based plasma processes, because the Si atom is a reactive species with a high surface loss probability.[1] Therefore, the Si atom in the plasma greatly affects the deposition of high-quality thin films and the precise etching of materials.

The neutral gas temperature is one of the most important plasma parameters for understanding and controlling the plasma process because the gas temperature has a considerable effect on the density profiles and the transport of reactive radicals. Moreover, many chemical reaction rates are strongly related to functions of the temperature of the species. Recently, an interest in the behavior of the neutral gas temperature has intensified, while the diagnostics of radical densities remain important to understand the plasma processes and to control them. Usually the diagnostics of radicals are performed using laser induced fluorescence and absorption spectroscopy, and the values measured have to be corrected for the partition function that is a function of the gas temperature to obtain the absolute densities. The temperature of neutral radicals provides us with a lot of important information from the standpoint of understanding the reaction chemistries. However, there has been few reported about the

dependence of the excitation frequency on the temperature of radicals in addition to their absolute densities in the VHF plasma.

In this chapter, the translational temperature and the absolute density of Si atoms in the VHF-CCP at 27 MHz and 60 MHz employing SiF_4 were investigated using ultraviolet absorption spectroscopy (UVAS) with a ring dye laser and a hollow cathode lamp, and the absolute density and the translational temperature of the SiF_4 molecule by infrared diode laser absorption spectroscopy (IRLAS). Based on these results, the effect of excitation frequency on the translational temperature of the Si atoms in VHF SiF_4 CCP is discussed.

4.2 Estimation of translational temperature of Si atom

Figure 4-1 shows the typical absorption coefficient profile of the Si atom. The experimental condition was an excitation frequency of 60 MHz and an electron density of 3.8×10^{10} cm^{-3}. The Doppler broadening was dominant for the absorption line in the present experimental condition. Therefore, the translational temperature of the Si atom was evaluated accurately from the width of the absorption profile $\Delta\upsilon_D$. The translational temperature of the Si atom, that is, T was obtained by the following equation,

$$\Delta\upsilon_D = 2\sqrt{2\ln 2}\upsilon_0\left(\frac{k_B T}{mc^2}\right)^{1/2}, \tag{4-1}$$

where υ_0 is the laser frequency at the line center, k_B is the Boltzmann constant, c is the speed of light, and m is the mass of Si atom, respectively. As shown in **Fig. 4-1**, the line represents calculated absorption coefficient profile of Si atom at a translational temperature of 600 K and a Si density of 3.4×10^9 cm^{-3} at the $3p^2{}^1D_2$ level and agreed well with the measured profile. Therefore, $\Delta\upsilon_D$ was 3.45 GHz and the translational temperature was estimated to be 600 K. The Si atom densities at the $3p^2{}^1D_2$ level measured using a hollow cathode lamp were almost the same value as those using a ring dye laser. Therefore, both measurement techniques were successfully applied to evaluate the Si atom density in the plasma.

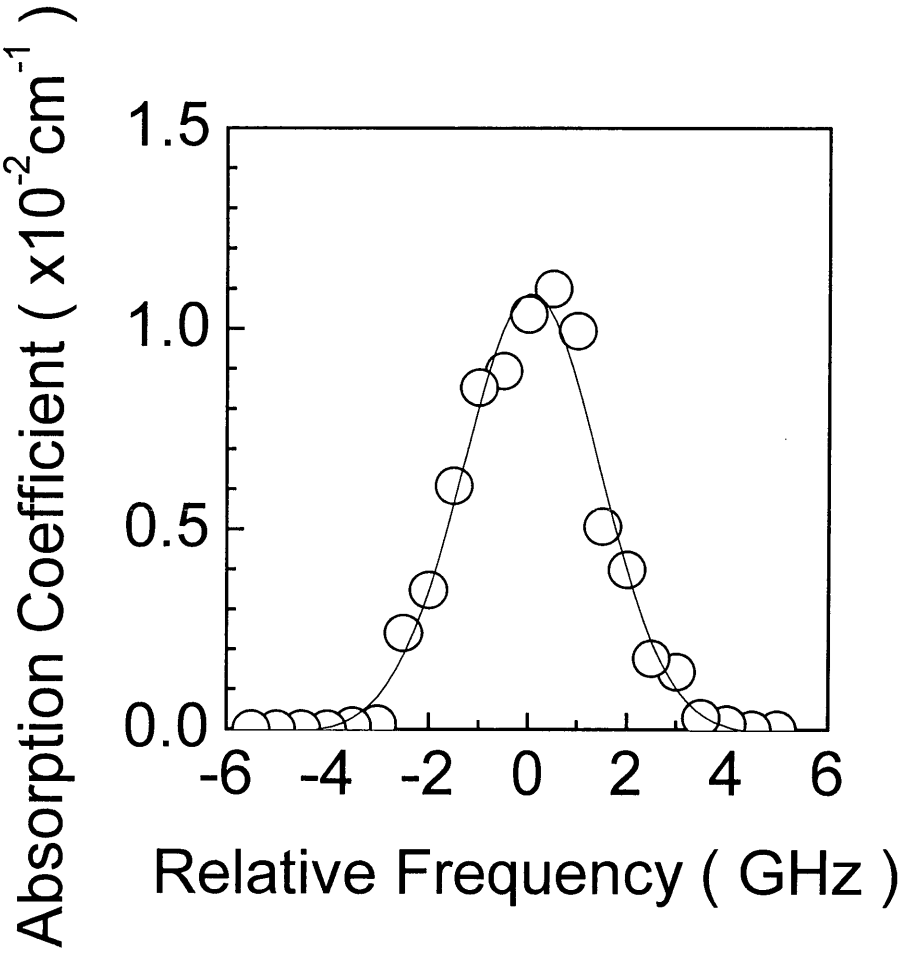

Figure 4-1 The absorption coefficient profile of the Si atom at the transition of $3p^{21}D_2$ - $3p4s^1P_1$ (288.2 nm).

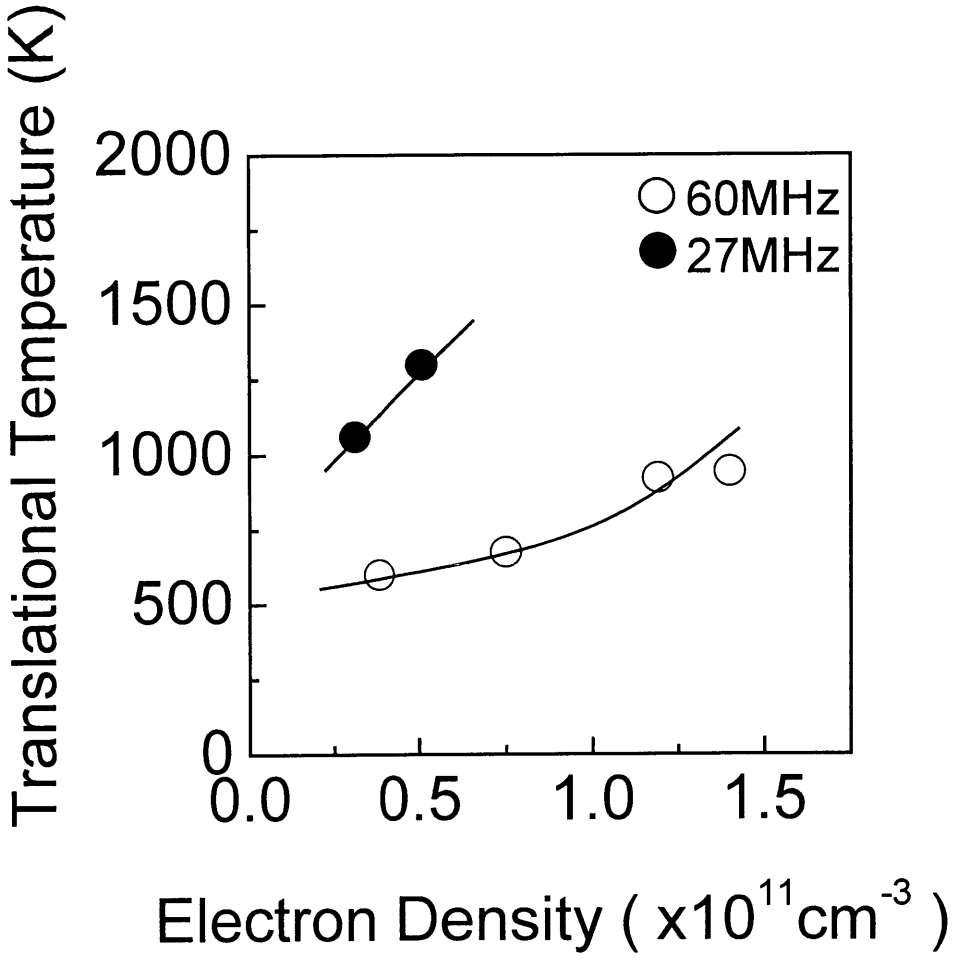

Figure 4-2 Si atom translational temperature as a function of electron density.

Figure 4-2 shows the translational temperature of the Si atom as a function of electron density. The electron densities obtained in **Figure 4-3** were used as the horizontal axis. The temperatures of the Si atom at 27 MHz and 60 MHz increased with increasing the electron density from 1060 K to 1300 K and from 600 K to 940 K, respectively. The temperatures at 27 MHz were considerably larger than those at 60 MHz. Moreover, the change in temperature slope agreed well with that of the Si atom densities at electron densities above 1.0×10^{11} cm^{-3} at 60 MHz as described below. Here, the spatially line-averaged temperatures of the Si atom express the temperature profile of the Si atom in the plasma region, because of the high loss probability of the Si atom.

4.3 Effect of excitation frequency on the translational temperature and absolute density of Si atoms

Figure 4-3 shows the electron density (N_e) and the electron temperature (T_e) as a function of VHF power. The plasma condition was maintained at a total pressure of 5.3 Pa and a SiF_4 flow rate of 90 sccm. The N_e at both frequencies increased with increasing VHF power from 0.5 kW to 2.0 kW. The N_e at 60 MHz was larger than that at 27 MHz at the same VHF power. It is reported that raising the excitation frequency at a constant amplitude of the applied voltage increases the plasma density approximately in proportion to the square of the excitation frequency.[2] In this study, however, the N_e at 60 MHz was approximately double that at 27 MHz, since the amplitude of the applied voltage was different. T_e decreased slightly from 3 eV to 2.3 eV at 60 MHz and from 4.1 eV to 3.8 eV at 27 MHz with increasing the VHF power.

Figure 4-4 shows the total Si atom density as a function of electron density. The total Si density was estimated by the Si density ratio at the $3p^2$ level from the assumption of Boltzmann distribution that is a function of the translational temperature, and the translational temperatures as shown in **Fig. 4-2** were used for estimating Si densities.[3] The Si atom densities at 27 MHz were larger than those at 60 MHz at the same N_e due to the high T_e at 27 MHz. It is noteworthy that the Si atom densities at both frequencies

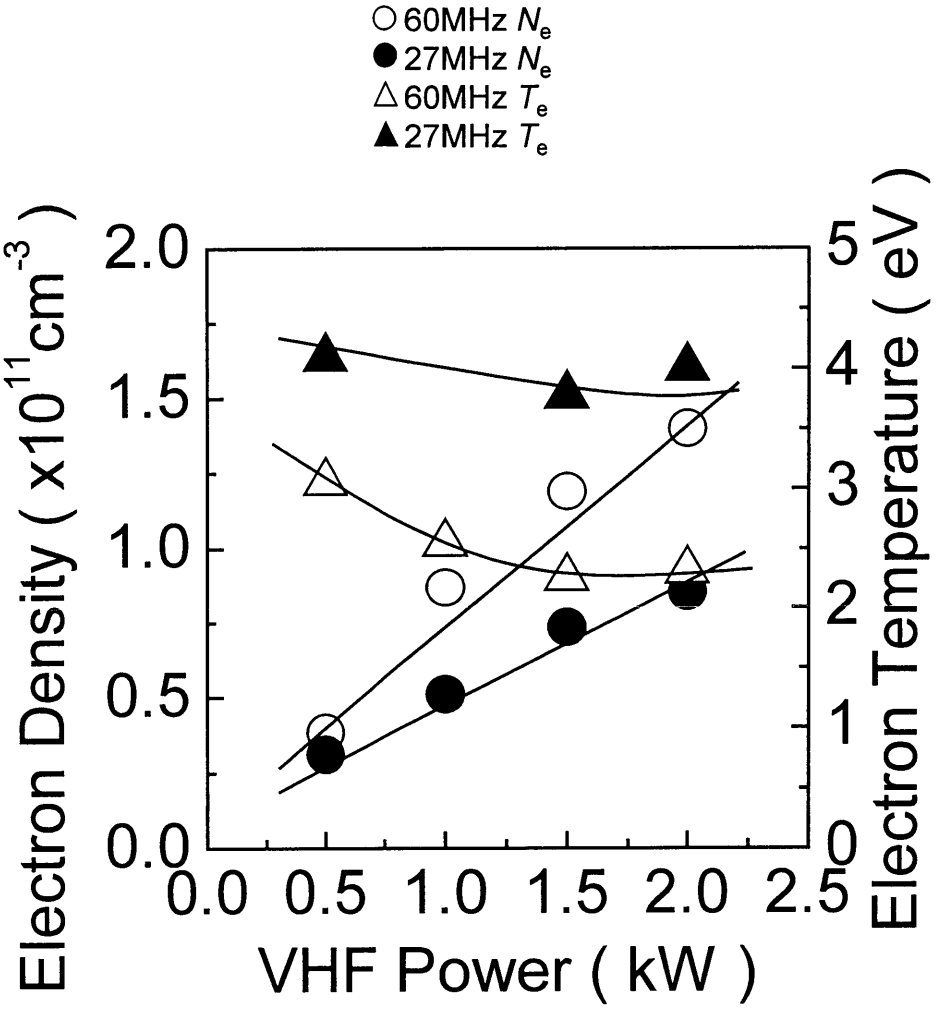

Figure 4-3 Electron density and electron temperature as a function of VHF power.

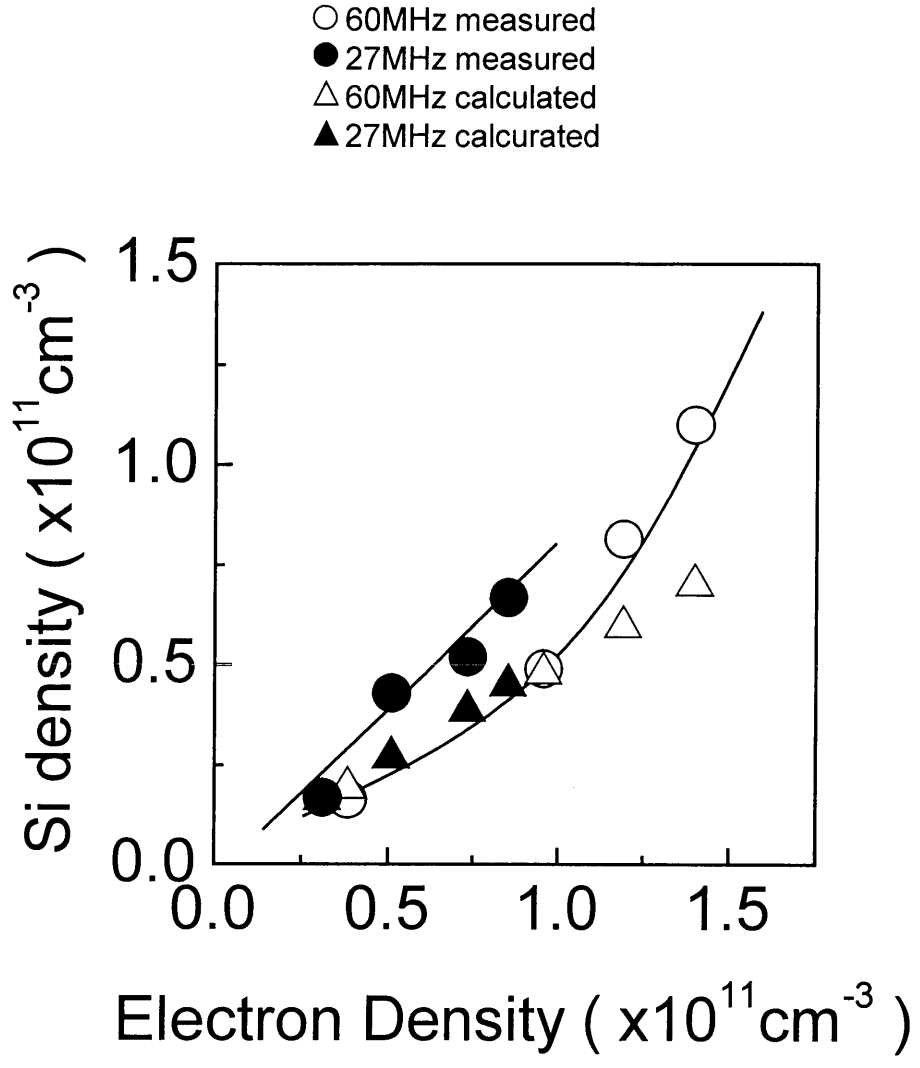

Figure 4-4 Si atom density as a function of electron density.

were increased linearly with increasing N_e up to $1.0 \times 10^{11}cm^{-3}$, and the gradient of the Si atom density was changed remarkably at N_e of $1.0 \times 10^{11}cm^{-3}$ at 60 MHz. Here, the production and loss processes of Si atoms were the electron impact dissociation of SiF_x (x = 1-4) and the reaction with the SiF_4 molecule, respectively, as described in chapter 3. In this study, the Si atom densities were calculated on the assumption that the main production of Si atom was the electron impact dissociation of SiF_4 molecule and the loss was the reaction with SiF_4 molecule, and represented by triangles as shown in **Fig. 4-4**. The SiF_4 densities measured by IRLAS were used as described below. The gradients of measured Si densities at N_e above 1.0×10^{11} cm^{-3} at 60 MHz and the Si densities at 27 MHz were estimated as being larger than those of calculated densities. As a result, the Si atoms were produced more by the electron impact dissociation of SiF_x (x = 1-3) radicals than the SiF_4 molecules at 27 MHz and high N_e above 1.0×10^{11} cm^{-3} at 60 MHz, because the SiF_4 molecules were depleted as described below.

Figure 4-5 shows the SiF_4 molecule density as a function of electron density. The SiF_4 density at 27 MHz decreased up to N_e of 5×10^{10} cm^{-3}, and saturated with further increasing N_e. The dissociation ratio of the SiF_4 molecules at 27 MHz was estimated about 89% at N_e of 8.5×10^{10} cm^{-3}, while the dissociation ratio of the SiF_4 molecules at 60 MHz was 63%. The SiF_4 density at 27 MHz was smaller than that at 60 MHz at the same N_e, since T_e at 27 MHz was larger than that at 60 MHz as shown in **Fig.4-3**.

4.4 Mechanism for translational temperature of Si atom

The mechanism for the gas temperature has been reported by simulations and models. Here, some of these reports are shown as follows.

Kiehlbauch *et al.* reported a simulation and experiment of the gas temperature in the PPA (point-of-use plasma abatement) system using CF_4 and O_2 gases. [4] The neutral temperature were measured using the rotational spectrum of an electronic transition between an excited state and a ground state by OES. The rotational temperature was estimated by assuming a Boltzmann distribution of the rotational energy, and assumed

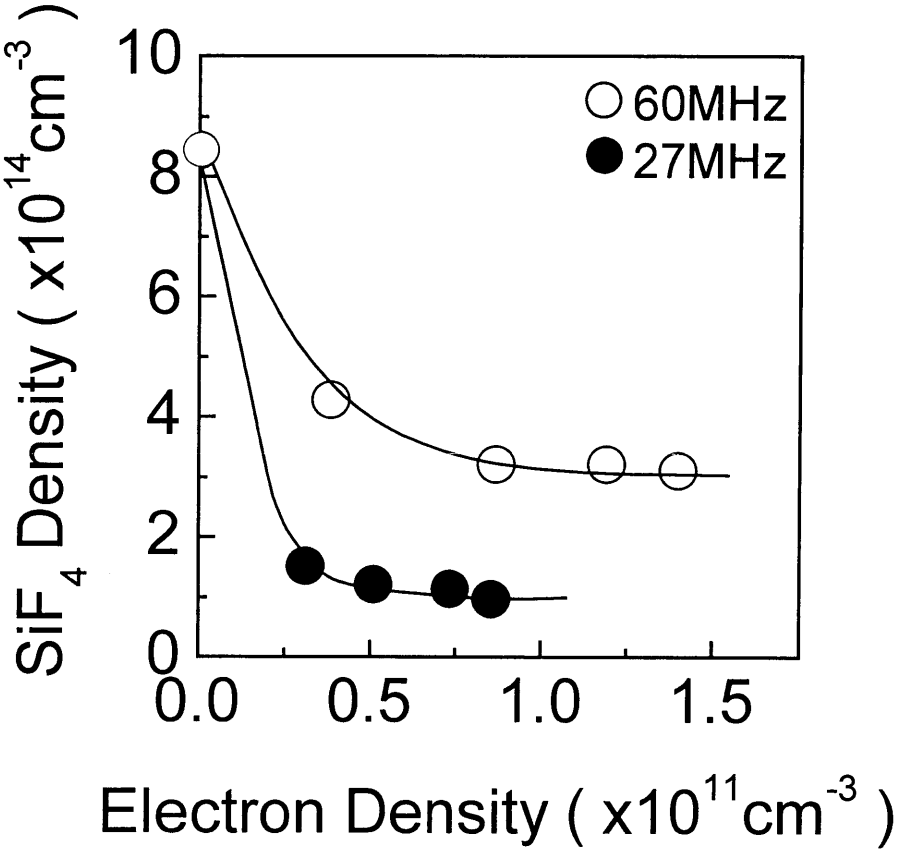

Figure 4-5 SiF_4 molecule density as a function of electron density.

to be in equilibrium with the translational temperature. This model was described as follows.

The neutral balance written in terms of mass density is

$$\frac{\partial}{\partial t}(\rho c_v T)+\nabla\cdot(\rho c_v T u)+\nabla\cdot q=-p(\nabla\cdot u)+S_n. \tag{4-2}$$

The conductive heat flux is expressed by

$$q=-\kappa\nabla T, \tag{4-3}$$

where ρ is the total neutral mass density, c_v is the mixture heat capacity, T is the neutral temperature, u is the mass-average convective velocity, p is the total pressure, and κ is the mixture thermal conductivity. The summation is over all neutral species. The second term and third term on the left-hand side of eq. (4-2) represent the transport of energy by convective flow and thermal conduction. The thermal conductivity is a function of temperature and mixture composition. The first term on the right-hand side is the pressure-volume work.

S_n is the source term for collisional energy transfer from the charged species to the neutrals,

$$S_n=\sum_n(E_n+FC_n+GP_n+IE_n). \tag{4-4}$$

The terms FC_n, IE_n, GP_n, and E_n represent the heating due to the Frank-Condon effect, the electron impact vibrational excitation of the neutral molecules, the heating due to gas phase thermochemistry, and ion/neutral charge exchange and elastic collisions, respectively. The neutral gas is assumed to follow Maxwell-Boltzmann statics.

Frank-Condon heating for species n is expressed by

$$FC_n=\sum_r k_r N_e N_n \Delta E_r, \tag{4-5}$$

where the summation is over all electron impact dissociation reactions for species n that release Frank-Condon energy, k_r is the rate coefficient for the reaction involving species n, N_e and N_n are the electron and neutral number densities, respectively, and ΔE_r is the Frank-Condon energy released in reaction r. The Frank-Condon effect occurs when an

electron strikes a neutral molecule with sufficient energy to raise the molecule to a dissociative state. In general this energy is greater than the dissociation energy, which results in the dissociated fragments obtaining extra kinetic energy.

Electron impact vibrational excitation was included only the one excited state of CF_4 and the three excited states of O_2.

The termodynamics of the gas phase chemistry is another source of neutral heating. This is the enthalpy of reaction at the neutral temperature times the rate of the reaction.

The final neutral heating term represents gas phase collisions with the ions. Ions transfer energy to the neutral through change exchange collisions and elastic collisions. Ion/neutral collisions were handled as a constant due to the hardsphere model for collision cross section. The total rate of ion/neutral energy transfer is calculated by integrating over ion and neutral velocity distributions. The ion/neutral energy transfer is dominated by the sheaths, where the ion velocity is high.

The simulation shows that the power transferred to the neutrals is typically 25-30 % of the rf power. Frank-Condon heating and ion/neutral heating are dominant for the heating mechanism, each accounting for about 40 % of the neutral energy source term. Gas phase chemistry and vibrational excitation are each 10 % of the neutral energy source term. It is found that PPA system using CF_4 and O_2 gases is dominated by electron impact dissociation.

Cruden *et al.* have reported the neutral temperature in $CF_4/O_2/Ar$ ICP.[5] The rotational temperature of CF radical was estimated from *B-X* band system near 203 nm by OES.

The dependence of gas temperature on pressure can be estimated by considering the steady-state heat balance, and approximated expressed by

$$\int_V Q \mathrm{d}V = -k_{\mathrm{gas}} \nabla T \cdot S, \tag{4-6}$$

where the heat input Q is balanced by conduction of heat through the gas to the chamber walls and k_{gas} is the thermal conductivity. If the heat input is dominated by electron impact processes, then Q will be approximately proportional to the product of electron

and neutral densities.

One of primary production mechanisms of CF is the electron impact dissociation of CF_4. The energy threshold for CF_4 dissociation to CF is near 20 eV, although the thermodynamic heat of reaction for this process is only 14.7 eV, meaning that approximately 5.3 eV of additional energy is imparted into neutral reaction products. This was termed Frank-Condon heating. This excess energy will be divided into translational energy for fluorine atoms and rotational, vibrational, and translational modes of CF. For a rough estimate of how much energy goes into CF, it is assumed that the translational energy is partitioned among the CF and F species and CF will have about 0.77 eV (9000 K) of translational energy, immediately following CF_4 dissociation.

Donnelly *et al.* reported the rotational temperature of N_2 as a trace gas from the $C^3\Pi_u$-$B^3\Pi_g$ near 337 nm in the Cl_2 ICP. [6] The mechanism for gas heating was described as follows.

Power (W/cm^3) is transferred from the electrons to the gas (Cl and Cl_2) by

(a) dissociation

$$W_d = 2k_d n_e n_{Cl_2} \delta_d , \tag{4-7}$$

(b) rotational excitation

$$W_{rot} = n_e n_{Cl_2} \left(\frac{2E_e}{m_e} \right)^{\frac{1}{2}} \sigma_{rot}(E_e) \delta_{rot}(e_e) f_e(e_e) dE_e , \tag{4-8}$$

(c) momentum transfer

$$W_m^g = \frac{\sqrt{8} n_e n_g}{M_g m_e} \int E_e^{\frac{3}{2}} \sigma_m(E_e) f_e(E_e) dE_e , \tag{4-9}$$

where k_d is the electron impact dissociation rate constant (dissociative attachment and dissociative ionization contribute much less), δ_d is the energy released into each Cl atom in Cl_2 dissociation, $\sigma_{rot}(E_e)$ is the total rotational scattering cross section, $\delta_{rot}(E_e)$ is the energy converted into Cl_2 rotational energy, $f_e(E_e)$ is the electron energy (E_e) distribution function, $\sigma_m(E_e)$ is the momentum transfer cross section for Cl or Cl_2, and n_g and M_g are the number density and mass of Cl or Cl_2, respectively. Consequently, the

energy released in Cl_2 dissociation dominates electron induced heating.

Power transfer from the ions occurs when they collide (including charge exchange) with the neutral gas in the presheath region,

(d) ion heating

$$W_i = n_{i,s}^{+} v_B \left(\delta_{ips} + \delta_{iw}\right)\frac{A}{V}, \tag{4-10}$$

where $n^{+}_{i,s}$ is the positive ion density at the sheath edge, v_B is the Bohm velocity, δ_{ips} is the energy transferred to neutrals per ion collision in the presheath, δ_{iw} is the energy of the ion (presumably neutralized) scattering from the walls and wafer, and V and A are the total plasma volume and effective area of the chamber. The ion heating was small from the calculation. However, W_i scales with n_i+T_e which decreases with increasing pressure. Near rf-biased electrodes and in plasmas with higher T_e, the mechanism should be more important, even if δ_{iw} is less than 10 % of the incident ion energy. Presumably, this mechanism plays a major role in the cooler Ar plasmas.

Heat is lost by collision of hot neutrals at the chamber walls. Because of the large thermal gradients, the temperature-dependent thermal conductivity of the gas (k_g), the higher k_g for Cl vs Cl_2, the concentration gradients of Cl and Cl_2 near the walls, and other complexities in the heat input process (e.g., its spatial dependence).

As a result, they concluded that heating is most likely due to primarily to the energy released in Cl_2 dissociation.

Here, electron impact dissociation as in the following reaction is considered for explaining the Frank-Condon effect.[7]

$$AB + e \rightarrow A + B + e\,.$$

The variety of some processes is illustrated in **Figure 4-6**. In collisions a or a', the v=0 ground state of AB is excited to a repulsive state of AB. The required threshold energy (ε_{thr}) is ε_a for collision a, and $\varepsilon_{a'}$ for collision a'. This energy leads to energy of products (here, A and B) after dissociation. Typically ε_a-ε_{thr} is few volts; consequently, hot neutral fragments are typically generated by dissociation processes. In collision b, the ground state AB is excited to an attractive state of AB at an energy ε_b that exceeds the binding

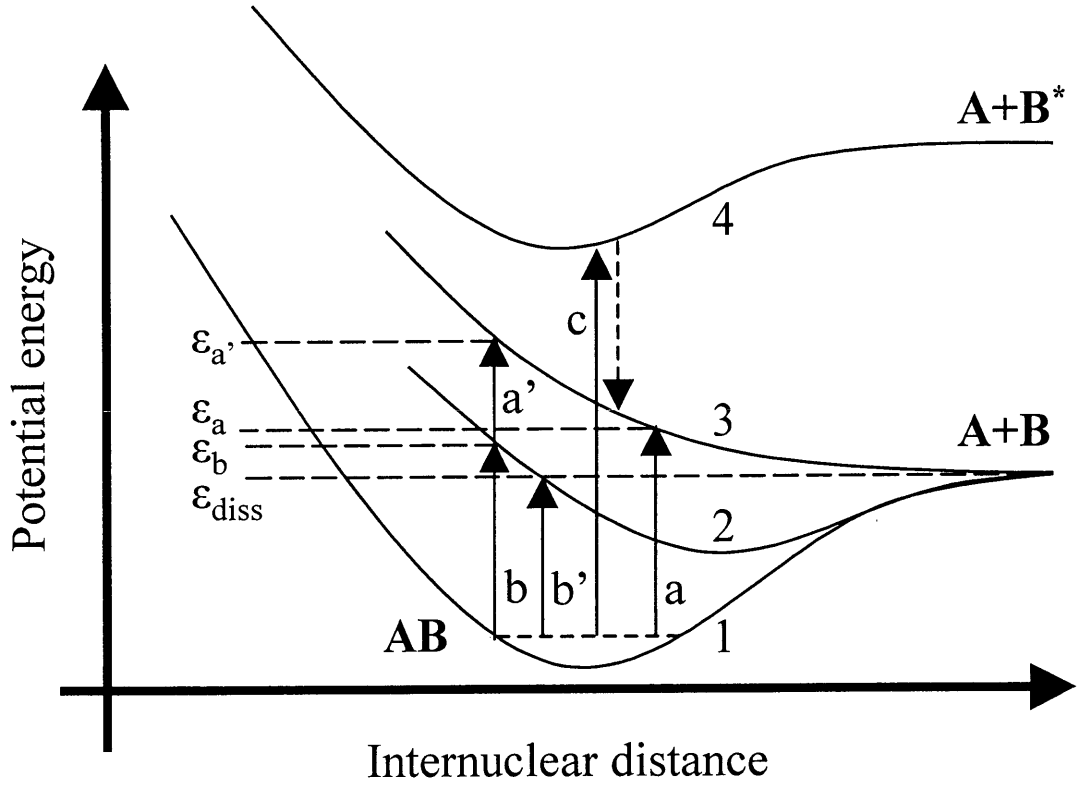

Figure 4-6 Frank – Condon effect.

energy ε_{diss} of the AB molecule, resulting in dissociation of AB with fragment energy ε_b-ε_{diss}. In collision b', the excitation energy $\varepsilon_{b'}$ equals ε_{diss}, and the fragments have low energies; hence this process creates fragments having energies ranging from essentially thermal energies up to $\varepsilon_{b'}$-ε_{diss} with few bolts. In collision c, the AB atom is excited to the bound excited state AB* (labeled 4), which subsequently radiates to the unbound AB state (labeled 3), which then dissociated. The threshold energy required is large, and the fragments are hot.

In the SiF_4 plasma, the Si atom produced from SiF_4 molecule reacted with the SiF_4 molecule immediately, because the reaction rate constant was 2.2×10^{-11} cm^3s^{-1},[8] therefore, it is assumed that the heat loss of thermal diffusion to the wall is negligible. The translational temperatures would increase with increasing SiF_4 density. However, the translational temperature of 1060 K at 27 MHz was larger than that of 600 K at 60 MHz, although the SiF_4 density of 1.5×10^{14} cm^{-3} at 27 MHz was smaller than that of 4.3×10^{14} cm^{-3} at 60 MHz. It is assumed that the major heating process of Si atoms is the Franck-Condon effect. This effect occurs when the electron collides with a neutral molecule with sufficient energy to raise the molecule to a dissociative state. This energy is larger than the electron impact dissociation energy of the neutral molecule. Consequently, dissociated fragments with excess energy are produced. This excess energy is divided into translational energy.

T_e increased with decreasing the excitation frequency, and so the Si atoms were produced more from radicals such as SiF_x (x = 1-3) radicals than SiF_4 molecules by the electron impact dissociation due to depletion of the SiF_4 molecule. Therefore, the hot Si atom is created due to the difference of energy of Si atom produced from electron impact dissociation of SiF_x (x = 1-3) radicals and SiF_4 molecules., resulting in an increase in translational temperature of the Si atoms.

4.5 Summary

In summary, UVAS techniques employing a ring dye laser and a hollow cathode lamp were applied to investigate the effects of excitation frequency on the density and the translational temperature of the Si atom in CCPs excited with VHF at 27 MHz or 60 MHz employing a SiF_4 gas. The translational temperature of the Si atom was very high, a value above 1060 K, especially at 27 MHz, and this was explained by the heating effect due to Frank-Condon effect and the hot Si atom is created due to the difference of energy of Si atom produced from electron impact dissociation of SiF_x (x = 1-3) radicals and SiF_4 molecules. These results of the high temperature of Si atoms are very important not only for the application of VHF plasma, but also for fundamental reactions in the plasma process.

References for chapter 4

[1] T. Nakano and H. Sugai, J. Phys. D : Appl. Phys., **26** 1909 (1993).

[2] S. Oda, Plasma Souces Sci. Technol., **2**, 26 (1993).

[3] Y. Yamamoto, H. Nomura, T. Tanaka, M. Hiramatsu, M. Hori and T. Goto, Jpn. J. Appl. Phys., **33**, 4320 (1994).

[4] M.W. Kiehlbauch and D. B. Graves, J Appl. Phys., **89**, 2047 (2001).

[5] B. A. Cruden, M. V. V. S. Rao, M. Surendra, P. Sharma and M. Meyyappan, Appl. Phys. Lett., **81**, 990 (2002).

[6] V. M. Donnelly and M. V. Malyshev, Appl. Phys. Lett., **77**, 2467 (2000).

[7] M. A. Lieberman and A. J. Lichtenberg: *Principles of Plasma Discharges and Materials Processing* (John Wiley & Sons, Inc. New York 1994).

[8] D. R. Harding and D. Husain, J. Chem. Soc. Faraday. Trans., **82,** 937 (1986).

Chapter 5

Effect of excitation frequency on absolute density and translational temperature of Si atom in SiH_4 plasma with Ar, H_2, and N_2 dilution gases

5.1 Introduction

SiH_4 based plasmas have been employed with some kinds of dilution gases such as noble gases, N_2 and H_2 gases. For example, SiH_4/H_2 plasma is used for depositing microcrystalline silicon films (μc-Si) and hydrogenated amorphous silicon films (a-Si:H) in thin film transistors (TFTs) and solar cells.[1],[2] SiH_4/N_2 plasma is used for synthesizing silicon nitride films as a passivation layer of Organic Light Emitting Devices (OLEDs) and a gate insulating films of ultralarge scale integrated circuits (ULSIs).[3],[4] It is well known that neutral radical species (Si_xH_y) are responsible for the thin-film formation in SiH_4 based plasma. It is indispensable for synthesizing these functional films with high quality to understand and control the behaviors of neutral radical species in reactive plasmas. Therefore, in order to understand the mechanism of thin-film formation quantitatively, it is demanded strongly to characterize the neutral radicals in the plasma.

The Si atom in SiH_4 based plasma processes influences the film formation because the Si atom is one of most reactive species with the high loss probability in the gas phase and surface. Yamamoto *et al.* reported that the contribution of Si atom to the thin-film formation was about 3.3 times as large as that of SiH_3 radical in the ECR SiH_4/H_2 plasma.[5] Murata *et al.* reported that the growth of microcrystalline silicon with preferential crystalline orientation would be dependent on the balance between silicon and hydrogen atom densities in the pulse modulated ultrahigh frequency SiH_4/H_2

plasma.[6] Moreover, the Si atom reacts with the SiH_4 molecule with a high reaction rate and produces the higher order silane-related radicals. These radicals with high loss probability make a significant influence on the film quality such as defects, which causes the photo-induced degradation of a-Si:H films for the solar cell even if the density of these radicals is low in the plasma.[7] Therefore, the quantitative information of behaviors of Si atoms in SiH_4 based plasma is very important for the formation of high quality-thin films.

In the SiH_4/H_2 plasma for hydrogenated amorphous silicon, many research by using VHF-CCP have been investigated as described in chapter 1. For example, the increase of the excitation frequency decreases the sheath thickness,[8] resulting in the reduction of ion bombardment energy incident on the a-Si:H and μc-Si films, which is usually favorite for the synthesis of high quality films. Takai *et al.* reported that increasing excitation frequency led to reducing the T_e, resulting in the reduction of the high order silane-related radicals in the plasma. Accordingly, a-Si:H films were formed with considerably less photo-induced degradation.[9] The increase of the excitation frequency, therefore, has given the great advantages to the thin films formation. The good performances of VHF-CCP processes in synthesizing thin films have been reported. However, it has not been studied enough on the plasma chemistry such as radical density, radical temperature, and so on in VHF-CCP. The plasma chemistry brought about in the VHF-CCP and the effect of the excitation frequency on radical species still has never been clarified in detail. Therefore, the diagnostics of radicals in VHF-CCP is indispensable and hereby to elucidate the neutral radical chemistry in VHF-CCP is very important.

Up to now, Tanaka *et al.* measured the absolute density and the translational temperature of Si atoms in the RF (13.56MHz) SiH_4/Ar plasma using the ultraviolet absorption spectroscopic technique employing a ring dye laser.[10] The translational temperatures were varied from 380 K to 700 K increasing SiH_4 flow rate ratio from 0 to 100 %. In chapter 4, the effect of excitation frequencies above 13.56 MHz on the translational temperature of Si atoms in VHF-CCP employing SiF_4 gas was measured. The translational temperatures of Si atoms at the excitation frequency of 27 MHz were

larger than those at 60 MHz at the same N_e. The results were explained by the difference in the energy of Si atoms released from the electron impact dissociation of SiF_x (x = 1-3) radicals and SiF_4 molecule. Therefore, it is very important to clarify the dependence of the excitation frequency and the effect of dilution gas on the temperature of Si atoms in the VHF-CCP employing the SiH_4 based plasma. As long as we know, the characteristics of the translational temperature of Si atoms have never been reported in VHF SiH_4 based plasma with dilution gases.

In this chapter, the absolute density and the translational temperature of Si atoms in the VHF-CCP employing SiH_4 were investigated using the ultraviolet absorption spectroscopy (UVAS) with a ring dye laser and a hollow cathode lamp. The absolute density of SiH_4 molecule was measured by infrared diode laser absorption spectroscopy (IRLAS). Based on these results, the effect of the different excitation frequencies (27 or 60 MHz) and the dilution of Ar, N_2, and H_2 gases are discussed.

5.2 Behavior of Si atom density

Figure 5-1 shows the electron density (N_e) as a function of SiH_4 flow rate ratio with dilution gases of Ar, N_2, and H_2 in 27 MHz or 60 MHz plasmas. The plasma condition was maintained at a total pressure of 11 Pa, a VHF power of 1500 W, and a dilution gas flow rates of 100 sccm. The substrate temperature was kept below 373 K by using helium-backside gas cooled by a water flow. The SiH_4 flow rate was varied from 0 to 15 sccm. N_e in the SiH_4/Ar and SiH_4/N_2 plasmas were of the order of $10^{11}cm^{-3}$, on the other hand, N_e in the SiH_4/H_2 plasma was of the order of $10^{10}cm^{-3}$. N_e in the SiH_4/Ar plasma decreased with increasing SiH_4 flow rate ratio, while the densities in the SiH_4/N_2 and SiH_4/H_2 plasmas were almost constant. The rate coefficients of the total electron impact ionization for SiH_4, Ar, N_2, and H_2 were calculated to be 2.8×10^{-11} cm^3s^{-1}, 1.4×10^{-10} cm^3s^{-1}, 7.9×10^{-11} cm^3s^{-1}, and 7.8×10^{-11} cm^3s^{-1}, respectively.[11]-[13] In the SiH_4/Ar plasma, the decrease in N_e with increasing SiH_4 flow rate ratio is due to the low ionization rate coefficient of SiH_4 in comparison with that of Ar. The constant value in N_e with increasing SiH_4 flow rate ratio in the SiH_4/N_2 and SiH_4/H_2 plasma is due to the

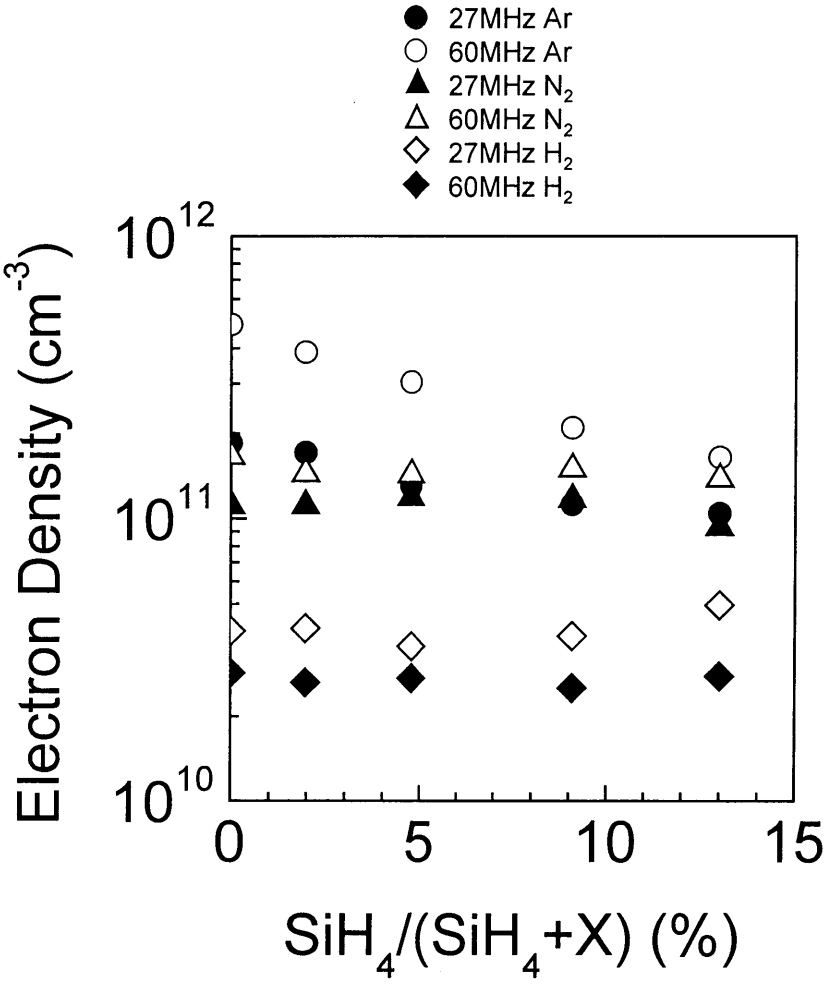

Figure 5-1 Electron density as a function of SiH_4 flow rate ratio.

same order of the ionization rate coefficients. N_e at 60 MHz were larger than those at 27 MHz in each dilution plasma.

Figure 5-2 shows the absolute density and emission intensity of Si atoms as a function of SiH_4 flow rate ratio with dilution gases of Ar, N_2, and H_2. The total Si density was estimated from the Si density ratio at each $3p^2$ level measured using a hollow cathode lamp and from the translational temperature measured, assuming that Boltzmann distribution is a function of the translational temperature.[5] The Si atom densities at the $3p^{21}D_2$ level measured using a hollow cathode lamp were almost the same values as those using a ring dye laser. The Si densities increased with increasing SiH_4 flow rate ratio and the Si densities at 27 MHz were larger than those at 60 MHz in each dilution plasma. Here, there is one possibility that the Si atoms are produced from the very thin Si films deposited at electrode by sputtering. It is generally reported that the sheath thickness increases with increasing electron temperature. The sputtering effect increases with increasing the sheath thickness. Therefore, in order to investigate the effect of Si densities sputtered for the electrode. Si atom density was measured at a SiH_4 flow rate ratio of 0 % in 27 MHz or 60 MHz plasmas using Ar, N_2, and H_2 gases by UVAS techniques. The absorption of Si atom was not obtained in a wide range of power and pressure for all of dilution gases in both 27 MHz or 60 MHz plasmas. The Si density produced by sputtering was below $1 \times 10^9 cm^{-3}$ (at absorption intensity of 1 %). Accordingly, Si density measured is considered to be not due to sputtering from the electrodes, but the gas phase reaction in the plasma.

The main production and loss processes of Si atoms are assumed to be due to the electron impact dissociation of SiH_4 and the reaction with the SiH_4 molecule, respectively.[5] These reactions are described as follows,

$$R1: SiH_4 + e \xrightarrow{k_1} Si + products + e$$

$$R2: Si + SiH_4 \xrightarrow{k_2} products$$

The rate coefficient k_2 was 3.5×10^{-10} cm^3s^{-1}.[10] Therefore, the balance equation for the production and loss processes of the Si atom can be expressed as the following equation,

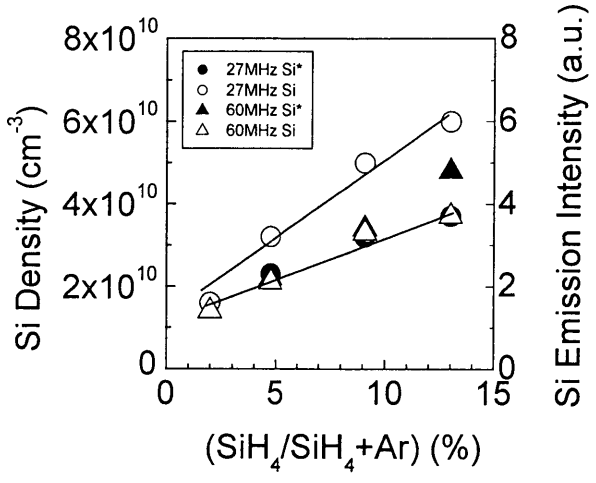

(a)

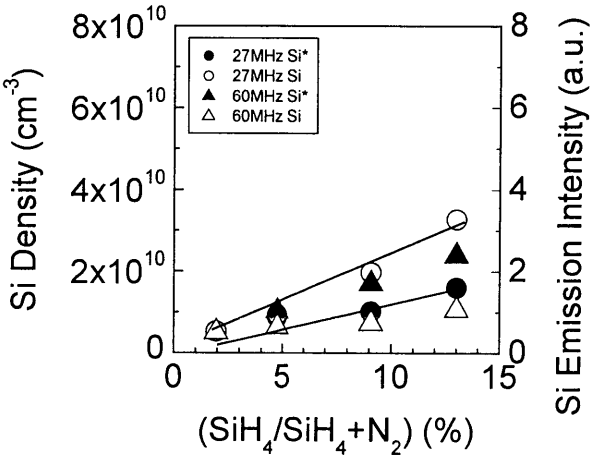

(b)

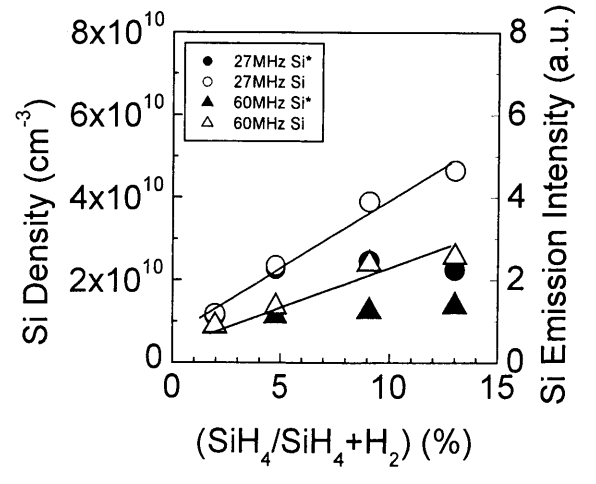

(c)

Figure 5-2 Si density and emission intensity as a function of SiH_4 flow rate ratio.
(a) Ar (b) N_2 (c) H_2.

$$\frac{d}{dt}[Si] = k_1 N_e [SiH_4] - k_2 [Si][SiH_4] - \frac{[Si]}{\tau_{d1}}, \quad (5\text{-}1)$$

where N_e, [Si] and [SiH_4] are the densities of the electron, Si, and SiH_4, respectively. k_1 and k_2 are the rate coefficients for reactions $R1$ and $R2$, respectively. τ_{d1} is the diffusion lifetime of the Si atom. The Si atom density in a steady-state is expressed as

$$[Si] = \frac{k_1 N_e [SiH_4]}{k_2 [SiH_4] + \frac{1}{\tau_{d1}}}. \quad (5\text{-}2)$$

The first term of the denominator in eq. (5-2) is explained as follows. As shown in **Fig. 5-3**, SiH_4 density was of the order of 10^{12}-10^{13} cm^{-3} described below in detail. Thus, the first term of the denominator in eq. (5-2) is estimated to be of the order of 10^2-10^3 s^{-1}. The second term is expressed by the following equation,[14]

$$\tau_d = \frac{p\Lambda_0^2}{D} + \frac{2l_0(2-\alpha)}{v\alpha}, \quad (5\text{-}3)$$

where p is the pressure and Λ_0 is the geometrical diffusion length determined by the chamber structure as expressed by the following equation. In this study, the electrode gap of 2.5 cm is much smaller than the chamber length 54 cm. Therefore, Λ_0 is expressed by the following equation,

$$\Lambda_0 = \frac{L}{\pi}, \quad (5\text{-}4)$$

where L is 2.5 cm, l_0 is expressed by V/S with V and S being the volume and surface area of the chamber, respectively. v is the velocity of the Si atom given by $(8kT/\pi m)^{1/2}$ (T and M are the temperature and mass of the Si atom, respectively, and k is the Boltzmann constant). α is the surface loss probability on the chamber wall, and α was assumed to be 1.[5],[15] D is the diffusion coefficient for the Si atom in the Ar, N_2, and H_2, and is calculated to be 1334, 1255, and 4518 $cm^2 \cdot Torr \cdot s^{-1}$, respectively, using the Chapman-Enskog theory with the Lennard-Jones intermolecular potential.[16],[17] Thus, the diffusion loss of Si atom in the SiH_4/H_2 plasma is about four times larger than that in the SiH_4/N_2 and SiH_4/Ar plasmas. The second term of the denominator in eq. (5-2) is estimated to be of the order of 10^2 s^{-1}. The value of the first term is determined by the

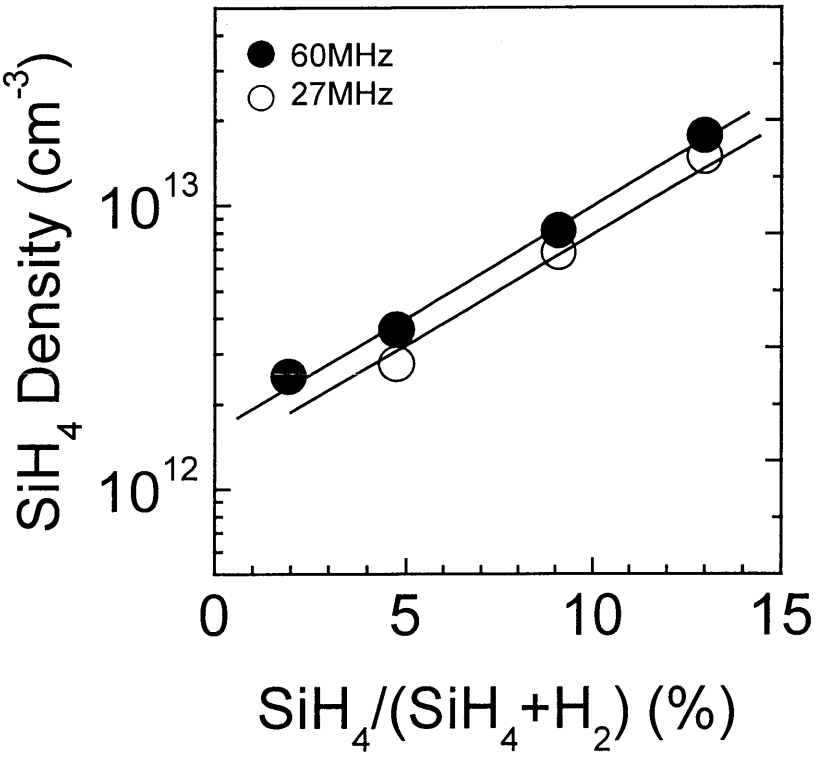

Figure 5-3 SiH_4 molecule density as a function of SiH_4 flow rate ratio in SiH_4/H_2 plasma.

SiH_4 density present in the plasma measured by IRLAS as shown in **Fig. 5-3**. The value of the first term was found to be larger than that of the second term in higher SiH_4 flow rate ratio above 10 %. Accordingly, the reaction of Si atoms with the SiH_4 molecule becomes dominant as the loss process in SiH_4 flow rate ratio above 10 %, and the reaction of Si atoms with the SiH_4 molecule and the diffusion to the wall becomes dominant as the loss process in low SiH_4 flow rate ratio below 10 % under the present experimental condition.

In the SiH_4/H_2 and SiH_4/N_2 plasmas, the loss processes of the reaction with H_2 molecule and N_2 molecule are also described as follows,

$$R3: \mathrm{Si} + \mathrm{H_2} \xrightarrow{k_3} \mathrm{SiH_2}$$

$$R4: \mathrm{Si} + \mathrm{N_2} + \mathrm{M} \xrightarrow{k_4} \mathrm{SiN_2}$$

The rate coefficients k_3 and k_4 were 6.6 × 10^{-12} cm^3s^{-1} and 6.6 × 10^{-32} cm^6s^{-1}, respectively.[18],[19] However, $R4$ was negligible because the rate coefficient k_4 was extremely small. Therefore, the Si atom density in the SiH_4/H_2 plasma is expressed from eq. (5-2),

$$[\mathrm{Si}] = \frac{k_1 N_e [\mathrm{SiH_4}]}{k_2[\mathrm{SiH_4}] + k_3[\mathrm{H_2}] + \dfrac{1}{\tau_{\mathrm{dH_2}}}}. \tag{5-5}$$

The first term of the denominator in eq. (5-5) is estimated to be of the order of 10^2-10^3 s^{-1} as described above. The H_2 density is estimated to be of the order of 10^{13}-10^{14} cm^{-3} from the equation of state assuming H_2 dissociation ratio of 90 %. The second term of the denominator in eq. (5-5) is estimated to be of the order of 10^2 s^{-1}. Accordingly, the reaction of Si atoms with the SiH_4 molecule becomes dominant as the loss process in SiH_4 flow rate ratio above 10 %, and the reaction of Si atoms with the H_2 molecule in addition to SiH_4 molecule becomes large in low SiH_4 flow rate ratio below 10 % under the present experimental condition. Therefore, Si atoms in the SiH_4/H_2 plasma extinguished faster than those in the SiH_4/N_2 and SiH_4/Ar plasmas through the reactions with H_2 molecules in addition to SiH_4 molecules.

The emission intensity of Si^* provides information on the production process of the Si atom from the electron impact dissociation of SiH_4 molecule. Kampas *et al.* reported

that Si* was mainly produced from the dissociative excitation of SiH_4 and the Si^* from the direct excitation of Si atom at the steady-state can be negligible.[20] The threshold energy of the electron impact dissociation of SiH_4 molecule for the production of Si atom and electron impact excitation of SiH_4 molecule for Si* are 10.3 eV and 10.5 eV, respectively.[21] The rate equation of Si^* atom is expressed by the following equation,

$$I_{Si^*} \propto c k_{Si^*} N_e [SiH_4], \tag{5-6}$$

where c is constant, k_{Si^*} is the excitation rate constant, N_e is electron density, and [SiH_4] is the density of SiH_4 molecule. Therefore, Si* gives the information on the production of Si atom from the electron impact dissociation of SiH_4.

The absolute density of SiH_4 measured by IRLAS is shown in **Fig. 5-3**. The density was line-averaged one in the plasma chamber, because the absorption of SiH_4 molecules in IRLAS measurement was obtained by using the multiple reflection White-type cell. In the SiH_4/H_2 plasma, the line-averaged absolute density of SiH_4 molecule was of the order of 10^{12}-$10^{13}cm^{-3}$ and the very high dissociation ratio of about 90-95 % was obtained. The absorption due to SiH_4 molecule in the SiH_4/Ar and SiH_4/N_2 plasmas could not be obtained, because SiH_4 molecules were dissociated almost completely by the electron impact due to high N_e in comparison with the SiH_4/H_2 plasma. The dissociation ratio of SiH_4 molecule was estimated to be above 95 % taking account of measurement error of about 5 %. Therefore, the SiH_4 gas injected into the plasma through the showerhead was dissociated almost completely in the SiH_4/Ar and SiH_4/N_2 plasmas and only few SiH_4 molecules will exist out of the plasma region. In the SiH_4/H_2 plasma, the SiH_4 density was increased with increasing SiH_4 flow rate ratio at both frequencies, because the partial pressure of SiH_4 molecule increased with present conditions. The SiH_4 density at 60 MHz was larger than that at 27 MHz.

The Si density increased with increasing SiH_4 flow rate ratio in each dilution plasma as shown in **Fig. 5-2**. These results were explained by the increase of the production of Si atom through the electron impact dissociation of SiH_4 molecule, since the SiH_4 densities increased with increasing SiH_4 flow rate ratio as shown in **Fig. 5-3**. However, the gradient of Si density was larger than that of Si^* at all of dilution plasmas in the 27 MHz. The behaviors of Si^* as shown in **Fig. 5-2** indicate mainly the production rate of

Si atom from the dissociation of SiH_4 molecule. Although the N_e at 60 MHz were larger than those at 27 MHz as shown in **Fig. 5-1**, the electron temperatures (T_e) at 27 MHz were larger than those at 60 MHz. At the SiH_4 flow rate ratio of 0 %, the T_e at 60 MHz and 27 MHz measured by the double probe were 2.3 eV and 3.2 eV in the SiH_4/Ar plasma, 2.5 eV and 3.3 eV in the SiH_4/N_2 plasma, and 3.5 eV and 4.4 eV in the SiH_4/H_2 plasma, respectively. Considering the result that the SiH_4 molecule was depleted at 27 MHz described above, the larger gradient of Si density than that of Si^* as shown in **Fig. 5-2** is due to the additional production process of Si atom from SiH_x (x = 1-3) radicals because Si* is mainly produced from the electron impact of SiH_4 molecule. In the only case of SiH_4/H_2 at 60 MHz plasma, the gradient of Si density is larger than that of Si^*. This result would be also explained using the difference of SiH_4 density described above. Thus, the T_e in H_2 dilution plasmas is large in comparison with that in Ar or N_2 dilution plasmas. Therefore, Si atom will be dominantly produced not only from SiH_4 molecules but also from SiH_x (x = 1-3) radicals. In the SiH_4/H_2 at 60 MHz plasma, therefore, the gradient of Si density will become larger than that of Si^*.

5.3 Behavior of Si atom temperature

Figure 5-4 shows the typical absorption coefficient profile of the Si atom measured by using the ring dye laser. The experimental condition was an excitation frequency of 27 MHz, a SiH_4 flow rate of 15 sccm, and an Ar flow rate of 100 sccm. The Doppler broadening was dominant for the absorption line in the present experimental condition. Therefore, the translational temperature of the Si atom was evaluated accurately from the width of the absorption profile $\Delta\upsilon_D$. The translational temperature of the Si atom, that is, T was obtained by the following equation,

$$\Delta\upsilon_D = 2\sqrt{2\ln 2}\upsilon_0\left(\frac{kT}{mc^2}\right)^{1/2}, \tag{5-7}$$

where υ_0 is the laser frequency at the line center, k is the Boltzmann constant, c is the speed of light, and m is the mass of Si atom, respectively. As shown in **Fig. 5-4**, the line represents the absorption coefficient profile of Si atom calculated assuming the

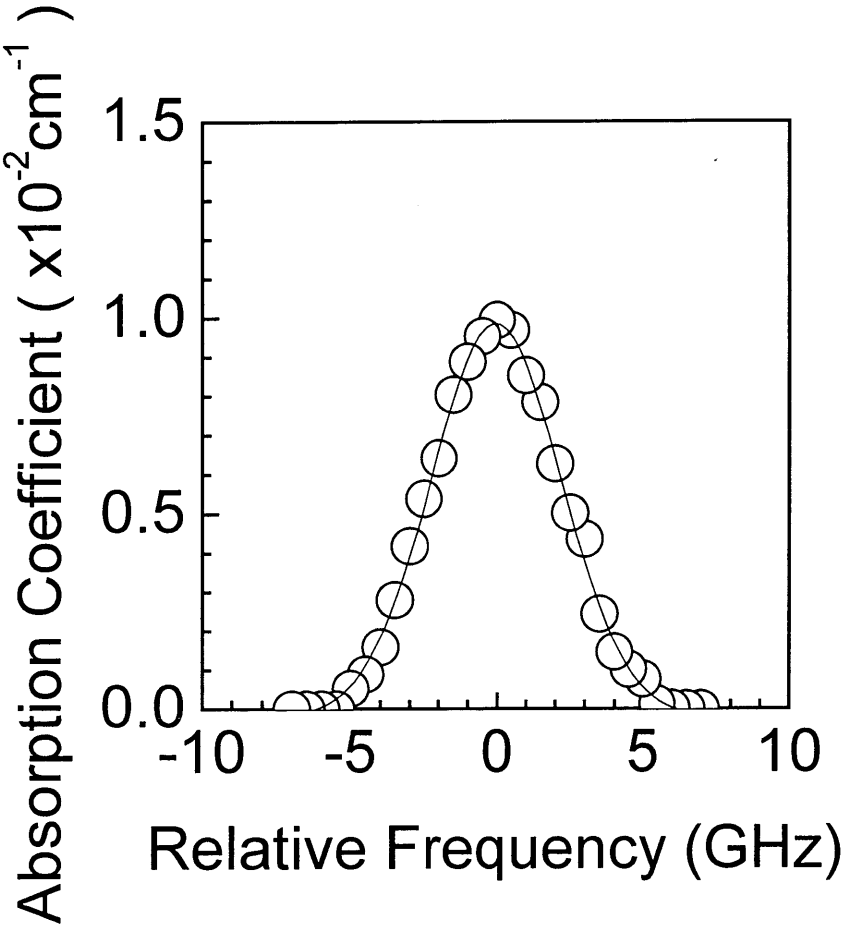

Figure 5-4 The absorption coefficient profile of the Si atom at the transition of $3p^{21}D_2$ - $3p4s^1P_1$ (288.2 nm).

translational temperature is 1260 K and the measured density of 3.2×10^9 cm^{-3} at the $3p^2{}^1D_2$ level. The calculated profile agreed well with the measured one. Therefore, $\Delta\upsilon_D$ was 5 GHz and the translational temperature was estimated to be 1260 K. Here, the spatially line-averaged temperatures of the Si atom was obtained in the present experiment. It expresses the temperature of Si atom existing in the plasma region. Since the Si density was decreased rapidly outside the plasma region due to the high reaction loss rate of 3.5×10^{-10} cm^3s^{-1} for the reaction with SiH_4 molecules and the high surface loss probability of about 1.[5],[15]

Figure 5-5 shows the translational temperature of Si atom as a function of SiH_4 flow rate ratio. The translational temperatures of Si atom at both frequencies increased with increasing SiH_4 flow rate ratio. The value of the temperature was estimated to be from 580 K to 1260 K at 27 MHz, and from 460 K to 880 K at 60 MHz. Si atoms produced by electron impact dissociation of SiH_4 molecule collide elastically with Ar atoms in many times before they are lost by the reaction with SiH_4 molecule. Moreover, SiH_4 density increased with increasing SiH_4 flow rate ratio as shown in **Fig. 5-3**. Therefore, the translational temperature increased with increasing SiH_4 flow rate ratio due to the loss process of the reaction with SiH_4 molecule. Therefore, the translational temperatures of Si atom increased with increasing SiH_4 flow rate ratio.

In the dissociation process of SiH_4 molecule, the electrons with the sufficient energy collide with a SiH_4 molecule to raise the SiH_4 molecule to a dissociative-state, resulting in the production of Si atom due to Frank-Condon effect. Consequently, the dissociated fragments with excess energy are produced. The excess energy is divided into the translational energy of species produced.[22] The threshold energy of the electron impact dissociation of SiH_4 molecule producing Si atom is about 10.3 eV, while the thermodynamic heat energy of the reaction for $SiH_4 \rightarrow Si+2H_2$ is 4.2 eV.[23] This fact indicates that the excess energy of 6.1 eV is divided into the Si atom and H_2 molecules. Therefore, the dominant driving factor for Si atom heating is considered due to the energy of Si atoms released from the electron impact dissociation of SiH_x (x = 1-4).

The translational temperatures at 27 MHz were larger than those at 60 MHz as shown in **Fig. 5-5**. The production rate of Si atoms at 27 MHz was larger than at 60 MHz

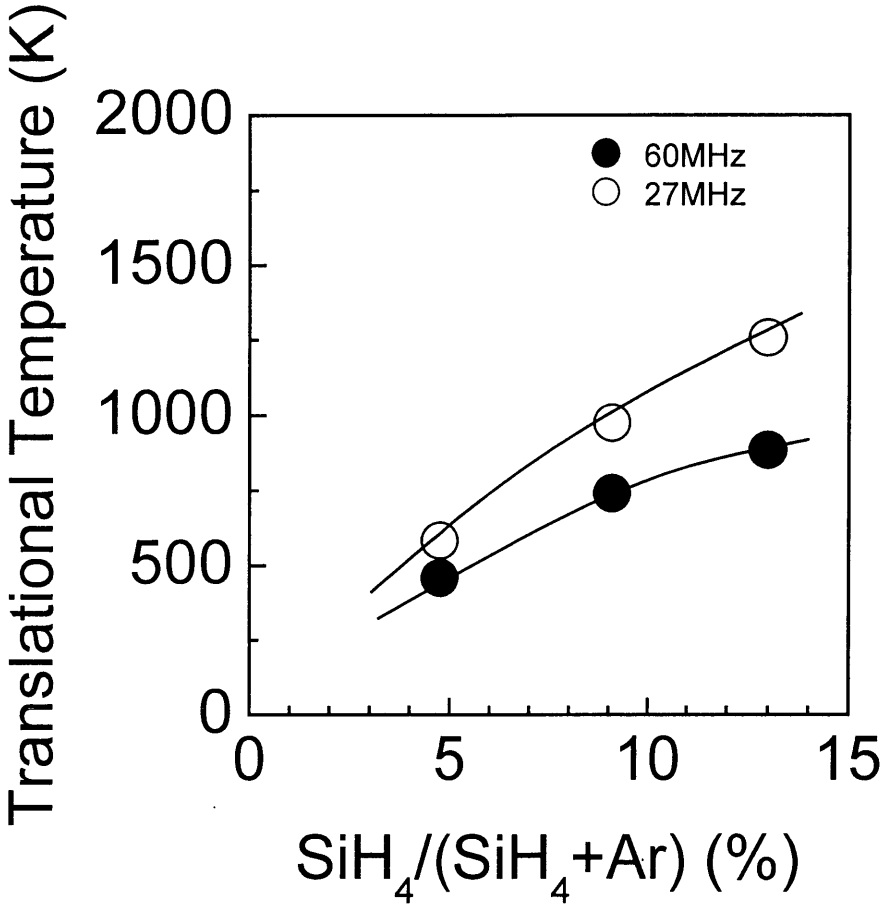

Figure 5-5 Translationl temperature of Si atom as a function of SiH_4 flow rate ratio.

because of high T_e. The Si atoms at the 27 MHz plasma were produced more from radicals such as SiH_x (x = 1-3) radicals than SiH_4 molecules by the electron impact dissociation as described above. Accordingly, it is considered that the translational temperatures of Si atoms at 27 MHz will become larger than those at 60 MHz.

Figure 5-6 shows the translational temperature of Si atom as a function of SiH_4 flow rate ratio in SiH_4/N_2 with 27 MHz and 60 MHz plasmas. The N_e was maintained at a constant of 1.1×10^{11} cm^{-3}. The translational temperatures increased with increasing SiH_4 flow rate ratio. SiH_4 density increased with increasing SiH_4 flow rate ratio as shown in **Fig. 5-3**. Therefore, the translational temperature increased with increasing SiH_4 flow rate ratio due to the loss process of the reaction with SiH_4 molecule. The translational temperatures at 27 MHz were larger than those at 60 MHz. The production rate of Si atoms at 27 MHz was larger than at 60 MHz because of high T_e. The Si atoms at the 27 MHz plasma were produced more from radicals such as SiH_x (x = 1-3) radicals than SiH_4 molecules by the electron impact dissociation as described above. Accordingly, it is considered that the translational temperatures of Si atoms at 27 MHz will become larger than those at 60 MHz.

Table 5-1 shows the translational temperature of Si atoms with dilution gases of Ar, N_2, and H_2. The condition is an excitation frequency of 27 MHz, a dilution gas flow rate of 100 sccm, a SiH_4 flow rate of 10 sccm, and a VHF power of 1500 W. The translational temperature of Si atoms in the SiH_4/Ar plasma indicated the lowest value. Si atoms produced by electron impact dissociation of SiH_4 molecule collide elastically with Ar atoms in many times before they are lost by the reaction with SiH_4 molecule. Therefore, it is considered that the translational temperature of Si atoms in the SiH_4/Ar plasma becomes low. The temperature of Si atoms in the SiH_4/H_2 plasma was the highest value, while the N_e was the lowest. The reaction of Si atoms with the SiH_4 molecule becomes dominant as the loss process in SiH_4 flow rate ratios above 10 % in the SiH_4/H_2 plasma. However, the reaction with H_2 molecule cannot be negligible as a loss process. Therefore, it is considered that Si atoms in the SiH_4/H_2 plasma extinguished faster than those in the SiH_4/Ar and SiH_4/N_2 plasmas. Moreover, the mass of H_2 molecule is small in comparison with that of Ar atom and N_2 molecule, hereby the

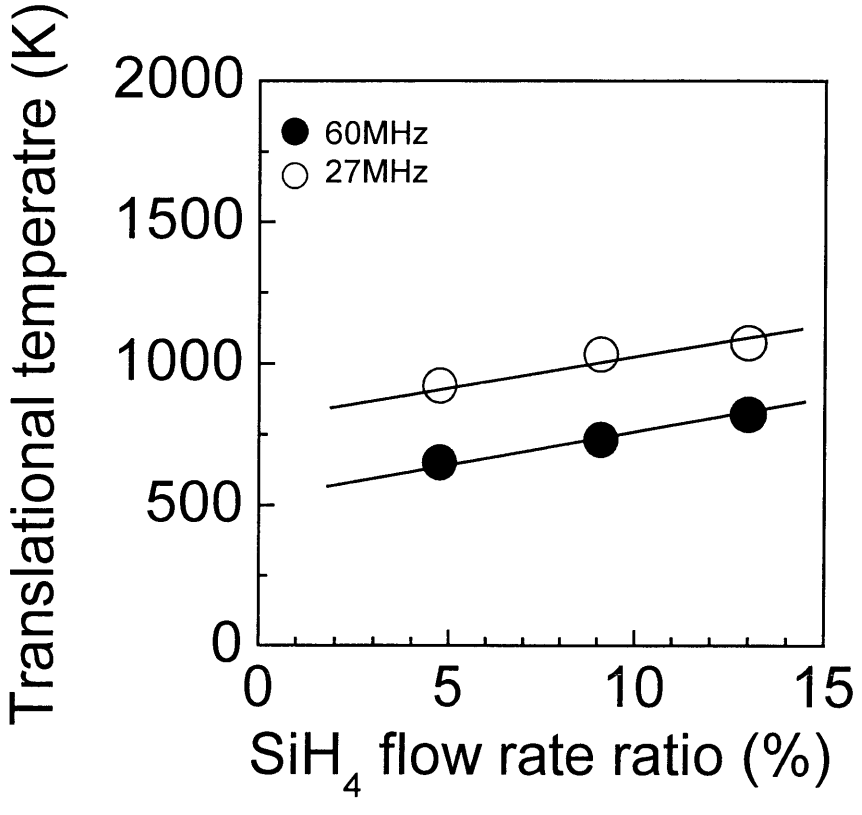

Figure 5-6 Translationl temperature of Si atom as a function of SiH_4 flow rate ratio in SiH_4/N_2 plasma.

Table 5-1 Translationl temperature at 27 MHz.

Dilution gas	Electron density (cm^{-3})	Si density (cm^{-3})	Si temperature (K)
Ar	1.2×10^{11}	5.0×10^{10}	970
N_2	1.1×10^{11}	2.0×10^{10}	1030
H_2	2.5×10^{10}	3.9×10^{10}	1130

loss energy of Si atom in the SiH_4/H_2 plasma would be small in comparison with the SiH_4/Ar and SiH_4/N_2 plasmas when Si atoms elastically collide with species. The Si atoms in the SiH_4/H_2 plasma were produced more from radicals such as SiH_x (x = 1-3) radicals than SiH_4 molecules by the electron impact dissociation in comparison with the SiH_4/Ar and SiH_4/N_2 plasmas due to high T_e. Accordingly, the temperature of Si atoms in the SiH_4/H_2 plasma was the highest value.

Here, there is one possibility for Si atom heating mechanism that the upper electrode heating by the bombardment of charged species would affect the translational temperature. Therefore, the electrode heating effect was investigated by measuring the temperature of upper electrode by using a pyrometer. In general, the light radiation from the plasma disturbs the temperature measurement of the surface of the electrode. To avoid this problem, the decay of the surface temperature of electrode in the afterglow was measured. **Figure 5-7** shows the decay time of the upper electrode temperature in the afterglow. The condition was an excitation frequency of 27 MHz or 60 MHz, a SiH_4 flow rate of 15 sccm, and a VHF power of 1500 W with diluted Ar, N_2, and H_2 gases. At the excitation frequency of 27 MHz, the electrode temperature in the plasma was estimated in the range of 500-505 K, and the difference of the electrode temperature in the plasma was not observed among dilution plasmas. At the excitation frequency of 60 MHz, the temperature at the upper electrode was not measured after 4 sec since the lower limit of the pyrometer was 473 K. If the gradient of temperature decay at 27 and 60 MHz plasmas was assumed to be the same, the electrode temperature at 60 MHz was estimated to be about 480 K. The temperature of upper electrode at 60 MHz plasma was

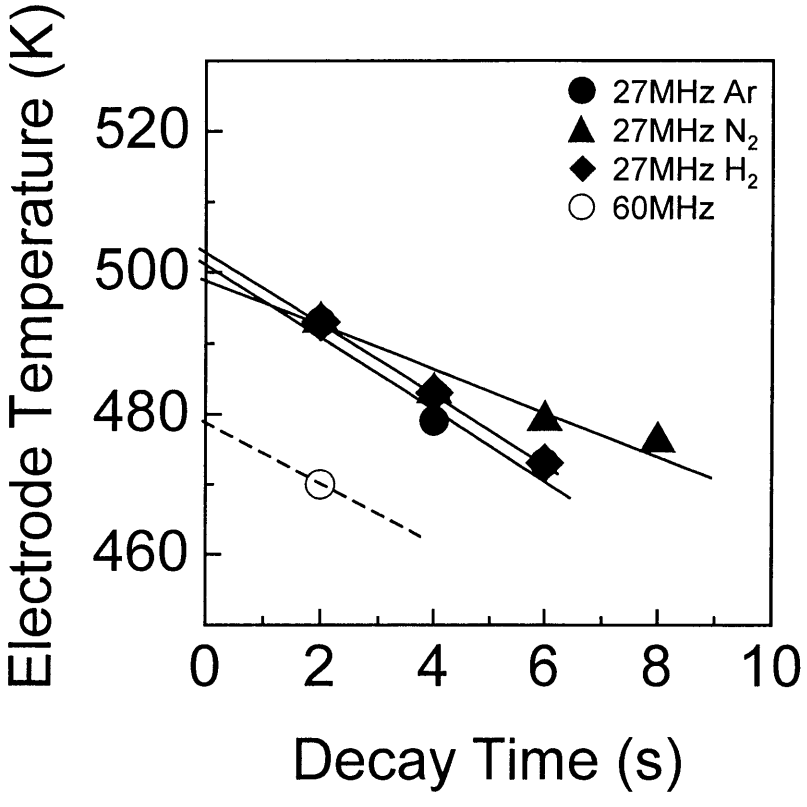

Figure 5-7 Decay time of surface temperature of upper electrode.

found to be lower than that at 27 MHz and the difference of the electrode temperature between 27 and 60 MHz plasmas was about 20 K. The difference of the electrode temperature was much small in comparison with that of the translational temperature of Si atoms. Therefore, the heating effect from upper electrode temperature by the bombardment of charged species did not affect the translational temperature.

5. 4 Summary

In summary, the behaviors of absolute densities and translational temperatures of Si atoms in very high frequency capacitively coupled SiH_4 plasmas with Ar, N_2, and H_2 dilution gases were measured by ultraviolet absorption spectroscopy employing a ring dye laser and a hollow cathode lamp.

Si atoms were mainly produced by the electron impact dissociation of SiH_4 molecules, and extinguished by the reaction with the SiH_4 molecules and the diffusion. However, the Si atoms at the 27 MHz plasmas were produced more from radicals such as SiH_x (x = 1-3) radicals than SiH_4 molecules by the electron impact dissociation in comparison with 60 MHz plasmas. Moreover, the Si atom heating was due to the energy of Si atoms released from the electron impact dissociation of SiH_x (x = 1-4). Therefore, the densities and translational temperatures of Si atoms at 27 MHz were larger than those at 60 MHz in each dilution plasma.

The translational temperatures in the SiH_4/Ar, SiH_4/N_2, and SiH_4/H_2 27 MHz plasmas were estimated to be 970, 1030, and 1130 K, respectively. In the SiH_4/Ar plasma, Si atoms collide elastically with Ar atoms in many times before they are lost by the reaction with SiH_4 molecule, resulting in the lowest value of the translational temperature of Si atoms. In the SiH_4/H_2 plasma, on the other hand, Si atoms extinguished faster than those in the SiH_4/Ar and SiH_4/N_2 plasmas due to the reaction with H_2 and SiH_4 molecules and the low loss energy of Si atom with elastically collision, resulting in the highest value of the temperature.

References for chapter 5

[1] T. Nagahara, K. Fujimoto, N. Kohno, Y. Kashiwagi, and H. Kakinoki, Jpn. J. Appl. Phys., **31**, 4555(1992).

[2] R. C. Ross and J. Jaklick, Jr., J. Appl. Phys., **55**, 3785 (1984).

[3] H. Ohta, .A Nagashima, M. Hori, and T. Goto, J. Appl. Phys., **89**, 5083 (2001).

[4] W. Huang, X. Wang, M. Sheng, L. Xu, F. Stubhan, L. Luo, T. Feng, X. Wang, F. Zhang, and S. Zou, Materials Science and Engineering, **B98,** 248 (2003).

[5] Y. Yamamoto, H. Nomura, T. Tanaka, M. Hiramatsu, M. Hori, and T. Goto, Jpn. J. Appl. Phys., **33**, 4320 (1994).

[6] K. Murata, Y. Mizutani, E. Iwasaka, S. Takashima, M. Hori, T. Goto, S. Samukawa, and T. Tsukada, Jpn. J. Appl. Phys., **40**, L4 (2001).

[7] T. Takagi, R. Hayashi, G. Ganguly, M. Kondo, A. Matsuda, Thin Solid Films, **345**, 75 (1999).

[8] M. Surendra and D. B. Graves, Appl. Phys. Lett., **59**, 2091 (1991).

[9] M. Takai, T. Nishimoto, T. Nakagi, M. Kondo, and A. Matsuda, J. Non-Crystalline Solid, **266-269**, 90 (2000).

[10] T. Tanaka, M. Hiramatsu, M. Nawata, A. Kono, and T. Goto, J. Phys. D: Appl. Phys., **27**, 1660 (1994).

[11] H. C. Straub, P. Renault, B. G. Lindsay, K. A. Smith, and R. F. Stebbings, Phys. Rev., **A52**, 1115 (1995).

[12] H. C. Straub, P. Renault, B. G. Lindsay, K. A. Smith, and R. F. Stebbings, Phys. Rev., **A54**, 2146 (1996).

[13] N. O. J. Malcolm and D. L. Yeager, J. Chem. Phys., **113**, 8 (2000).

[14] P. J. Chantry, J. Appl. Phys., **62**, 1141 (1987).

[15] Y. Nozaki, K. Kongo, T. Miyazaki, M. Kitazoe, K. Horii, H.Uemoto, A. Masuda, and H. Matsumura, J. Appl. Phys., **88**, 5437 (2000).

[16] R. C. Reid, J. M. Prausnitz, and T. K. Sherwood, *The Properties of Gases and Liquids* (McGraw-Hill, New York, 1977).

[17] R. A. Svehla, NASA Tech. Report No. R-132, Lewis Research Center, 1962.

[18] M. J. Kushner, J.Appl.Phys., **63**, 2532 (1988).

[19] M. J. Kushner, J.Appl.Phys., **74**, 6538 (1993).

[20] F. J. Kampas, J.Appl. Phys., **54**, 2276 (1983).

[21] M. Takai, T. Nishimoto, M. Kondo, and A. Matsuda, Appl. Phys. Lett., **77**, 2828 (2000).

[22] B. A. Cruden, M. V. V. S. Rao, Surendra P. Sharma, and M. Meyyappan, Appl. Phys. Lett., **81**, 990 (2002).

[23] M. Tsuda, S. Oikawa, and K. Sato, J. Chem. Phys., **91**, 6822 (1989).

Chapter 6

Effect of excitation frequency on thin film formation in SiH_4 plasma

6.1 Introduction

The behavior of absolute density and translational temperature of Si atom in the VHF CCP employing SiH_4 based gas were discussed in chapter 5. In this chapter, the correlation between the behavior of Si atom and the thin film formation in VHF SiH_4 CCP is investigated. The estimation for the contribution of Si atom to the film deposition is calculated by using the flux of Si atom and SiH_3 radical to the substrate. Moreover, the effect of excitation frequency is investigated for the film deposition.

6.2 Estimation for contribution of radicals to film deposition

The contribution of Si atoms to the film deposition in VHF-CCP was estimated from the densities and translational temperatures. Here, the mean free path of molecule at 11 Pa and 800 K is about 0.2 cm. The Si atom produced in the plasma will collide with other neutral species at least about 12 times due to the electrode gap of 2.5 cm before the Si atoms react the substrate. In fact, even if taking account that the contribution of the diffusion loss is large in low SiH_4 flow rate ratio region below 10 %, Si atoms will react with other species such as H_2 molecule with its high reaction rate before reaching the substrate. Therefore, it is difficult to estimate accurately the direct contribution ratio of Si atoms to the film deposition. It is focused on SiH_3 radicals in this study, which are the major species to the deposition. Here, the density of SiH_3 radical is roughly estimated assuming that SiH_3 radical is produced by the electron impact dissociation of

SiH_4 and loss by the diffusion. The reaction constant of the electron impact dissociation of SiH_4 molecule producing SiH_3 radical is 7.4×10^{-9} cm^3s^{-1} on the assumption of a Maxwellian energy distribution function at the electron temperature of 3.2 eV measured at 27 MHz Ar plasma as described in chapter 5.[1] The density of SiH_3 radical was estimated to be of the order of 10^{11}-$10^{12}cm^{-3}$. Assuming that all of Si atom and SiH_3 radicals generated in the plasma region will diffuse to the substrate at the average velocity determined by its temperature, the flux density Γ of Si atom and SiH_3 radical to the substrate is given by the following equation,[2]

$$\Gamma = \frac{n}{4}\sqrt{\frac{8k_BT}{\pi m}}, \tag{6-1}$$

where n is the radical density, k_B is the Boltzmann constant, T is the temperature of radical, and m is the mass of the radical. The flux is a function of the radical temperature and density. The growth rate of the film due to Si atoms and SiH_3 radicals was estimated by following equation,

$$R_d = \Gamma \times s \times \frac{m}{\rho}, \tag{6-2}$$

where s is the sticking probability, ρ is the mass density of the film, m is the mass of the radical. ρ of a-Si:H and Si_3N_4 was assumed to be 2.2 gm^{-3} and 3.3 gm^{-3}, respectively. In this study, s is assumed to be 1 for Si and 0.1 for SiH_3.[3],[4] The ratio of SiH_3 radical and Si atom to the film deposition, that is, Si/SiH_3 was estimated.

Figure 6-1 shows the deposition rate and the contribution ratio of SiH_3 radical and Si atom to the film deposition as a function of SiH_4 flow rate ratio in SiH_4/Ar 27 MHz and 60 MHz plasmas. The plasma condition was maintained at a total pressure of 11 Pa, and an Ar flow rate of 100 sccm. The SiH_4 flow rate was varied from 0 to 15 sccm. The VHF power was maintained at a constant of 1500 W. The Si atom density at 27 MHz plasma was larger than those at 60 MHz as shown in **Fig. 5-2**, and the deposition rate at 60 MHz was larger than that at 27 MHz. The SiH_3 density at 60 MHz calculated was larger in comparison with that at 27 MHz. The contribution ratio of Si atom to the film deposition at 27 MHz was larger than that at 60 MHz because the Si densities and the

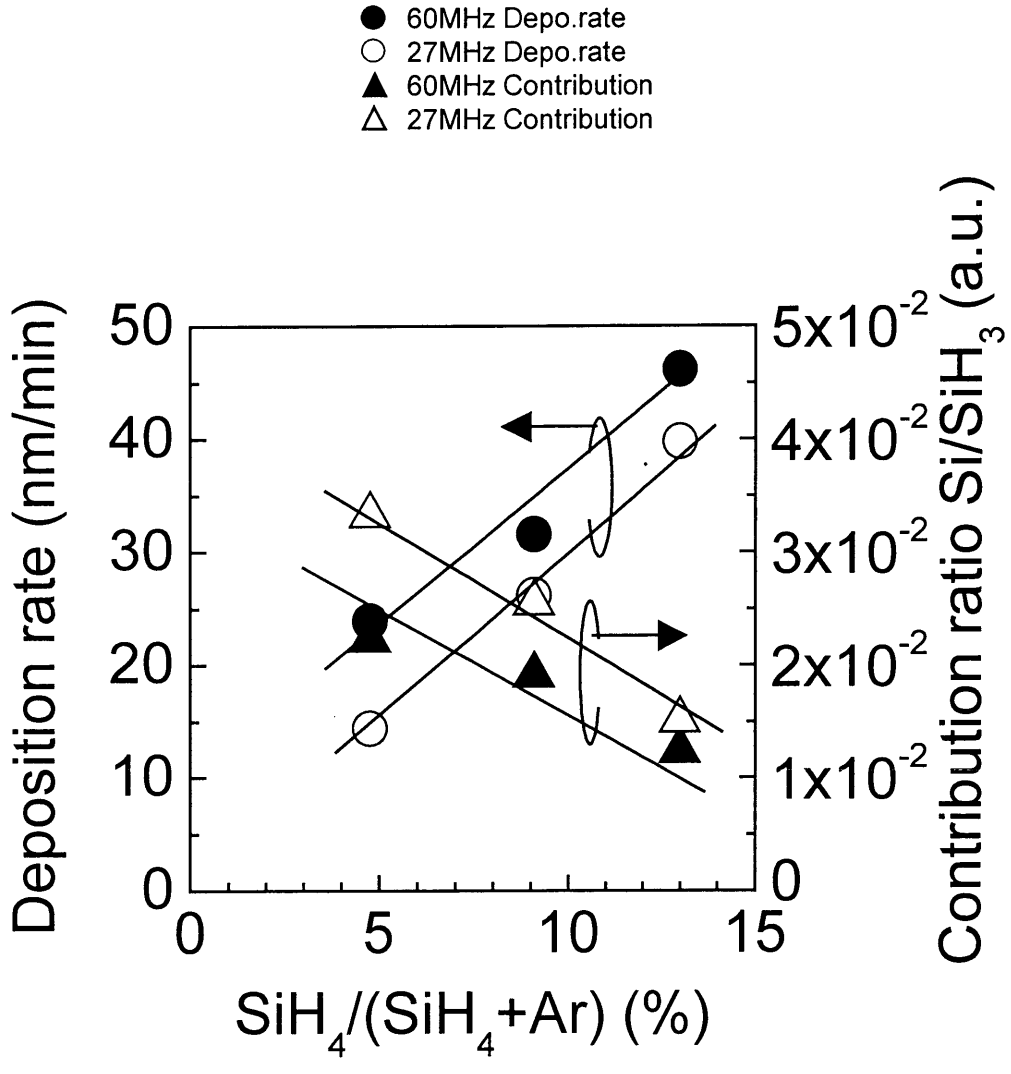

Figure 6-1 Deposition rate and contribution to thin film deposition as a function of SiH_4 flow rate ratio in SiH_4/Ar.

translational temperatures at 27 MHz were larger than those at 60 MHz. The ratio of Si/SiH_3 decreased with increasing SiH_4 flow rate ratio.

Figure 6-2 shows the deposition rate and the contribution of SiH_3 radical and Si atom to the film deposition as a function of SiH_4 flow rate ratio in SiH_4/N_2 plasma. The plasma condition was maintained at a total pressure of 11 Pa, and N_2 flow rate of 100 sccm. The SiH_4 flow rate was varied from 0 to 15 sccm. The electron density was maintained at a constant of 1.1×10^{11} cm^{-3}. The deposition rates at 27 and 60 MHz were almost the same, while the deposition rate at 60 MHz was larger than that at 27 MHz under the same VHF power as shown in **Fig. 6-1**. The contribution of the Si atom to the film deposition at 27 MHz was larger than that at 60 MHz. The fact indicates that the contribution of Si atom is larger with decreasing the excitation frequency.

Figure 6-3 shows Fourier transform infrared absorption spectroscopy (FTIR) spectra of SiN film as a function of the excitation frequency. The plasma condition was maintained at a total pressure of 11 Pa, a N_2 flow rate of 100 sccm, a SiH_4 flow rate of 5 sccm, and an electron density of 1.1×10^{11} cm^{-3}. The absorption peaks at 910 cm^{-1} of Si-N, 2210 cm^{-1} of Si-H, 1200 cm^{-1} and 3350 cm^{-1} of N-H were observed. The peak of Si-H bond decreased and those of N-H and Si-N bonds increased with increasing the excitation frequency. The film deposited at 60 MHz became nitride rich composition in comparison with that at 27 MHz. In the SiH_4/N_2 plasma, it is reported that SiN_x films was formed by surface reaction between SiH_x radicals and N atoms.[5] Moreover, it is reported that the N-rich SiN_x films with high quality as an insulator film was observed a high (N-H)/(Si-H) peak ratio and the insulator characteristics were degraded with increasing the peak of Si-H bond due to the formation of Si-rich films.[6] Therefore, in this study, it was found that the film at 60 MHz would have high quality in comparison with that at 27 MHz and the film structure was changed with increasing the excitation frequency. This fact suggests the contribution of the radicals to the film composition is changed with increasing the excitation frequency.

In the case of SiH_4/H_2 plasma, the analysis of Si atom for the deposition rate is very complicated because of the reaction of Si atom with SiH_4 and H_2 molecules in the gas

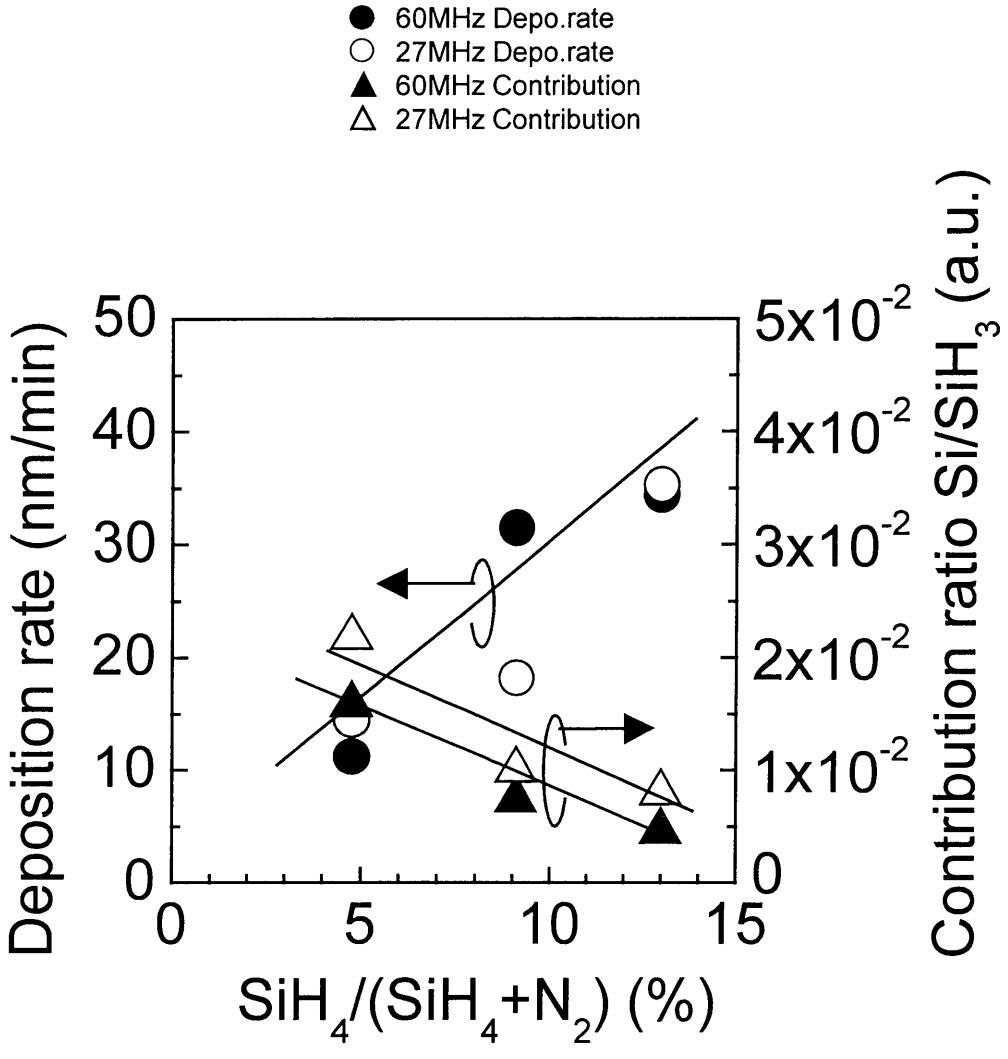

Figure 6-2 Deposition rate and contribution to thin film deposition as a function of SiH_4 flow rate ratio in SiH_4/N_2.

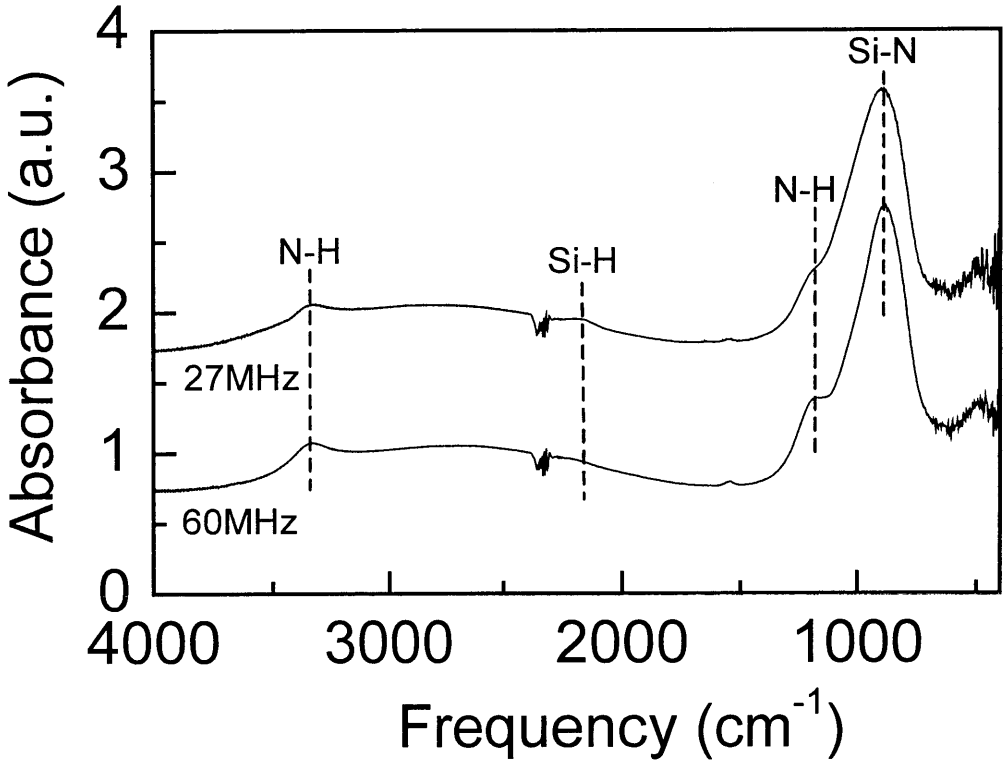

Figure 6-3 FT-IR spectra as a function of excitation frequency.

phase and surface. Further accurate work will be necessary to clarify the reaction mechanism of Si atoms. The Si atom reacts with the SiH_4 molecule at a high reaction rate and produces the higher order silane-related radicals. These higher radicals make a lot of defects in the film, which causes the photo-induced degradation of a-Si:H films for solar cell. Actually, it is reported that the photo-induced degradation of a-Si:H film was decreased by using VHF-CCP.[7] However, the effects of the temperature and density of radicals on the film quality in VHF-CCP still have not been clarified. In this study, depositing films with high quality may be indirectly realized by the decrease of Si density, resulting in the decrease of the higher order silane-related radicals. It is indicated that the change of excitation frequency with VHF-CCP can control the film structure and the plasma chemistry and give great advantage to high performance of the high quality thin films.

6.2 Summary

In this chapter, the effect of the excitation frequency on thin film formation in SiH_4 based plasma was discussed. The effect of Si atoms and SiH_3 radicals on the contribution to the deposition film was investigated in 27 MHz or 60 MHz plasmas. The ratio of Si/SiH_3 ratio decreased with increasing the excitation frequency. The SiN film deposited at 60 MHz became nitride-rich composition more than that at 27 MHz because of the low ratio of Si/SiH_3. This fact suggests the contribution of the radicals to the film composition is changed with increasing the excitation frequency. It is indicated that increasing the excitation frequency has the advantages for obtaining the high-quality films and controlling the plasma chemistry.

References for chapter 6

[1] E. Meeks, R. S. Larson, P. Ho, C. Apblett, S. M. Hann, E. Edelberg, and E. S. Aydil, J. Vac. Sci. Technol., **A16**, 544 (1998).

[2] B. Chapman, *Glow Discharge Processes : Sputtering and Plasma Etching* (Wiley, New York, 1980).

[3] Y. Yamamoto, H. Nomura, T. Tanaka, M. Hiramatsu, M. Hori, and T. Goto, Jpn. J. Appl. Phys., **33**, 4320 (1994).

[4] Y. Nozaki, K. Kongo, T. Miyazaki, M. Kitazoe, K. Horii, H.Uemoto, A. Masuda, and H. Matsumura, J. Appl. Phys., **88**, 5437 (2000).

[5] D. L. Smith, A. S. Alimonda, and F. J. vonPreissig, J. Vac. Sci. Technol., **B8**, 551 (1990).

[6] N. Lustig and J. Kanicki, J. Appl. Phys., **65**, 3951 (1989).

[7] M. Takai, T. Nishimoto, T. Nakagi, M. Kondo, and A. Matsuda, J. Non-Crystalline Solid, **266-269**, 90 (2000).

Chapter 7

Conclusions

7.1 Summary of this thesis

The effect of the excitation frequency on the neutral radical and the contribution to the film deposition in VHF-CCP was investigated in this thesis. In chapter 1, the trend of the excitation frequency was shown as an introduction. The importance of the radical temperature in plasma processing and the purpose of this thesis were also described. In chapter 2, the experimental apparatus and UVAS, IRLAS, LIF, AOES, wave diagnostics, double probe technique, and pyrometer for the diagnostic techniques of plasma were described.

In chapter 3, the densities of the Si, SiF and SiF_2 radical and the SiF_4 molecule in VHF 60 MHz CCP employing SiF_4 gas were measured as a function of N_e using LIF, IRLAS and UVAS techniques. The behavior of their radicals and the SiF_4 molecule was characterized using an internal plasma parameter of N_e. The SiF_4 density decreased with increasing N_e, and the dissociation ratio of SiF_4 was saturated at about 63% at N_e of 8.7 $\times 10^{10}$ cm^{-3}. SiF_2 radical density decreased while Si and SiF densities increased with increasing N_e above 1.2×10^{11} cm^{-3}. The SiF_2 radical is mainly produced by the electron impact dissociation of SiF_4 and extinguished by the diffusion to the wall at the N_e below 1.2×10^{11} cm^{-3} and by the electron impact dissociation at N_e above 1.2×10^{11} cm^{-3}. SiF radical density increased linearly with increasing N_e. The SiF radical is mainly produced by the electron impact dissociation of the SiF_4 molecule and extinguished by the reaction with the SiF_4 molecule. The total density of the Si atom was estimated to be of the order of 10^{10} - 10^{11} cm^{-3}. The Si atom is mainly produced by the electron impact dissociation of SiF_4 molecule at N_e below 1.0×10^{11} cm^{-3} and by the electron impact dissociation of SiF_x (x = 1-3) radicals in addition to the SiF_4 molecule at the N_e above

1.0×10^{11} cm^{-3}. The kinetics of species in SiF_4 plasma has been clarified quantitatively. The spatial distribution of SiF, SiF_2 and SiF_4 densities was also measured by LIF and IRLAS, showing an almost flat distribution inside the plasma region. This result indicated VHF-CCP had an advantage for large area process within above 8-inch diameter.

In chapter 4, UVAS techniques employing a ring dye laser and a hollow cathode lamp were applied to investigate the effect of the excitation frequency on the density and the translational temperature of the Si atom in VHF-CCP VHF at 27 MHz or 60 MHz employing a SiF_4 gas. The translational temperature of the Si atom was very high at the same N_e, especially above 1060 K at 27 MHz, and this was explained by the Frank-Condon effect and the hot Si atom is created due to the difference of energy of Si atom produced from the electron impact dissociation of SiF_x (x = 1-3) radicals and SiF_4 molecules.

In chapter 5, the behaviors of absolute densities and translational temperature of Si atoms in VHF SiH_4 CCP with Ar, N_2, and H_2 dilution gases were measured by UVAS employing a ring dye laser and a hollow cathode lamp. Si atoms were mainly produced by the electron impact dissociation of SiH_4 molecules, and extinguished by the reaction with the SiH_4 molecules and the diffusion. However, the Si atoms at the 27 MHz plasmas were produced more from radicals such as SiH_x (x = 1-3) radicals than SiH_4 molecules by the electron impact dissociation in comparison with 60 MHz plasmas. It is found that the Si atom heating was due to the energy of Si atoms released from the electron impact dissociation of SiH_x (x = 1-4). The temperatures at 27 MHz were larger than that at 60 MHz and the temperatures increased with increasing SiH_4 flow rate ratio. The temperatures in the SiH_4/Ar, SiH_4/N_2, and SiH_4/H_2 27 MHz plasmas were estimated to be 970, 1030, and 1130 K, respectively.

In chapter 6, the effect of the excitation frequency for the contribution of the deposition film was estimated. The contribution ratio of Si/SiH_3 ratio decreased with increasing the excitation frequency. The SiN film deposited at 60 MHz became nitride-rich composition more than that at 27 MHz because of the low ratio of Si/SiH_3.

Therefore, the contribution of the radicals to the film composition is changed with increasing the excitation frequency. It is indicated that increasing the excitation frequency has the advantages for obtaining the high-quality films and controlling the plasma chemistry.

These results are very important from the viewpoint of diagnostics of plasma chemistries and important information to control film deposition.

7.2 Scopes for future works

In the present study, behaviors of radicals in VHF-CCP were investigated by UVAS, IRLAS, and LIF. The production and loss processes of radicals and the radical temperature were clarified in VHF-CCP. Moreover, the correlation between Si atom and thin film deposition were discussed on the bases of the effects of the excitation frequency.

In chapter 3, the densities of the Si, SiF and SiF_2 radical and the SiF_4 molecule in VHF 60 MHz CCP employing SiF_4 were measured and the kinetics of these radicals were systematically discussed. However, only relative densities of SiF and SiF_2 radical were measured. It is important to measure the absolute density for clarifying the behaviors of radicals quantitatively. SiF_3 radical density has not been measured yet. These radicals density may be as large as or larger than Si atom density, and will affect much the film deposition. In this study, radical densities have been measured as a function of electron density under limited condition of SiF_4 100 % plasma. Therefore, in the future work, the radical density must be measured systematically in various plasma processes such as etching plasma, various plasma sources, and various plasma conditions (pressure, gas composition). For example, the SiF_4 based gases have been employed for the deposition of μc-Si:H and SiO_2 etching processes. In this study, VHF-CCP has a good uniformity for the large area process of the Si wafer of 8-inch in diameter. In the future, the wafer of 12-inch in diameter will be used soon in comparison with the current wafer of 8-inch in diameter, and the expansion of wafer

size is one of the most effective ways to reduction of the production cost. It is necessary to investigate the characteristics of VHF-CCP in which will be available in 12-inch process.

In chapter 4 and 5, the translational temperature of Si atom was measured and the effects of the excitation frequency and dilution gases on the behaviors of Si atoms were clarified. Various frequencies such as 13.56 MHz, 500 MHz, and 2.45 GHz were used for the plasma processes in addition to VHF. It is important to clarify the effect of the excitation frequency of the radical temperature systematically. In this study, the heating mechanism of Si atom has been mainly discussed by the Frank-Condon effect. The elastically collision with ion and the diffusion to the electrode will cause one of the heating mechanism in addition to the Frank-Condon effect. In order to clarify this mechanism in detail, it is necessary to discuss then quantitatively and systematically.

In chapter 6, the correlation between Si atom and thin film deposition was discussed on the basis of the effect of the excitation frequency. However, SiH_3, SiH_2, and SiH radical densities may be as large as or larger than Si atom density, and will affect the film deposition considerably. Therefore, it is necessary to discuss the contribution of all radicals to the thin film deposition with consideration of various radicals in addition to Si atom. Moreover, it is considered that the distribution of ion energy between 27 MHz and 60 MHz affects the film structure. Therefore, it is necessary to consider ion energy distribution in order to clarify the deposition mechanism of the films with high quality.

At last, it is found that VHF-CCP has advantages for plasma processing in this study. VHF-CCP will be the most useful plasma source for plasma processing. Furthermore, the mechanism of plasma chemistry in the VHF-CCP will be clarified in detail for realizing highly precise plasma processing.

Acknowledgments

The present research was performed in Professor Goto's Laboratory, Department of Quantum Engineering, Nagoya University. The author would like to thank sincerely his research advisor, Professor Toshio Goto, Department of Quantum Engineering, Nagoya University, for his guidance, advice, and encouragement throughout the course of this work. He also would like to thank his vice-advisor, Professor Akihiro Kono, Department of Electronics, Nagoya University, for guidance and valuable suggestion in preparing this thesis. He would also like to thank his vice-advisor, Associate Professor Masaru Hori, Department of Quantum Engineering, Nagoya University for a lot of their valuable discussions, advice, and comments in preparing this thesis.

The author would like to thank Associate Professor Masafumi Ito, Department of Opto-mechtronics, Wakayama University for their helpful advice and discussions, Assistant Professor Norihiko Nishizawa at Nagoya University for their useful advices and suggestions in day-to-day research.

The author would like to thank to Dr. Seigou Takashima at Nippon Laser & Electronics LAB., Dr. Kazushi Fujita at Fujitsu Ltd., and Dr. Hisao Nagai at Matsushita Electric Industrial Co., Ltd., for their discussions and useful suggestions in this research.

He also thanks heartily Mr. Ken-ichiro Hara at Canon Inc., and Mr. Tetsuro Ishida who aided experimental works carried out in this study. The author thanks to Mr. Junichi Higuchi, Mr. Koji Yamakawa, Mr. Takashi Hori, Mr. Mikio Nagai, Mr. Souichi Ikuma, Mr. Akira Suzuki, Mr. Kouichiro Homma, Mr. Akio Matsushita, Mr. Hori Naoki, Mr. Mouri Junpei, Mr. Masahiro Yamamoto, Mr. Eiji Tamura, and all other students who have studies in Professor Goto's Laboratory for their encouragement and cooperation.

Finally, the author owes great deals to his parents and brother, to all his teachers, and all his good friends.

Takayuki Ohta

January, 2004

List of Papers

1. Original Papers

Title	Journal	Authors (Related Chapters)
1. Measurement of Si, SiF, SiF_2, radicals and SiF_4 molecule using very high frequency capacitivery coupled plasma employing SiF_4	Journal of Applied Physics, **94**, (2003) 1428.	T.Ohta, K.Hara, T.Ishida, M.Hori, T.Goto, M.Ito, S.Kawakami, N.Ishii (chapter 3)
2. Effect of driving frequency on density and temperature of Si atom using capacitively coupled SiF_4 plasma	Japanese Journal of Applied Physics, **42**, (2003) L1532.	T.Ohta, M.Hori, T.Ishida, T.Goto, M.Ito, S.Kawakami, N.Ishii (chapter 4)
3. Effects of Ar dilution and exciting frequency on absolute density and translational temperature of Si atom in very high frequency-capacitively coupled SiH_4 plasmas	Japanese Journal of Applied Physics, **43**, (2004) L94.	T.Ohta, T.Ishida, M.Hori, T.Goto, M.Ito, S.Kawakami (chapter 5)
4. Study on the absolute density and the translational temperature of Si atom in very high frequency capacitively coupled SiH_4 plasma with Ar, N_2, and H_2 dilution gases	Japanese Journal of Applied Physics (submitted).	T.Ohta, M.Hori, T.Ishida, T.Goto, M.Ito, S.Kawakami (chapter 5 and 6)

2. International Conferences

Title	Conference	Authors
1. Monitoring of F, Si, SiFx (x=1-2) and SiF_4 molecule in RF60MHz Parallel-plate capacitively coupled plasma employing SiF_4	16th European Conference on Atomic & Molecular Physics of Ionized Gases and 5th International Conference on Reactive Plasmas joint conference, Grenoble, France, July 2002.	T.Ohta, K.Hara. M.Hori, T.Goto, M.Ito, S.Kawakami, N.Ishii
2. Behaviors of Si, SiF, SiF_2 radicals and SiF_4 molecule using RF60MHz capacitively coupled SiF_4 plasma	24th International Symposium on Dry Process, Tokyo, Japan, October 2002.	T.Ohta, T.Ishida, M.Hori, T.Goto, M.Ito, S.Kawakami, N.Ishii
3. Kinetics of SiFx (x=0-2) and SiF_4 molecule in RF60MHz parallel-plate capacitively coupled plasma employing SiF_4	55th Annual Gaseous Electronics Conference, Minneapolis, Minnesota, USA, October 2002.	M.Hori, T.Ohta, K.Hara, T.Goto, M.Ito, S.Kawakami, N.Ishii
4. The behavior of Si atoms in capacitively coupled VHF plasma employing SiF_4	XXVI International Conference on Phenomena in Ionized Gases, Greifswald, Germany, July 2003.	T.Ohta, T.Ishida, M.Hori, T.Goto, M.Ito, S.Kawakami, N.Ishii